DCAF16-Based Covalent Handle for the Rational Design of Monovalent Degraders

By

Melissa Lim

A dissertation submitted in partial satisfaction of the

requirements for the degree of

Doctor of Philosophy

in

Chemistry

in the

Graduate Division

of the

University of California, Berkeley

Committee in charge:

Professor Daniel K. Nomura, Chair

Professor Ziyang Zhang

Professor Roberto Zoncu

Spring 2026

Abstract

DCAF16-Based Covalent Handle for the Rational Design of Monovalent Degraders

By

Melissa Lim

Doctor of Philosophy in Chemistry

University of California, Berkeley

Professor Daniel K. Nomura, Chair

Targeted protein degradation (TPD) has emerged as a powerful therapeutic strategy that co-opts the cell's endogenous ubiquitin-proteasome system to selectively eliminate disease-causing proteins. Unlike traditional occupancy-driven inhibitors, which are limited to roughly 10% of the proteome featuring identifiable binding pockets or catalytic active site, TPD modalities operate through an event-driven and catalytic mechanism, inducing proximity between an E3 ubiquitin ligase and a protein of interest to promote its ubiquitination and proteasomal degradation at sub-stoichiometric concentrations. Molecular glue degraders in particular represent a compelling TPD approach, offering superior drug-like properties by virtue of their lower molecular weights and linker-less architecture, while enabling engagement of shallow binding surfaces of proteins previously deemed "undruggable". However, the rational design of molecular glue degraders remains a central challenge in the field as most known degraders were identified serendipitously or through phenotypic screens and the structural principles governing a productive E3 ligase-degrader-target ternary complex formation are still poorly understood.

In this dissertation, we sought to address this gap by identifying transplantable covalent chemical handles that could be appended onto the exit vectors of existing protein-targeting ligands to convert them into monovalent degraders of their respective targets. Using the BET family inhibitor JQ1 as a testing platform, we synthesized and screed a series of covalent JQ1 analogs and identified a vinylsulfonyl piperazine moiety that, when appended onto JQ1, enabled potent and selective proteasomal degradation of BRD4. Chemoproteomic profiling revealed that this handle covalently engages C119 on DCAF16, a CUL4 substrate receptor, as the E3 ligase responsible for the BRD4 degradation. This DCAF16-recruiting handle was successfully transplanted across a chemically diverse panel of protein-targeting ligands to induce the degradation of CDK4, the androgen receptor, BTK, SMARCA2/4, and BCR-ABL/c-ABL, spanning multiple protein classes. Together, these findings established a generalizable framework for a target-centric molecular glue degrader design that expands the repertoire of ligandable E3 ligases beyond the extensively exploited $CRL4^{CRBN}$ and VHL.

Table of Contents

Abstract **1**
Table of Contents ..... **i**
List of Figures ..... **iii**
Abbreviations ..... **iv**
Dedications ..... **ix**
Acknowledgements ..... **xi**
CHAPTER 1: Targeted Protein Degradation via Molecular Glue Degraders **1**
1.1 Targeted Protein Degradation 2
1.2 Modalities of Targeted Protein Degradation 2
1.3 Challenges in Molecular Glue Degrader Discovery 3
1.4 Rational Discovery of Molecular Glue Degraders 3
1.5 Figures 5
CHAPTER 2: Discovery of a DCAF16-Based Transplantable Covalent Handle for the Rational Design of Monovalent Degraders **8**
2.1 Summary 9
2.2 Introduction 9
2.3 Results 10
2.3.1 Identifying Covalent Handles that Enable the Degradation of BRD4 10
2.3.2 Mapping the E3 Ligase Responsible for BRD4 Degradation 11
2.3.3 Exploring the Applicability of the Covalent Handle Against Other Target Proteins 12
2.4 Discussion and Conclusion 14
2.5 Figures 16
2.6 Methods 26
2.6.1 Cell Culture 26
2.6.2 Western Blotting 26
2.6.3 Bortezomib or MLN4924 Rescue Studies 27
2.6.4 Cell Viability Assay 27
2.6.5 Isotopic desthiobiotin (isoDTB)-ABPP Cysteine Chemoproteomic Profiling of ML1-50 27
2.6.6 IsoDTB-ABPP Mass Spectrometry Analysis 28
2.6.7 Gel-Based ABPP 29
2.6.8 ML1-50-Competed Targets from ML2-33 Probe Pulldown Proteomics 29

2.6.9 Mapping of ML1-50 Site of Modification on DCAF16 by LC-MS/MS 29
2.6.10 Quantitative TMT Proteomics Analysis 30
2.6.11 Knock Out Cell Line Generation 31
2.6.12 Site-Directed Mutagenesis on FLAG-tagged DCAF16 Plasmid 31
2.6.13 Plasmid Isolation 31
2.6.14 Expression of FLAG-tagged Wild Type DCAF16 and Mutants in DCAF16 Knockout Cells 31
2.6.15 DCAF16 Knockdown Studies 32
2.6.16 RT-qPCR Analysis 32
Concluding Remarks 33
References 36
Appendices 44
Supplementary Figures 45
Supporting Table Legends 50
Synthetic Methods and Characterization 51

List of Figures

Figure 1.1 Mechanism of the Ubiquitin-Proteasome System (UPS)

Figure 1.2 Targeted Protein Degradation via PROTACs and Molecular Glue Degraders

Figure 1.3 Proposed Rational Chemical Design Strategy

Figure 1.4 Chemical Modifications on the Protein Inhibitors Render Molecular Glue Degrader Discoveries

Figure 2.1 Identifying Covalent Handles that Enable the Degradation of BRD4

Figure 2.2 Characterization of the Monovalent and Covalent BRD4 Degrader ML 1-50

Figure 2.3 Identifying the E3 Ligase Responsible for ML 1-50-Mediated BRD4 Degradation

Figure 2.4 Testing the Dependence of Covalent Monovalent BRD4 Degraders on DCAF16 versus RNF126

Figure 2.5 Characterization of CDK4 Monovalent Degrader

Figure 2.6 Characterization of AR and BTK Monovalent Degraders

Figure S1 Characterization of ML 1-50

Figure S2 ML 1-71 effects on cell viability

Figure S3 Characterization of SMARCA2 Monovalent Degrader

Figure S4 Characterization of AR and BCR-ABL/c-ABL Monovalent Degraders

Figure S5 Characterization of the BTK Degrader TH 1-9

Abbreviations

AASDHPPT	L-aminoadipate-semialdehyde dehydrogenase-phosphopantetheinyl transferase
ABPP	Activity-based protein profiling
ADCY5	Adenylate cyclase type 5
ADRBK1	Adrenergic receptor kinase 1
ALDH6A1	Aldehyde dehydrogenase 6 family member A1
ANOVA	Analysis of variance
AR	Androgen receptor
AR-V7	Androgen receptor variant 7
ATCC	American Type Culture Collection
ATP	Adenosine triphosphate
Aux/IAA	Auxin/Indole-3-acetic acid
BCA	Bicinchoninic acid
BCL6	B cell lymphoma 6 protein
BCR-ABL	Breakpoint cluster region-Abelson tyrosine protein kinase 1
BET	Bromodomain and extra-terminal domain
BRD2	Bromodomain-containing protein 2
BRD3	Bromodomain-containing protein 3
BRD4	Bromodomain-containing protein 4
BRD9	Bromodomain-containing protein 9
BSA	Bovine serum albumin
BTB	Broad-complex, Tramtrack and Bric-a-brac domain
BTK	Bruton tyrosine kinase
BTZ	Bortezomib
c-ABL	Abelson tyrosine protein kinase 1
C119	Cysteine at position 119
C177	Cysteine at position 177
C179	Cysteine at position 179
C2H2	Cys2-His2
C58	Cysteine at position 58
CCCNB1	Cyclin B1
CDK1	Cyclin-dependent kinase 1
CDK12	Cyclin-dependent kinase 12
CDK4	Cyclin-dependent kinase 4
CDK6	Cyclin-dependent kinase 6
CDKN2A	Cyclin-dependent kinase inhibitor 2A

cDNA	Complementary DNA
CHEK1	Checkpoint kinase 1
CK1α	Casein kinase 1 alpha
CLK3	CDC-like kinase 3
COI1	Coronatine-insensitive 1
CRBN	Cereblon
CRISPR	Clustered regularly interspaced short palindromic repeats
CRL	Cullin-RING E3 ubiquitin ligase
CRL4	Cullin-RING ligase 4
cryo-EM	Cryogenic electron microscopy
CuAAC	Copper-catalyzed azide-alkyne cycloaddition
CUL4	Cullin-4
CV	Compensation voltages
DCAF11	DDB1 and CUL4 Associated Factor 11
DCAF16	DDB1 and CUL4 Associated Factor 16
DCM	Dichloromethane
DDB1	DNA damage-binding protein 1
DIPEA	N,N-diisopropylethylamine
DMEM	Dulbecco's Modified Eagle Medium
DMF	N,N-dimethylformamide
DMSO	Dimethyl sulfoxide
DTT	Dithiothreitol
DUS3L	Dihydrouridine synthase 3 like
ESI	Electrospray ionization
EtOAc	Ethyl acetate
FA	Formic acid
FAIMS	High-field asymmetric waveform ion mobility spectroscopy
FAM204A	Family with sequence similarity 204 member A
FASN	Fatty acid synthase
FBS	Fetal bovine serum
FBXO22	F-box protein 22
FBXO28	F-box protein 28
FDR	False discovery rate
FEM1B	Fem-1 homolog B
FGD6	FYVE, RhoGEF and PH domain-containing protein 6
FKBP12	FK506-binding protein 12
FLAG	DYKDDDDK polypeptide protein tag
FRB	FKBP12-rapamycin binding domain

GAPDH	Glyceraldehyde 3-phosphate dehydrogenase
GART	Trifunctional purine biosynthetic protein adenosine-3
GSPT1	G1 To S Phase Transition 1
HATU	Hexafluorophosphate azabenzotriazole tetramethyl uronium
HCD	Higher-energy collision dissociation
HDAC1	Histone deacetylase 1
HDAC2	Histone deacetylase 2
HEK	Human embryonic kidney
HPLC	High-performance liquid chromatography
HRMS	High-resolution mass spectrometry
IA	Iodoacetamide
IKZF1	Ikaros family zinc finger 1
IKZF2	Ikaros family zinc finger 2
IKZF3	Ikaros family zinc finger 3
IKZF4	Ikaros family zinc finger 4
IMDM	Iscove's Modified Dulbecco's Medium
IMiD	Immunomodulatory imide drug
IRS1	Insulin receptor substrate 1
isoDTB-ABPP	Isotopically labeled desthiobiotin azide-tag-based activity-based protein profiling
JAZ	Jasmonate ZIM-domain
KEAP1	Kelch-like ECH-associated protein 1
KIAA0101	PCNA-associated factor
KIFC1	Kinesin family member C1
KLHDC2	Kelch domain-containing protein 2
KO	Knockout
LC-MS/MS	Liquid chromatography-mass spectrometry
LNCaP	Lymph node carcinoma of the prostate
MAP2K4	Dual specificity mitogen-activated protein kinase kinase 4
MDA-MB-231	MD Anderson-metastatic breast-231
MeOH	Methanol
MGD	Molecular glue degrader
MID1IP1	Mid1-interacting protein 1
MND1	Meiotic nuclear divisions 1
mRNA	Messenger RNA
MRTO4	mRNA turnover protein 4 homolog
MS1	First MS for detection of initial ionization in MS/MS
MS2	Second MS for detection of fragment ionization in MS/MS

mTOR	Mechanistic target of rapamycin
mTORC1	Mechanistic target of rapamycin complex 1
NEDD8	Neural precursor cell expressed developmentally downregulated protein 8
NEK7	NIMA-related kinase 7
NFKB1	Nuclear factor kappa B subunit 1
NFκB	Nuclear factor kappa-light-chain-enhancer of activated B cells
NMR	Nuclear magnetic resonance
NOSIP	Nitric oxide synthase-interacting protein
NP-40	Nonyl phenoxypolyethoxylethanol
PARP2	Poly(ADP-ribose) polymerase 2
PBK	Lymphokine-activated killer T-cell-originated protein kinase
PBS	Phosphate-buffered saline
POI	Protein of interest
PPI	Protein-protein interaction
PROTAC	Proteolysis-targeting chimera
PSMG1	Proteasome assembly chaperone 1
RIPA	Radio-immunoprecipitation assay
RNF114	Ring finger protein 114
RNF126	Ring finger protein 126
RNF4	Ring finger protein 4
RP-HPLC	Reversed phase high-performance liquid chromatography
RPMI	Roswell Park Memorial Institute Medium
RPS6KA4	Ribosomal protein S6 kinase A4
RSBN1L	Round spermatid basic protein 1 like
RT	Room temperature
RTFDC1	Replication termination factor 2 domain containing 1
SALL4	Spalt-like transcription factor 4
SBNO1	Strawberry notch homolog 1
SCF	Skp1-cullins-F-box protein
SDS	Sodium dodecyl sulfate
SDS/PAGE	Sodium dodecyl sulfate-polyacrylamide gel electrophoresis
SFC	Supercritical fluid chromatography
sgRNA	Single guide RNA
shRNA	Short hairpin RNA
SIAH1	Seven in absentia homolog 1
SKP1	S-phase kinase-associated protein 1
SMARCA2	SWI/SNF related, matrix associated, actin dependent regulator of chromatin, subfamily A, member 2

SMARCA4	SWI/SNF related, matrix associated, actin dependent regulator of chromatin, subfamily A, member 4
SPIN4	Spindlin family member 4
SRSF9	Serine/arginine-rich splicing factor 9
STK4	Serine/threonine-protein kinase 4
SYK	Spleen tyrosine kinase
T3P	Propylphosphonic anhydride
TBS-T	Tris-buffered saline containing Tween 20
TBTA	Tris(benzyltriazolylmethyl)amine
tBuOH	tert-Butyl alcohol
TCEP	Tris(2-carboxyethyl)phosphine
TEAB	Triethylammonium bicarbonate
TFA	Trifluoroacetic acid
TGX	Tris-Glycine eXtended
TIR1	Transport inhibitor response 1
TLC	Thin layer chromatography
TLK2	Tousled-like kinase 2
TMT	Tandem mass tag
TOE1	Target of EGR1 protein 1
TPD	Targeted protein degradation
TUBB2B	Tubulin beta-2B chain
UBE2C	Ubiquitin-conjugating enzyme E2 C
UBE2D	Ubiquitin-conjugating enzyme E2 D
UPS	Ubiquitin-proteasome system
UV	Ultraviolet
VAV1	Vav guanine nucleotide exchange factor 1
VHL	Von Hippel-Lindau tumor suppressor
WT	Wild type
ZBTB16	Zinc finger and BTB domain-containing protein 16
β-TrCP	Beta-transducin repeat-containing protein

Dedications

This dissertation is dedicated to the incredible people who have always been there for me, believed in me, supported me and made this chapter of my life truly unforgettable.

To my Ph.D. advisor and mentor, Dan Nomura, thank you for taking me into the lab as a first-year student four years ago and for believing in what I am capable of achieving. Your guidance and encouragement at every step of this journey have meant a lot to me. Your optimism and faith in my abilities, despite all the challenges and failed experiments across every project I have worked on, have pushed me to be a better scientist every single day.

To Dr. Thang Do Cong, an incredible collaborator, desk mate, mentor, friend, and brother, thank you for coming onboard with this project three years ago. You are truly the best teammate anyone could ever ask for. I have learned so much from you and I truly appreciated your support, both in and outside of the lab. I will dearly miss the hours we spent discussing science and dreaming up our wildest ideas together. To future Dr. Zoe Tuong Nghi Duong, you have always been so kind and so present, standing by my side through the highs and lows, the excitement and frustration, and everything in between. Your words of encouragement and moments of "goofiness" have always brightened my days, especially the discouraging ones. Thang, Zoe, and Lydia Zhang, I am so grateful our paths crossed. Having you around made me genuinely look forward to coming into lab every day, and every failed experiment felt a little less heavy knowing you were always there. I will truly miss the spontaneous boba runs, late-night lab dinners, and the weekend food adventures we shared.

To Dr. Ethan Toriki, who helped me find my footing in the lab during my first year, thank you for your patience in training me on new techniques and for your support in those early days of my research. Your dedication and work ethic (particularly the long hours you poured into the lab) set a standard that I still aspire to as a scientist. To Elijah and Yihan, it was an honor to mentor you both and watch you grow as scientists. Thank you for the hard work you put into our projects. I really enjoyed working alongside you and I cannot wait to see where your research careers take you. To all past and present members of the Nomura Research Group, thank you for your warm welcome when I first joined, for all the scientific advice along the way, and for making the late nights and weekends in the lab so much more fun than they had any right to be.

To all my fellow Malaysian friends in the Bay Area, thank you for building such a wonderful community and making me feel at home away from home. To Marsya, Akmal and Ang, thank you for your warmth and friendship from the very first day I arrived in Berkeley. You are part of the reason I chose to come here for grad school, and the weekend food hunts, sleepovers, and road trips we went on are some of my favorite memories from this whole chapter of my life. To my real-life friends turned online/LDR ones, Erica, Jason, Lucas, and Stephanie, and to the entire extended Yeo Family, thank you for the love, encouragement and unwavering faith you have shown me throughout this journey no matter the distance between us. I am so grateful for every single one of you, and I truly could not have made it through these past few years without you.

Finally, and most importantly, to my mum, thank you for your unconditional love, and support in everything I have ever chosen to pursue: picking a major, leaving home for a university on the other side of the world, and deciding to take on a Ph.D. You have always been my greatest role model, and your belief in me has never once faltered. Thank you for listening to me rant about failed experiments, for genuinely trying to understand my research despite having no science background and for simply being there whenever I needed you. Every word of encouragement, every lesson and every sacrifice you have made has shaped me into who I am today. While I am the one receiving this degree, you have earned it just as much as I have. I could not have done any of this without you, and I am forever grateful to be your child.

Acknowledgements

This work in chapter 2 was adapted from the manuscript with permission from co-authors, Melissa Lim, Thang Do Cong, Lauren M. Orr, Ethan S. Toriki, Andrew C. Kile, James W. Papatzimas, Elijah Lee, Yihan Lin, Daniel K. Nomura, "DCAF16-Based Covalent Handle for the Rational Design of Monovalent Degraders." Copyright © 2024 ACS Central Science.

Thank you to the members of the Nomura Research Group and Novartis BioMedical Research for critical reading of the manuscript. This work was supported by Novartis BioMedical Research and the Novartis-Berkeley Translational Chemical Biology Institute (NB-TCBI) for all listed authors. This work was also supported by the Nomura Research Group and the Mark Foundation for Cancer Research ASPIRE Award. This work was also supported by grants from the National Institutes of Health (R01CA240981 and R35CA263814) and the National Science Foundation Molecular Foundations for Biotechnology Award (2127788). We also thank Drs. Hasan Celik, Raynald Giovine, and Pines Magnetic Resonance Center's Core NMR Facility (PMRC Core) for spectroscopic assistance. The instrument used in this work was in part supported by NIH S10OD024998.

CHAPTER 1

Targeted Protein Degradation via Molecular Glue Degraders

1.1 Targeted Protein Degradation

Protein homeostasis, or proteostasis, is fundamental to cell function and survival. Cells constantly maintain protein equilibrium through tightly regulated processes encompassing protein synthesis, folding, localization, and degradation, and any disruption to this balance can have serious pathological consequences. Aberrant upregulation or downregulation of protein expression, accumulation of misfolded, and protein aggregation have all been implicated in a wide spectrum of human diseases, including cancer, neurodegeneration, and immunological and metabolic disorders[1]. Cells have therefore evolved sophisticated quality control pathways to restore proteostasis, most notably the ubiquitin-proteasome system (UPS) and the autophagy-lysosome pathway, which collectively act to remove misfolded, damaged, or unwanted proteins and maintain the appropriate protein levels within the cell. Targeted protein degradation (TPD) is a therapeutic strategy that rewires these endogenous protein degradation pathways to eliminate disease-causing proteins. This work focuses on modalities that rely on the mechanisms of the UPS, in which protein substrates are labelled with a polyubiquitin chain through a series of ATP-dependent reactions involving an E1 ubiquitin-activating enzyme, an E2 ubiquitin-conjugating enzyme, and an E3 ubiquitin ligase. The resulting polyubiquitinated substrate is subsequently recognized and degraded by the 26S proteasome **(Figure 1.1)**.

1.2 Modalities of Targeted Protein Degradation

TPD approaches use small molecules that induce proximity between an E3 ubiquitin ligase and a target protein of interest (POI) to promote degradation of the latter. These molecules, referred to as degraders, are classified into heterobifunctional molecules, known as proteolysis targeting chimeras (PROTACs), and monovalent molecular glue degraders (MGDs) **(Figure 1.2)**. PROTACs consist of a ligand recruiting an E3 ubiquitin ligase and a flexible linker connecting another ligand engaging a POI, while MGDs are single, linker-less small molecules that (i) bind to either the E3 ligase or POI (with low or unmeasurable affinity to the other) and create a neo-interface to allow E3 ligase-POI interactions; or (ii) bind at the protein-protein interface and stabilize interactions between two protein partners that have intrinsic affinity for each other[2].

In contrast to traditional occupancy-driven inhibitors that require binding at a protein's active site to block its function **(Figure 1.3a)**, both PROTACs and MGDs offer a catalytic mechanism of action that allows therapeutic effect at a sub-stoichiometric level. Furthermore, TPD modalities do not have binding site requirements, as they can bind to anywhere on the POI, and even transient binding is sufficient to achieve degradation due to their event-driven pharmacology[3]. PROTACs' modular nature allows them to be rationally designed using existing E3 recruiting ligands and POI inhibitors; however, challenges arise as their large molecular weights limit bioavailability, and the "hook effect" can occur at high concentrations as a result of their bivalent nature, impeding ternary complex formation and drug efficacy. MGDs, on the other hand, present more promising therapeutic potential due to their (i) lower molecular weights and associated drug-

like properties; (ii) ability to engage shallow binding pockets of target proteins previously deemed "undruggable"; and (iii) non-saturable kinetics[2].

1.3 Challenges in Molecular Glue Degrader Discovery

Most MGDs have been discovered fortuitously or through phenotypic screens. The most prominent example of a molecular glue degrader is thalidomide, which was first used in the 1950s to treat morning sickness in pregnant women but was withdrawn from the market in 1961 due to its teratogenic side effects[4,5]. The drug was later reapproved for its anti-inflammatory and anti-angiogenic effects in treating erythema nodosum leprosum and multiple myeloma, even though the molecular mechanisms of action were still poorly understood at the time[4,6,7]. It was only in the 2010s that thalidomide was discovered to act as a molecular glue degrader[8,9]. Thalidomide and its structural analogs known as the immunomodulatory imide drugs (IMiDs) bind to the E3 ligase $CRL4^{CRBN}$ and induce protein-protein interactions (PPIs) with a range of POIs, including the C2H2-type zinc-finger transcription factors, Ikaros (IKZF1) and Aiolos (IKZF3), SALL4, GSPT1, and CK1α, leading to ubiquitination and proteasomal degradation of these targets[10–12,8,9,13–15]. This mechanistic elucidation laid an important foundation for the discovery of many MGDs to date.

Another example is the serendipitous discovery of the BCL6 degrader BI-3802 during screening for inhibitors of the oncogenic transcription factor[16]. In a later study, Słabicki *et al.* revealed that the compound engages the BTB domain of BCL6 and induces BCL6 polymerization through the assembly of the homodimers. BI-3802 does not directly induce interaction between BCL6 and an E3 ligase but instead promotes BCL6 polymerization, which facilitates substrate recognition by the E3 ligase SIAH1, resulting in the subsequent degradation **(Figure 1.4a)**[17]. These examples underscore a broader challenge in the field: the lack of experimental tools to discover MGDs and the complexity of their mechanism of action have made the systematic design of these molecules difficult.

1.4 Rational Discovery of Molecular Glue Degraders

Despite these challenges, the field has sought to develop more systematic strategies, such as phenotypic and biochemical screening, chemoproteomic profiling, and structure-based rational design to identify and design MGDs. Mayor-Ruiz et al. developed a phenotypic screening strategy exploiting hyponeddylated cell models to identify CRL-dependent MGDs, yielding dCeMM2/3/4, whose antiproliferative effects were abrogated in hyponeddylated cell lines[18]. Quantitative proteomics and genome-wide CRISPR screening revealed that these compounds induce proximity between CDK12 and DDB1, leading to the ubiquitination and degradation of the CDK12 binding partner cyclin K. However, target deconvolution in such target-agnostic workflows can be extensive and laborious. To circumvent this limitation, King et al. applied a similar screening approach coupled with covalent chemoproteomics for rapid mechanistic interrogation, leading to the discovery of an MGD that glues together UBE2D2 with NFKB1[19]. The discovery of NRX-

252114 illustrated a more target-directed biochemical screening strategy, in which a fluorescence polarization assay was designed to identify small molecules that enhance the PPI between β-catenin and its cognate E3 ligase, $SCF^{\beta\text{-}TrCP}$ [20]. This approach directly interrogates PPI stabilization rather than relying on cytotoxicity as a readout and highlights the therapeutic potential of MGDs in restoring native substrate-E3 ligase binding. Structure-based rational design efforts have largely focused on developing next-generation $CRL4^{CRBN}$ modulators derived from the thalidomide and IMiD scaffolds to expand the neosubstrate scope of $CRL4^{CRBN}$. In 2020, Matyskiela et al. discovered CC-3060 and CC-647, which promote degradation of the transcription factor ZBTB16[21]. Wang et al. reported the discovery of ALV1 and ALV, which induce the degradation Helios (IKZF2) and Eos (IKZF4), thereby weakening the anergic phenotype and reducing the suppressive activity of regulatory T cells on antitumor immune response[22]. More recently, Petzold et al. identified and validated over 20 previously unknown $CRL4^{CRBN}$ neosubstrates beyond the canonical β-hairpin G-loop class, such as NEK7, mTOR and VAV1, using three $CRL4^{CRBN}$-based MGDs[23].

While IMiD-based rational design strategy of MGDs has expanded the molecular glue landscape, these compounds rely on $CRL4^{CRBN}$ when there are over 600 E3 ligases encoded by the human genome. The Nomura lab recently has taken a different approach, by leveraging covalent chemistry and chemoproteomics to rationally design MGDs in a target centric manner while also identifying novel E3 ligase recruiter beyond $CRL4^{CRBN}$ and VHL ligands **(Figure 1.3b, 1.4c)**[24]. Previous reports on the discovery of the aforementioned BI-3802 and (*R*)-CR8, a close analog of the CDK12 inhibitor, (*R*)-roscovitine, that induce selective degradation of cyclin K through the same mechanism of action of dCeMM2/3/4 mentioned above, provided evidence that subtle modifications in inhibitor structures can convert the inhibition mechanism of action into degradation **(Figure 1.4a-b)**[17,18,25]. However, these independent examples of inhibitors-turned degraders offer distinct mechanisms of action and the underlying design principles are still poorly understood. Using a fumarate handle engaging the E3 ligase RNF126, Toriki et al. demonstrated the possibility of using a transplantable chemical modification capable of recruiting a E3 ligase onto existing protein-targeting ligand to design MGDs more systematically **(Figure 1.4c)**[24]. This work in Chapter 2 of this dissertation described the efforts of discovering additional transplantable chemical handles that could be appended onto protein-targeting ligands to convert these compounds into MGDs of their respective targets.

1.5 Figures

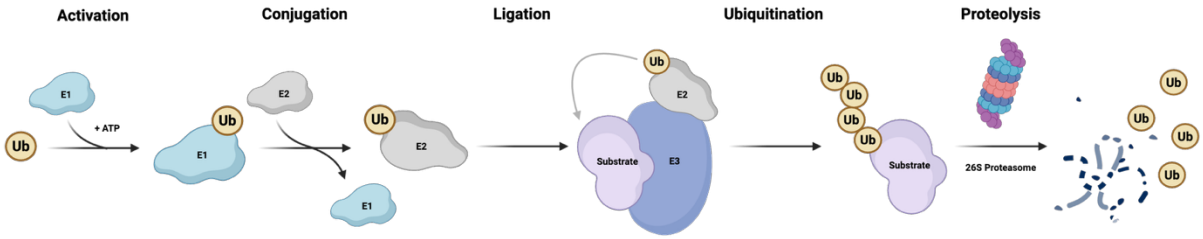

Figure 1.1. Mechanism of the Ubiquitin-Proteasome System (UPS). The ubiquitination cascade starts with the ATP-dependent activation of ubiquitin by an E1 ubiquitin-activating enzyme, followed by the transfer of the ubiquitin to an E2 ubiquitin-conjugating enzyme, and finally to the protein substrate via an E3 ubiquitin ligase, which mediates substrate recognition. Subsequent extension of the ubiquitin chain results in the formation of a polyubiquitin chain that ultimately signals the protein for proteasomal degradation.

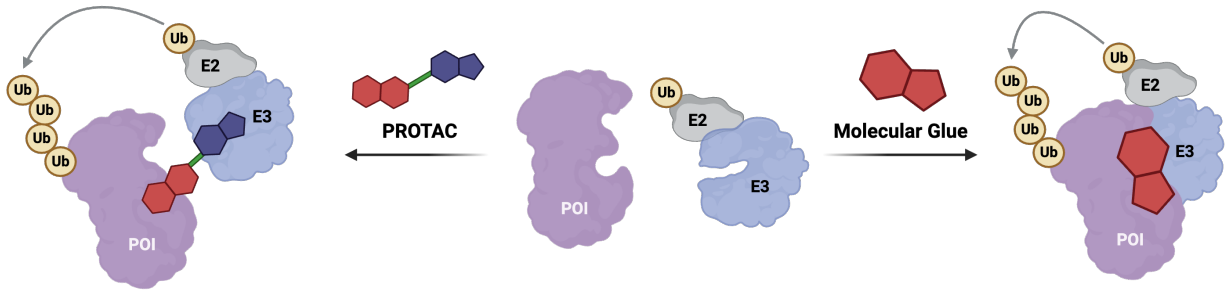

Figure 1.2. Targeted Protein Degradation via PROTACs and Molecular Glue Degraders. Proteolysis targeting chimeras (PROTACs) and molecular glue degraders induce proximity between an E3 ubiquitin ligase and a protein of interest (POI), also known as a target protein, to promote the ubiquitination and proteasomal degradation of the target protein. PROTACs are heterobifunctional molecules consist of two ligands, a target protein ligand and an E3 ligase ligand, connected by a flexible linker. Molecular glue degraders are monovalent compounds that bind to either the E3 ligase or the target protein to induce interaction between the two protein partners.

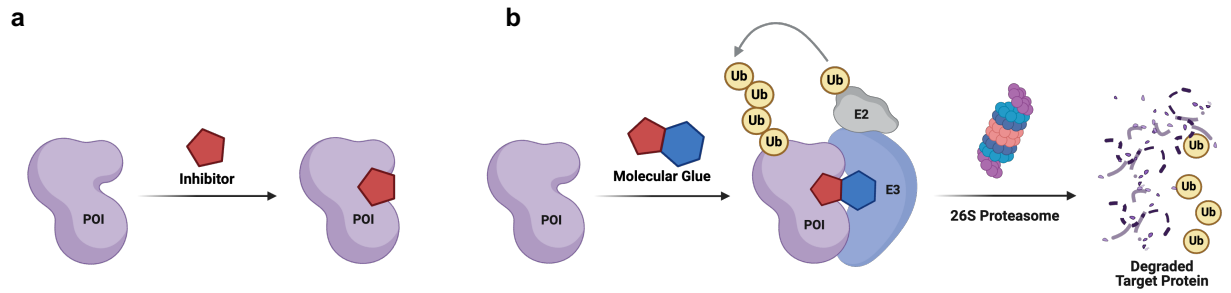

Figure 1.3. Proposed Rational Chemical Design Strategy. (a) Occupancy-based inhibitors bind to a well-defined binding pocket or active site on a protein, and require stoichiometric and sustained target binding to maintain functional effects. **(b)** Appending a transplantable chemical modification that engages an E3 ubiquitin ligase onto existing inhibitors converts non-degradative inhibitors into molecular glue degraders.

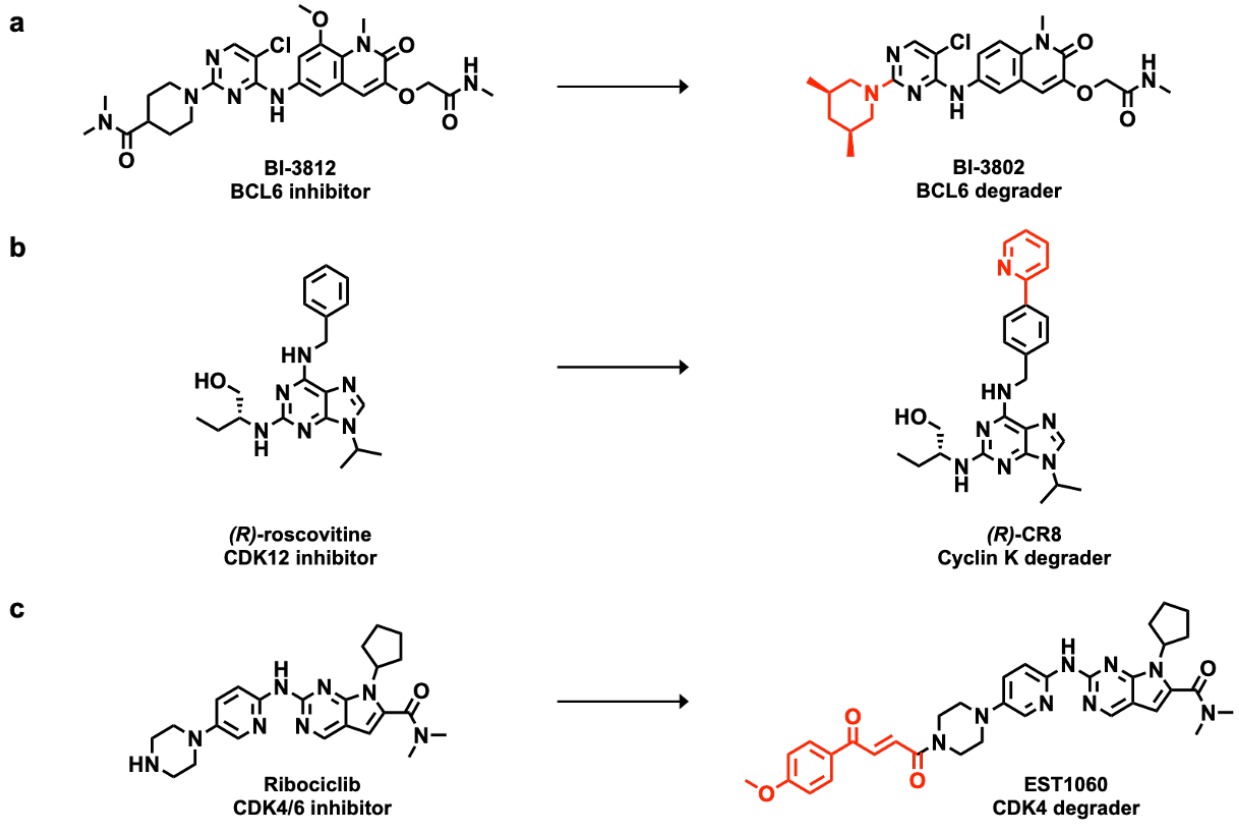

Figure 1.4. Chemical Modifications on the Protein Inhibitors Render Molecular Glue Degrader Discoveries. (a) Dimethyl-piperidine modification on the BCL6 inhibitor BI-3812 induces BCL6 polymerization via the BTB domain, making BI-3802 a BCL6 degrader. **(b)** Addition of a 2-pyridyl substituent on the CDK12 inhibitor *(R)*-roscovitine created *(R)*-CR8, which

induces selective degradation of cyclin K by strengthening protein-protein interaction between DDB1 and CDK12-cyclin K. **(c)** EST1060, a CDK4 degrader derived from the inhibitor ribociclib, contains a methoxyphenyl but-2-ene-1,4-dione ("fumarate handle") that covalently engages the E3 ligase RNF126 to induce degradation.

CHAPTER 2

Discovery of a DCAF16-Based Transplantable Covalent Handle for the Rational Design of Monovalent Degraders

This chapter is based on the *ACS Central Science* publication "DCAF16-Based Covalent Handle for the Rational Design of Monovalent Degraders"[26] and has been adapted with permission from all co-authors.

2.1 Summary

Targeted protein degradation with monovalent molecular glue degraders is a powerful therapeutic modality for eliminating disease causing proteins. However, rational design of molecular glue degraders remains challenging. In this study, we sought to identify a transplantable and linker-less covalent handle that could be appended onto the exit vector of various protein-targeting ligands to induce the degradation of their respective targets. Using the BET family inhibitor JQ1 as a testbed, we synthesized and screened a series of covalent JQ1 analogs and identified a vinylsulfonyl piperazine handle that led to the potent and selective degradation of BRD4 in cells. Through chemoproteomic profiling, we identified DCAF16 as the E3 ligase responsible for BRD4 degradation—an E3 ligase substrate receptor that has been previously covalently targeted for molecular glue-based degradation of BRD4. Interestingly, we demonstrated that this covalent handle can be transplanted across a diverse array of protein-targeting ligands spanning many different protein classes to induce the degradation of CDK4, the androgen receptor, BTK, SMARCA2/4, and BCR-ABL/c-ABL. Our study reveals a DCAF16-based covalent degradative and linker-less chemical handle that can be attached to protein-targeting ligands to induce the degradation of several different classes of protein targets.

2.2 Introduction

Monovalent molecular glue degraders have arisen as a powerful therapeutic modality for degrading therapeutic targets of interest through inducing the proximity of an E3 ubiquitin ligase with a neo-substrate protein to ubiquitinate and degrade the target through the proteasome [27,28]. Molecular glue degraders are potentially more promising compared to heterobifunctional Proteolysis Targeting Chimeras (PROTACs) because of their lower molecular weights and associated drug-like properties, as well as their potential to exploit shallow protein-protein interfaces between an E3 ligase and less tractable therapeutic proteins that may not possess deep binding pockets [27]. However, most molecular glue degraders have either been discovered fortuitously or through phenotypic screens [8,25,27,29–31]. Rational chemical design of molecular glue or monovalent degraders in a target-based manner remains challenging.

Many recent studies have reported how subtle chemical alterations to otherwise non-degradative small-molecule inhibitors converted them into molecular glue degraders of their respective targets [25,31–33]. These studies gave rise to the exciting possibility of transplantable chemical handles that could be appended onto the exit vector of protein-targeting ligands to convert these compounds into molecular glue degraders of their targets. E3 ligases have been shown to be ligandable with covalent small-molecules and chemoproteomic approaches [34–40]. Covalent handles have also been successfully used in heterobifunctional PROTACs to identify permissive chemical handle and ligandable E3 ligase pairs that can be exploited for targeted protein degradation applications. These studies have identified various covalent handles targeting cysteines in E3 ligase substrate receptors DCAF16 and DCAF11 [37,41,42]. Covalent ligand screens against specific ubiquitin proteasome system components have also yielded new E3 ligase, E2

ubiquitin conjugating enzyme, or Cullin adaptor recruiters against RNF114, RNF4, FEM1B, UBE2D, DDB1, and SKP1 that can be used for PROTACs [36,43–48].

Recent studies have also revealed that covalent chemistry can be used to identify potential chemical handles that enable the rational design of monovalent or molecular glue degraders. We previously discovered a covalent chemical handle that targets a cysteine in the quality control E3 ligase RNF126 that could be appended to the exit vector of a diverse range of protein-targeting ligands without the necessity for a linker to enable degradation of their respective targets [24]. Covalent molecular glue degraders have also been discovered that enhance weak existing interactions between DCAF16 and BRD4 to degrade BRD4 in a template-assisted covalent modification approach [49,50].

In this study, we sought to identify additional transplantable covalent chemical handles that can convert non-degradative inhibitors into molecular glue or monovalent degraders of their respective targets. We have identified a vinylsulfonyl piperazine handle that acts through targeting a cysteine within DCAF16 to not only enable the degradation of BRD4, but also several additional neo-substrates.

2.3 Results

2.3.1 Identifying Covalent Handles that Enable the Degradation of BRD4

To identify covalent chemical handles that could convert non-degradative inhibitors into molecular glue or monovalent degraders of their targets, we used the BET family inhibitor JQ1 as a testbed to generate a series of covalent JQ1 analogs bearing various electrophilic handles that could react with cysteines, lysines, or other nucleophilic amino acids on E3 ligases to degrade BRD4 **(Figure 2.1a)**. We synthesized and tested 18 derivatives. Among these compounds, only one compound, ML 1-50, led to the loss of both the long and short isoforms of BRD4 in HEK293T cells **(Figure 2.1b-c; Figure 2.2a)**. ML 1-50 reduced BRD4 levels in a dose-dependent manner with preferential degradation of the short BRD4 isoform with nanomolar potency in HEK293T cells **(Figure 2.2b-c)**. We observed hook effects with degradation of the long BRD4 isoform. ML 1-50 only showed modest cell viability impairments in HEK293T cells at the highest concentration of 10 mM tested **(Figure S1a)**. This BRD4 degradation was attenuated by pre-treatment with either proteasome inhibitor or NEDD8-activating enzyme inhibitor MLN4924 demonstrating that the loss of BRD4 was dependent on the proteasome and also a Cullin E3 ubiqutin ligase, respectively **(Figure 2.2d-g).** We had previously observed preference for degradation of the long versus short isoforms of BRD4 with covalent PROTACs that appeared be specific to HEK293T cells compared to other cell lines [47,48]. Similarly, we found that ML 1-50 potently degraded both the long and short BRD4 isoforms in the MDA-MB-231 breast cancer cell line, with no hook effects observed **(Figure 2.2h, Figure S1b).** Quantitative proteomic profiling of ML 1-50 in MDA-MB-231 cells showed relatively selective BRD4 degradation with only 11 other proteins that were significantly

reduced in levels by greater than 2-fold **(Figure 2.2i; Table S1)**. These 11 targets that are degraded are likely due to off-targets of our covalent degradative handle, which still requires further medicinal chemistry efforts to improve selectivity. These 11 targets included KIAA0101, RSBN1L, CCCNB1, MND1, UBE2C, RTFDC1, FAM204A, KIFC1, and IRS1 **(Table S1)**. JQ1 also engages BRD2 and BRD3 and JQ1-based PROTACs have led to the degradation of BRD2, BRD3, and BRD4 [51]. With ML 1-50, we did not observe BRD2 degradation, but we did observe loss of BRD3 below our statistical significance threshold **(Figure 2.2i; Table S1).**

2.3.2 Mapping the E3 Ligase Responsible for BRD4 Degradation

We next sought to identify the E3 ligase responsible for the BRD4 degradation observed with ML 1-50. We synthesized an alkyne-functionalized probe based on the vinylsulfonyl piperazine handle, ML 2-33 **(Figure 2.3a)**. Given the simplicity of this handle without a more elaborated ligand attached, we surmised that the handle would likely be more promiscuous compared to ML 1-50. We thus performed a competitive pulldown chemoproteomic experiment from ML 2-33-treated cells searching for proteins that were significantly outcompeted by ML 1-50 pre-treatment. The ML 2-33 pulldown proteomics experiment yielded 6259 proteins. Out of these proteins, we observed 133 proteins that were significantly out-competed by excess ML 1-50 (200 mM) ($p<0.03$, with $\log_2$ less than -0.6) spanning diverse protein classes **(Figure 2.3b-c; Table S2)**. Among these outcompeted targets, there was only one E3 ligase that was part of the Cullin E3 ligase family that could be regulated by NEDD8—DCAF16 **(Figure 2.3c; Table S2)**. Using competitive activity-based protein profiling (ABPP), competing *in situ* ML 1-50 target binding against *ex situ* proteome-wide cysteine labeling with a cysteine-reactive probe, we showed significant engagement of C119 of DCAF16 in cells with a control versus ML 1-50 treated ratio of the probe-modified tryptic peptide of 1.4, indicating a ~28 % engagement of this cysteine **(Figure S1c-d; Table S3)**. This modest degree of E3 ligase engagement is consistent with previous reports with covalent PROTACs showing that only a small fraction of the E3 ligase needs to be engaged to enable degradation of target proteins [36,37,41]. Site of modification analysis by liquid chromatography-mass spectrometry (LC-MS/MS) on tryptic digests of pure DCAF16 labeled with ML 1-50 also showed a single labeled site on C119 **(Figure S1e).** Our ABPP analysis identified 32 cysteines that were significantly engaged by >80 % among >10,000 cysteines profiled **(Table S3).** Interestingly, there was no overlap between the targets identified in ABPP versus ML 2-33 competitive pulldown experiments. While our chemoproteomic data collectively demonstrated that ML 1-50 likely possesses a significant number of off-targets and still requires further medicinal chemistry optimization, we sought to further characterize the role of DCAF16 in ML 1-50 mediated BRD4 degradation effects.

To further confirm direct interaction of ML 1-50 with DCAF16, we showed that ML 1-50 displaced cysteine-reactive probe labeling of pure DCAF16 protein by gel-based ABPP approaches without causing any precipitation of the protein **(Figure 2.3d)**. We further demonstrated that the ML 1-50-mediated degradation of BRD4 could be outcompeted with pre-

treatment of cells with excess JQ1 and that treatment of cells with the covalent alkyne-functionalized handle ML 2-33 alone did not alter BRD4 levels, indicating that the loss of BRD4 was likely through specific interactions with BRD4 and not through non-specific effects of the covalent handle **(Figure S1f-h).** Consistent with the role of DCAF16 in our observed effects, we showed that the BRD4 degradation from ML 1-50 treatment was significantly and completely attenuated in DCAF16 knockout cells compared to wild-type cells **(Figure 2.3e-g; Table S4).** Previous reports have identified a covalent molecular glue degrader between DCAF16 and BRD4, MMH2, in which the covalent warhead was attached to an orthogonal exit vector from JQ1, compared to our ML 1-50 compound[49]. Interestingly, MMH2 targeted C58 of DCAF16[49]. In this structure, C119 did not appear to be solvent exposed. Zhang and Cravatt *et al.* also demonstrated that their covalent DCAF16-based PROTACs acted through yet another set of cysteines, C177 and/or C179 [37]. As such, we were skeptical whether our covalent degraders really acted through targeting yet another cysteine on DCAF16—C119. As such, we expressed FLAG-DCAF16 WT, C58S, or C119S in DCAF16 knockout cells to determine which mutant may confer resistance to ML 1-50-mediated BRD4 degradation. Consistent with our site-of-modification analysis, we demonstrated that expression of the C119S DCAF16 mutant, but not the C58S mutant, conferred significant resistance to ML 1-50-mediated BRD4 degradation observed in DCAF16 WT-expressing cells **(Figure 2.3h-j)**. Interestingly, we also observed that ML 1-50 treatment consistently increased FLAG-DCAF16 protein levels even in the C119S mutant line, potentially suggesting that the previously reported weak ligand-induced interactions between DCAF16 and BRD4[33,49] may help to stabilize DCAF16 protein expression **(Figure 2.3h, j)**.

Given that several previous studies have identified DCAF16 as the E3 ligase substrate receptor responsible for the degradation of covalent BRD4 degraders bearing various different types of electrophilic handles, in part because of the native weak affinity between BRD4 and DCAF16 [37,42,49,50], we next determined whether our previously discovered covalent monovalent BRD4 degrader, JP-2-197, bearing a but-2-ene, 1,4-dione "fumarate" covalent degrader handle that targets RNF126 instead acts through DCAF16 [24]. We showed that the BRD4 degradation observed by JP-2-197 was not mitigated at all in DCAF16 knockout cells **(Figure 2.4a-b)**. In contrast, we observed complete and significant attenuation of BRD4 degradation in RNF126 knockout cells **(Figure 2.4c-d).** Furthermore, we demonstrated that ML 1-50-mediated degradation of BRD4 is not diminished in RNF126 KO cells compared to WT cells **(Figure 2.4e-f).** Our data thus indicate that different electrophilic degraders against the same target can act through distinct E3 ligases.

2.3.3 Exploring the Applicability of the Covalent Handle Against Other Target Proteins

While we identified a covalent handle that can convert the non-degradative JQ1 into a degrader of BRD4, BRD4 is extremely susceptible to targeted protein degradation and thus demonstrating proof-of-concept of a covalent handle that can degrade BRD4 does not speak to the broader applicability of this handle for other targets. Furthermore, previous studies have already

demonstrated covalent and noncovalent BRD4 molecular glue degraders that act through DCAF16, through strengthening already existing weak interactions between DCAF16 and BRD4 [32,33,49,50]. Previous studies have also used covalent DCAF16 recruiters to generate heterobifunctional PROTACs against other targets beyond BRD4 [37]. Whether a DCAF16-targeting covalent handle could be broadly transplanted across other protein-targeting ligands to generate linker-less monovalent degraders of neo-substrate proteins beyond BRD4 is unknown. We first appended the vinylsulfonyl piperazine handle onto the clinically approved CDK4/6 inhibitor ribociclib to generate ML 1-71 **(Figure 2.5a)**. ML 1-71 significantly degraded CDK4 in cells in a dose-dependent manner, albeit less potently compared to ML 1-50 and BRD4 **(Figure 2.5b-c)**. Despite the modest potency of this degrader, we still observed significant attenuation of CDK4 degradation in DCAF16 knockout cells **(Figure 2.5d-e).** We also did not observe degradation of CDK4 with ML 2-33 treatment and did not observe cytotoxicity with ML 1-71 treatment **(Figure 2.5f; Figure S2)**. Quantitative proteomic profiling of ML 1-71 in C33A cervical cancer cells also demonstrated relatively selective CDK4 degradation with only 15 other targets reduced in levels that may arise from transcriptional effects downstream of CDK4 inhibition or off-target effects **(Figure 2.5g; Table S5)**. These targets included CHEK1, PSMG1, STK4, KEAP1, FASN, GART, FGD6, AASDHPPT, PBK, MRTO4, TUBB2B, DUS3L, TUBB4A, MAP2K4. Given that CHEK1, STK4, PBK, and MAP2K4 are kinases, perhaps these may be off-targets of the CDK4/6 inhibitor ribociclib. We next generated a monovalent degrader for SMARCA2/4 bearing the vinylsulfonyl piperazine handle—ML 1-96 **(Figure S3a)** [52]. ML 1-96 significantly degraded both SMARCA2 and SMARCA4 in MV-4-11 leukemia cancer cells **(Figure S3b-c).** ML 1-96-mediated SMARCA2/4 degradation was attenuated in DCAF16 knockout cells **(Figure S3d-e).** We also demonstrated that ML 2-33 treatment does not affect SMARCA2/4 levels and ML 1-96 was not cytotoxic to cells **(Figure S3f-g).**

To further explore the substrate scope of our covalent degradative handle, we next generated an androgen receptor (AR) monovalent degrader consisting of the AR-targeting ligand from the AR PROTAC ARV-110 and the vinylsulfonyl piperazine handle—ML 2-9 **(Figure 2.6a)** [53]. ML 2-9 significantly degraded AR in LNCaP prostate cancer cells **(Figure 2.6b-c).** ML 2-33 did not alter AR levels **(Figure 2.6d)**. Interestingly, a hook effect was observed with this degrader. Proteomic data showed selective AR degradation with only 7 other proteins reduced in levels **(Figure 2.6e; Table S6)**. These proteins included ADCY5, CDK1, MID1IP1, KLHDC2, SBNO1, and FBXO28 **(Table S6)**. We also demonstrated that ML 2-9 did not show any cytotoxicity in LNCaP prostate cancer cells **(Figure S4a).** Unfortunately, we could not determine DCAF16 dependence because DCAF16 knockdown impaired cell viability of LNCaP cells, indicating that DCAF16 may be essential in this particular cell line. We also made a vinylsulfonyl piperazine bearing derivative of the BCR-ABL and c-ABL kinase inhibitor dasatinib, ML 2-5, and demonstrated the degradation of both the fusion oncogene and the parent kinase in K562 leukemia cancer cells **(Figure S4b-d).** We once again demonstrated that ML 2-33 treatment did not alter BCR-ABL or c-ABL levels and ML 2-5 only caused modest cytotoxicity in K562 cells **(Figure S4e-f)**. Importantly, DCAF16 knockdown significantly attenuated ML 2-5-mediated degradation

of both BCR-ABL and c-ABL, demonstrating that this degrader was still dependent on DCAF16 **(Figure S4g-i).** Finally, we also generated a vinylsulfonyl derivative of the BTK inhibitor ibrutinib, TH 1-9, and showed that this compound also degrades BTK in dose-dependent manner in MINO lymphoma cancer cells **(Figure 2.6f-h)**. We demonstrated that ML 2-33 treatment did not affect BTK levels **(Figure 2.6i).** Proteomic analyses revealed a higher number of proteins, 73 off-targets in total, beyond BTK that were lowered in levels compared to the other degraders **(Figure 2.6j; Table S7).** This may be due to the many off-targets of ibrutinib [54] at the high concentrations used in this study or may be due to downstream transcriptional changes resulting from BTK inhibition and degradation. The full list of the off-target proteins can be found in **Table S7**, but examples of off-targets included NOSIP, ALDH6A1, TOE1, SRSF9, SYK, CLK3, TLK2, DUS3L, KEAP1, CDK4, CDKN2A, and ADRBK1. Note that SYK, CLK3, TLK2, CDK4, and ADRBK1 are kinases and may potentially be off-targets of ibrutinib. Despite this moderate selectivity of degradation, we still observed significant partial attenuation of TH 1-9-mediated BTK degradation upon DCAF16 knockdown **(Figure S5a-c).** The incomplete rescue is likely due to partial DCAF16 knockdown in MINO cells. Overall, this degradative covalent handle thus enabled the degradation of not only BRD4, but also several other proteins, including CDK4, SMARCA2/4, AR, BTK, and BCR-ABL/c-ABL.

2.4 Discussion and Conclusion

Overall, we have identified a covalent DCAF16 degradative handle that can be transplanted across a diverse range of protein targeting ligands, without the need for a linker, to enable the degradation of several different protein classes. We note that this is a proof-of-concept study further demonstrating the possibility of covalent chemical handle and permissive E3 ligase pairs that can potentially be exploited towards rationally designing monovalent or molecular glue degraders, beyond our previously discovered covalent RNF126-targeting degradative handle[24]. While BRD4 has been shown to possess weak interactions with DCAF16, based on the UbiBrowser database, CDK4, SMARCA2/4, AR, BTK, and BCR-ABL/c-ABL do not appear to natively interact with DCAF16. As such, DCAF16 may have utility for both PROTACs[37] and molecular glue degraders of neo-substrates beyond BRD4.

We note that the potency, selectivity, and pharmacokinetic properties of our covalent handle would need to be substantially improved for future translational efforts. Each of our degraders in this study still shows off-target degradation, likely indicative of either off-targets of the protein-targeting ligands at the concentrations used or off-target effects resulting from our covalent degradative handle. For example, we saw that KEAP1 and DUS3L were common off-targets degraded by the CDK4 and BTK degraders **(Table S5, Table S7)**. While our genetic rescue studies demonstrate that the degradative on-target action of our degraders is resulting from DCAF16, we did observe that KEAP1 was likely a direct target of our covalent degradative handle from ML 2-33 pulldown chemoproteomic experiments, and that it did not pass our filtering criteria for ML 1-50-competed targets **(Table S2)**. KEAP1 has cysteines that are sensitive to oxidants and

electrophiles and we have previously shown that engagement of KEAP1 with bardoxolone-based PROTACs lowers KEAP1 levels in cells [55]. As such, future medicinal chemistry efforts would be required to further improve the selectivity of our covalent degradative handle.

Our study, coupled with several other prior studies, also demonstrates the unique susceptibility of DCAF16 to covalent targeting for monovalent or heterobifunctional targeted protein degradation applications [37,49,50]. This study also points to the potential permissiveness of DCAF16 in enabling the degradation of many different neo-substrate proteins, compared to other E3 ligases such as KEAP1 that may be much more restrictive in its substrate scope [56]. Intriguingly, our results indicate that our covalent DCAF16-dependent degraders act through targeting C119 on DCAF16. This is in contrast to previously reported DCAF16-dependent PROTACs and molecular glue degraders that have been shown to act through C58 or C177/C179 [37,49]. The permissiveness of DCAF16 for targeted protein degradation of neo-substrates may be in-part due to the several different cysteines that can be exploited on DCAF16. Understanding whether these cysteines on DCAF16 may generally act as an electrophile sensor for degradation of native DCAF16 substrates or whether these cysteines may be regulated by cellular redox balance will be of future interest. Furthermore, based on DCAF16 structures previously solved with previously discovered DCAF16-based BRD4 molecular glue degraders [33,49], C119 does not appear to be solvent-exposed. This C119 on DCAF16 may become exposed when the other neo-substrate binding pockets where C58 or C177/C179 reside are not occupied. Future structural biology studies will be useful in understanding the accessibility of C119. We also demonstrate that not every electrophilic monovalent degrader acts through DCAF16. We show that our previously discovered covalent BRD4 degrader bearing a "fumarate" handle acts through RNF126, and not through DCAF16. Our results are analogous to recent findings with covalent heterobifunctional BRD4 degraders bearing two different electrophilic handles that act through DCAF16 and DCAF11 [42]. Our study also suggests that pre-existing weak interactions between the E3 ligase and protein target may not be necessary to develop monovalent degraders. We also acknowledge that our covalent degraders show independent binding to both the target protein and DCAF16, analogous to one of the original molecular glues rapamycin that has independent binding to FKBP12 and the FRB domain of mTORC1 [28,57,58]. While we have chosen to call our degraders monovalent degraders or molecular glue degraders, one may also choose to classify these degraders as bivalent degraders or "mini-PROTACs" wherein the piperazine could be viewed as the linker with a minimum degradative covalent handle. Although not observed with most of our degraders, this may explain the "hook effect" observed with our AR degrader. Overall, our study underscores the utility of covalent chemoproteomic approaches in identifying covalent degradative handle and permissive E3 ligase pairs to expand the scope of targeted protein degradation applications.

2.5 Figures

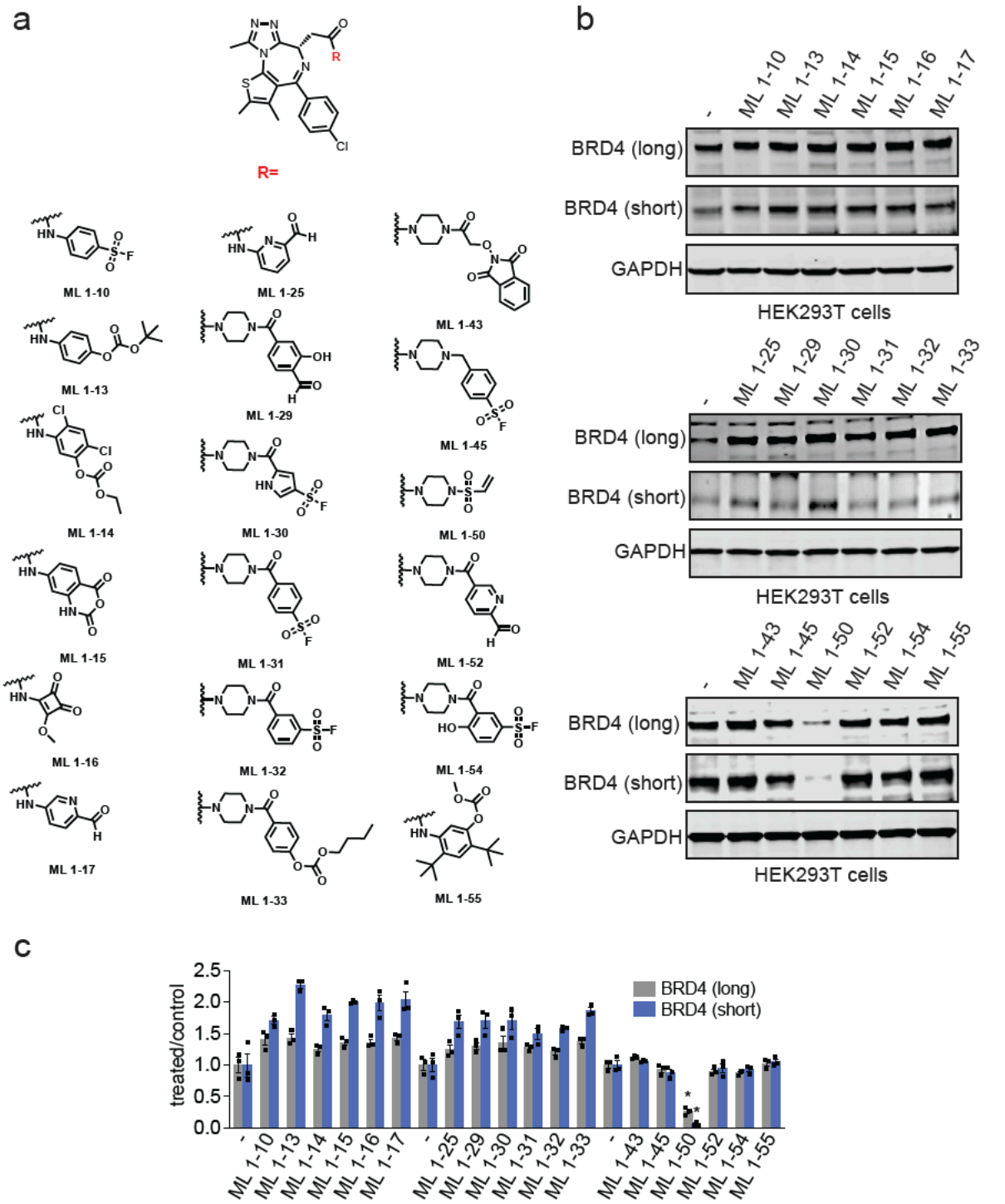

Figure 2.1. Identifying Covalent Handles that Enable the Degradation of BRD4. (a) Series of analogs of the BET family inhibitor JQ1 bearing various electrophilic handles. **(b)** Testing for BRD4 degradation with covalent JQ1 derivatives. HEK293T cells were treated with DMSO vehicle or covalent JQ1 derivatives (10 μM) for 24 h and BRD4 long and short isoforms and

GAPDH loading control levels were assessed by Western blotting. Shown are gels that are representative of n=3 biologically independent replicates per group. **(c)** Quantitation of BRD4 long and short isoforms from experiment described in **(b)** showing individual replicate values and average ± sem. Significance is expressed as *p<0.001 compared to vehicle-treated controls.

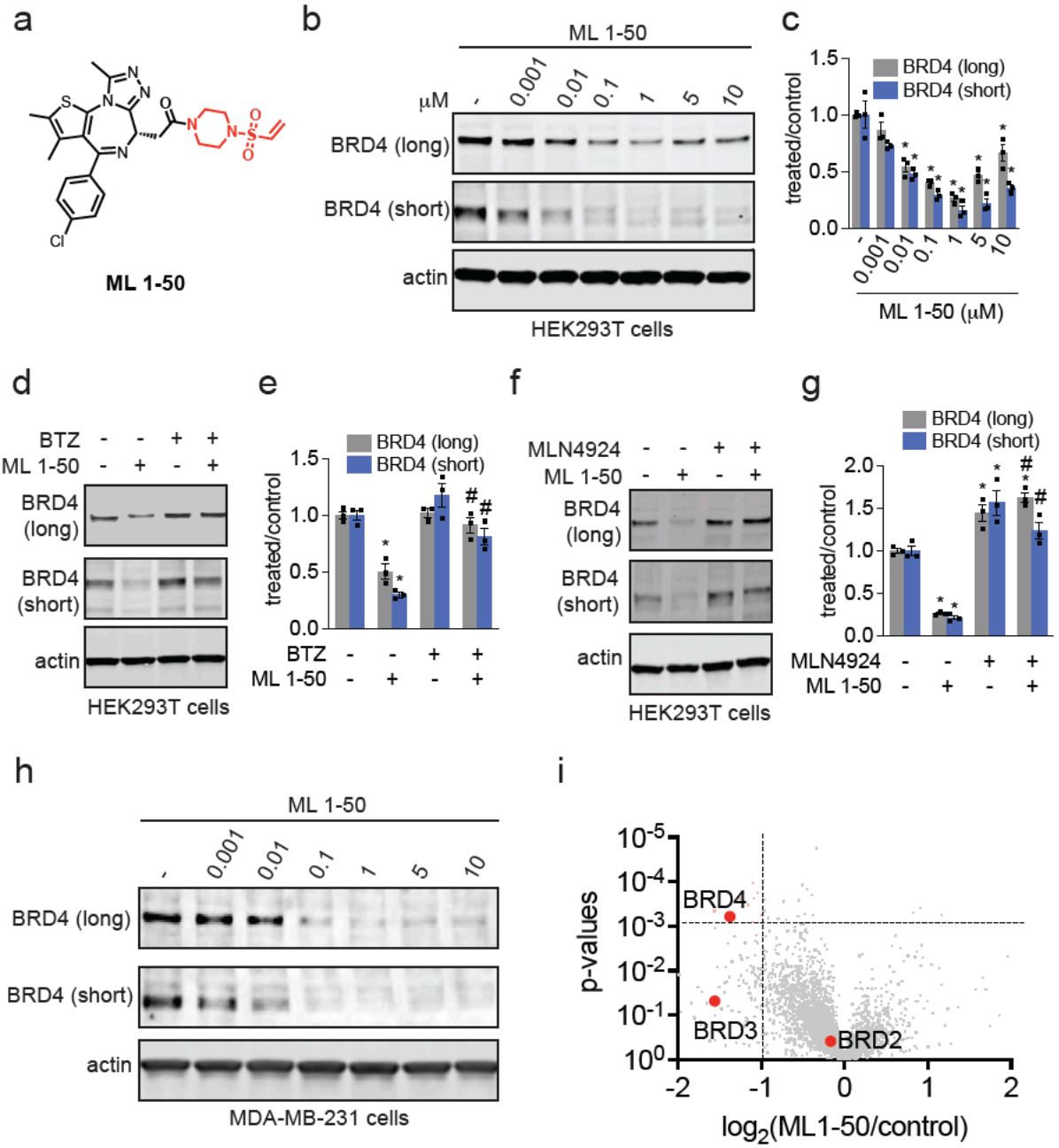

Figure 2.2. Characterization of the Monovalent and Covalent BRD4 Degrader ML 1-50. (a) Structure of ML 1-50 with the vinylsulfonyl piperazine covalent chemical handle in red. **(b, c)** Dose-response of BRD4 degradation. HEK293T cells were treated with DMSO vehicle or ML 1-50 for 24 h. BRD4 and actin loading control levels were assessed by Western blotting and quantified in **(c)**. **(d, e)** Proteasome inhibitor attenuation of BRD4 degradation. HEK293T cells were pre-treated with DMSO vehicle or bortezomib (1 μM) 1 h prior to DMSO vehicle or ML 1-50 (1 μM) treatment for 24 h. BRD4 and actin loading control levels were assessed by Western blotting and quantified in **(e). (f, g)** NEDD8 activating enzyme inhibitor attenuation of BRD4 degradation. HEK293T cells were pre-treated with DMSO vehicle or MLN4924 (1 μM) 1 h prior to DMSO vehicle or ML 1-50 (1 μM) treatment for 24 h. BRD4 and actin loading control levels were assessed by Western blotting and quantified in **(g). (h)** BRD4 degradation in MDA-MB-231 cells. MDA-MB-231 cells were treated with DMSO vehicle or ML 1-50 for 24 h and BRD4 and actin loading control levels were assessed by Western blotting. **(i)** Tandem mass tagging (TMT)-based quantitative proteomic profiling of ML 1-50 in MDA-MB-231 cells. MDA-MB-231 cells were treated with DMSO vehicle or ML 1-50 (1μM) for 24 h. Proteins that were lowered in levels by >2-fold with $p<0.001$ are highlighted in red with BRD4 specifically labeled, alongside other JQ1 targets BRD2 and BRD3. Data are from n=3 biologically independent replicates per group. Blots shown in **(b, d, f, h)** are representative of n=3 biologically independent replicates per group. Bar graphs in **(c, e, g)** show average ± sem. Significance is expressed as *$p<0.05$ compared to vehicle-treated controls and #$p<0.05$ compared to ML 1-50 treatment alone.

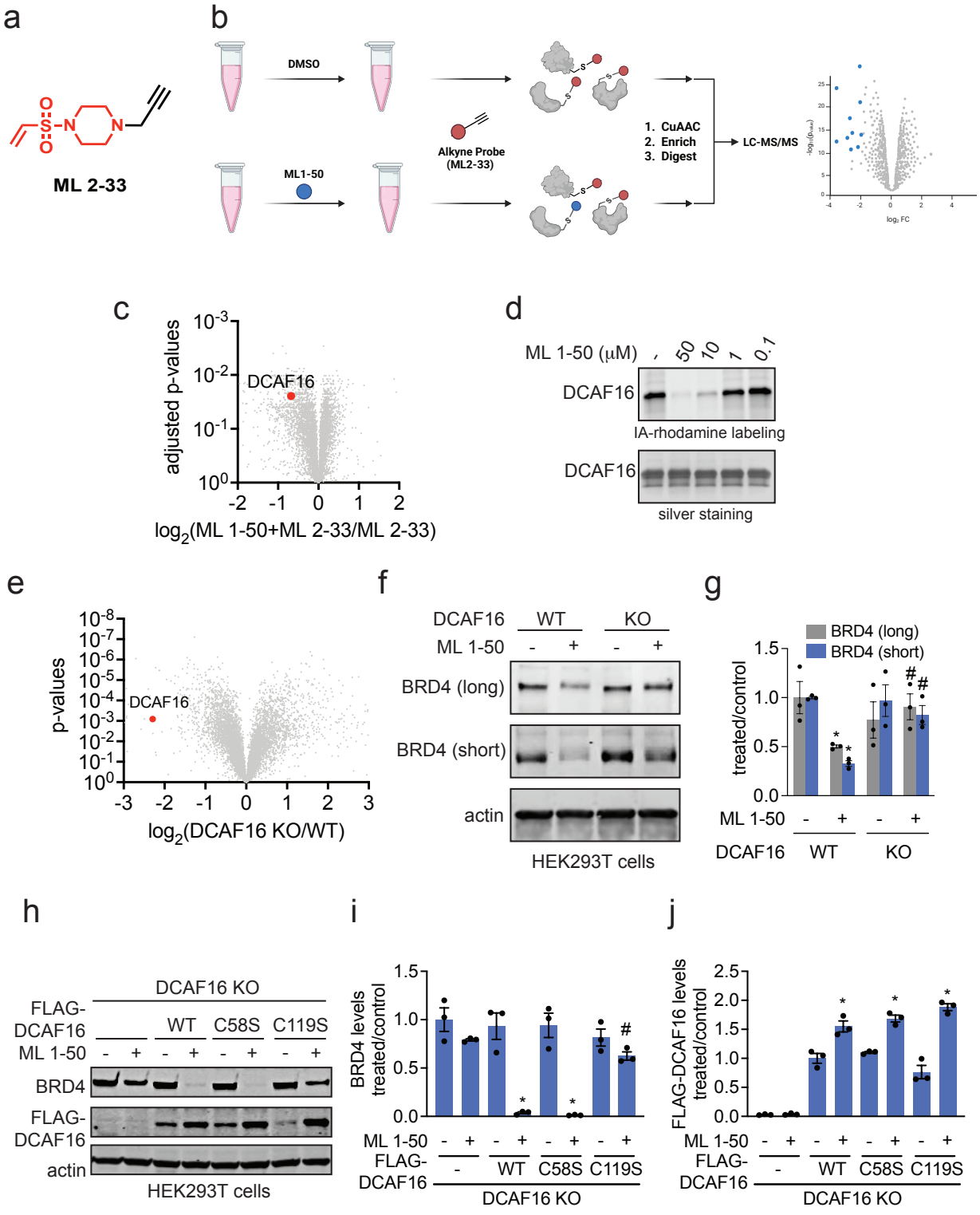

Figure 2.3. Identifying the E3 Ligase Responsible for ML 1-50-Mediated BRD4 Degradation.
(a) Structure of alkyne-functionalized probe of the vinylsulfonyl piperazine handle (highlighted in

red). **(b)** Workflow for competitive ML 2-33 probe pulldown chemoproteomic experiment. HEK293T cell lysate were pre-treated with DMSO vehicle or ML 1-50 (200 μM) 1 h prior to treatment with the ML 2-33 probe (20 μM). Probe-modified proteins were subjected to copper-catalyzed azide alkyne cycloaddition (CuAAC) with an azide-functionalized biotin enrichment handle. Probe-modified proteins were avidin-enriched, tryptically digested, and analyzed by TMT-based proteomics. **(c)** ML 1-50-outcompeted targets enriched by ML 2-33. Among the significantly outcompeted targets, DCAF16 highlighted in red was the only Cullin E3 ligase substrate receptor identified. **(d)** Gel-based ABPP of ML 1-50 against pure DCAF16. Pure DCAF16 protein was pre-incubated with DMSO vehicle or ML 1-50 for 30 min prior to addition of a rhodamine-functionalized cysteine-reactive iodoacetamide probe (IA-rhodamine) (250 nM) for 1 h. Proteins were resolved by SDS/PAGE and assessed by in-gel fluorescence and protein loading was assessed by silver staining. **(e)** TMT-based quantitative proteomic analysis of DCAF16 wild-type (WT) versus knockout (KO) cells. Because there was no commercial DCAF16 antibody, proteomic methods were used to confirm DCAF16 knockout. DCAF16 is labeled in red. **(f, g)** BRD4 degradation in DCAF16 WT and KO HEK293 cells. DCAF16 WT and KO cells were treated with DMSO vehicle or ML 1-50 (1 μM) for 24 h and BRD4 and actin loading control levels were assessed by Western blotting and quantified in **(g)**. **(h)** ML 1-50-mediated BRD4 degradation in DCAF16 KO HEK293 cells expressing WT, C58S, or C119S mutant FLAG-WT, C58S, or C119S DCAF16 was lentivirally and stably expressed in DCAF16 KO cells after which cells were treated with DMSO vehicle or ML 1-50 (1 μM) for 24 h and BRD4, FLAG-DCAF16, and loading control actin levels were assessed by Western blotting. **(i, j)** BRD4 and FLAG-DCAF16 levels from **(h)** were quantified. Proteomics experiments and blots in **(c-j)** are from n=3 biologically independent replicates per group and blots are representative. Bar graphs in **(g, i, j)** show individual replicate values average ± sem. Significance is expressed as *$p<0.05$ compared to vehicle-treated controls and #$p<0.05$ compared to ML 1-50 treated DCAF16 WT cells in **(g)** and compared to ML 1-50 treated FLAG-DCAF16 WT-expressing cells in **(i,j)**.

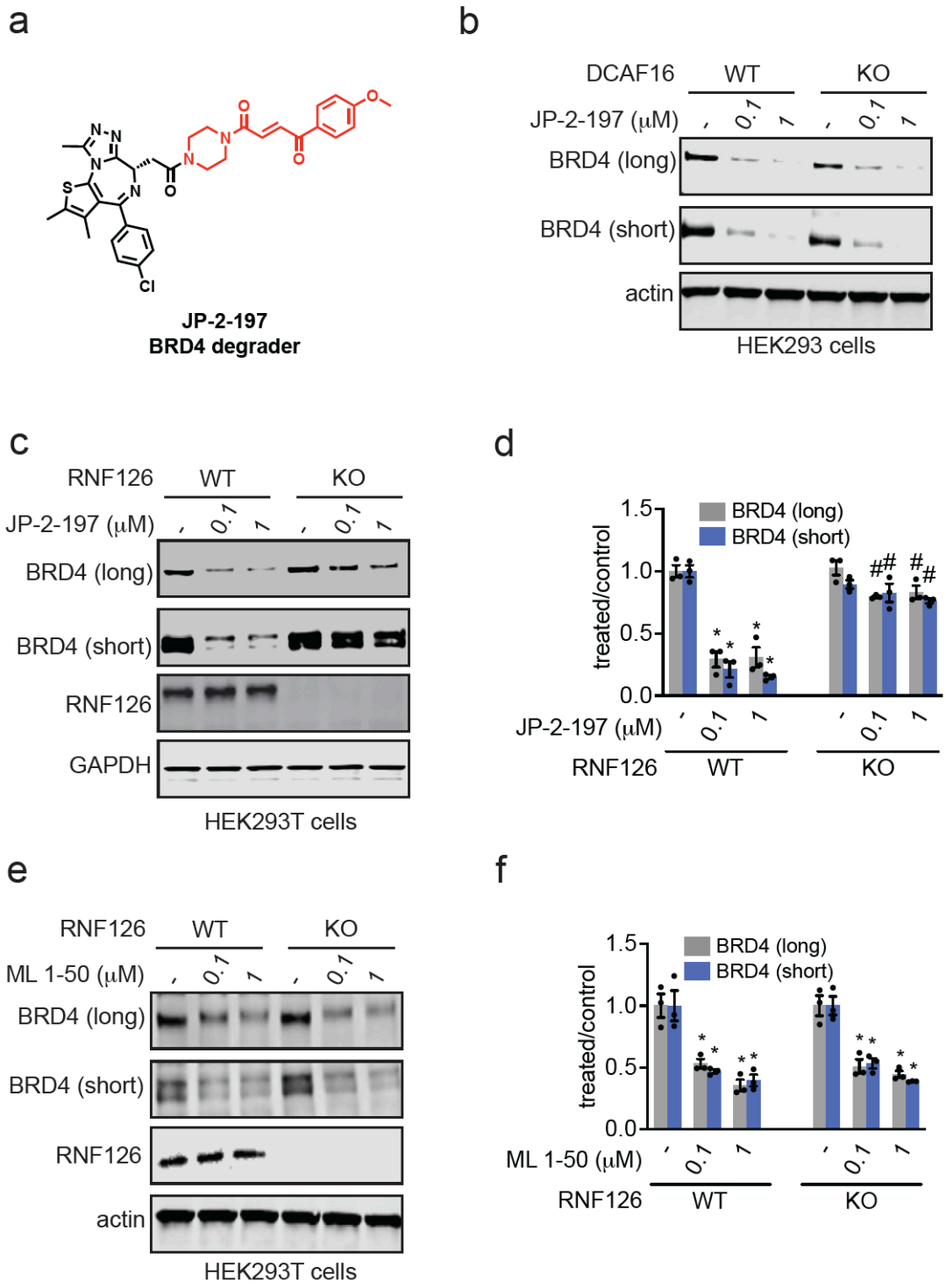

Figure 2.4. Testing the Dependence of Covalent Monovalent BRD4 Degraders on DCAF16 versus RNF126. (a) Structure of our previously published covalent monovalent BRD4 degrader JP-2-197 bearing the covalent "fumarate" handle shown in red. **(b)** BRD4 degradation in DCAF16 WT and KO HEK293 cells. DCAF16 WT and KO HEK293 cells were treated with DMSO vehicle or JP-2-197 for 24 h and BRD4 and actin loading control levels were assessed by Western blotting.

(c, d) BRD4 degradation in RNF126 WT and KO cells. RNF126 WT and KO HEK293T cells were treated with JP-2-197 for 10 h and BRD4, RNF126, and GAPDH loading control levels were assessed by Western blotting and quantified in **(d). (e, f)** BRD4 degradation in RNF126 KO HEK293T cells. RNF126 WT and KO HEK293T cells were treated with ML 1-50 for 16 h and BRD4, RNF126, and actin loading control levels were assessed by Western blotting and quantified in **(f)**. Blots in **(b, c, e)** are representative of n=3 biologically independent replicates per group. Bar graph in **(d, f)** shows individual replicate values and average ± sem. Significance is expressed as *p<0.05 compared to vehicle-treated controls and #p<0.05 compared to JP-2-197 or ML 1-50 treated RNF126 WT cells.

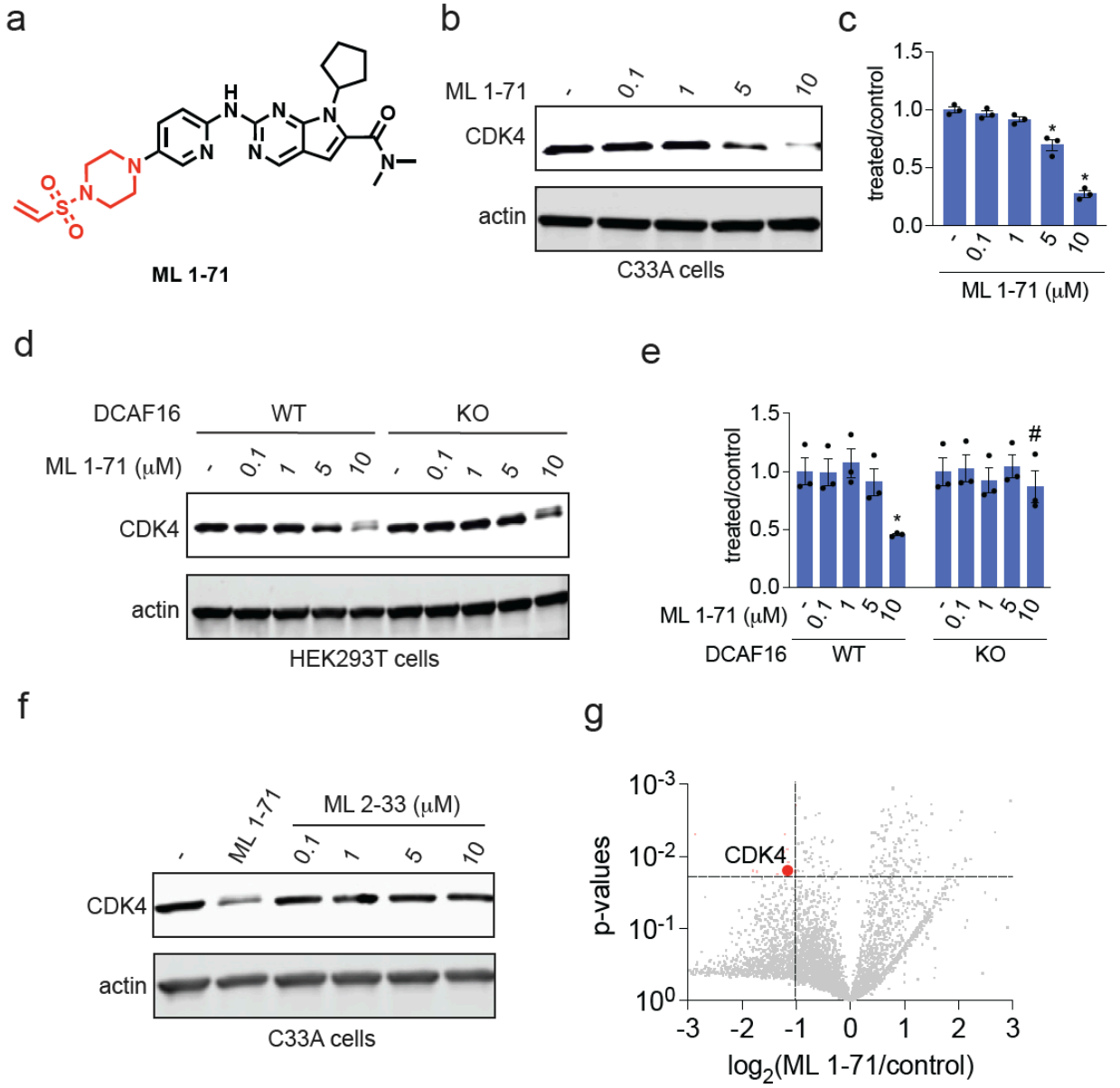

Figure 2.5. Characterization of CDK4 Monovalent Degrader. (a) Structure of ML 1-71, a CDK4 inhibitor ribociclib bearing a vinylsulfonyl piperazine handle highlighted in red. **(b, c)** CDK4 degradation in C33A cervical cancer cells. C33A cells were treated with DMSO vehicle or ML 1-71 for 24 h and CDK4 and actin loading control levels were assessed by Western blotting and quantified in **(c)**. **(d, e)** CDK4 degradation in DCAF16 WT and KO HEK293 cells. DCAF16 WT and KO HEK293 cells were treated with DMSO vehicle or ML 1-71 for 24 h and CDK4 and actin loading control levels were assessed by Western blotting and quantified in **(e). (f)** CDK4 levels in C33A cells. C33A cells were treated with DMSO vehicle, ML 1-71 (10 μM), or ML 2-33 for 24 h and CDK4 and loading control actin levels were assessed by Western blotting. **(g)** TMT-based quantitative proteomic profiling of ML 1-71 in C33A cells. C33A cells were treated with DMSO vehicle or ML 1-71 (10 μM) for 24 h. Proteins that were reduced in levels by >2-fold with $p<0.05$ are designated in red with CDK4 labeled. Data are from n=3 biologically independent replicates per group. Blots in **(b, d, f)** are representative of n=3 biologically independent replicates per group. Bar graph in **(e)** shows individual replicate values and average ± sem. Significance is expressed as *$p<0.05$ compared to vehicle-treated controls and #$p<0.05$ compared to ML 1-71 treated DCAF16 WT cells.

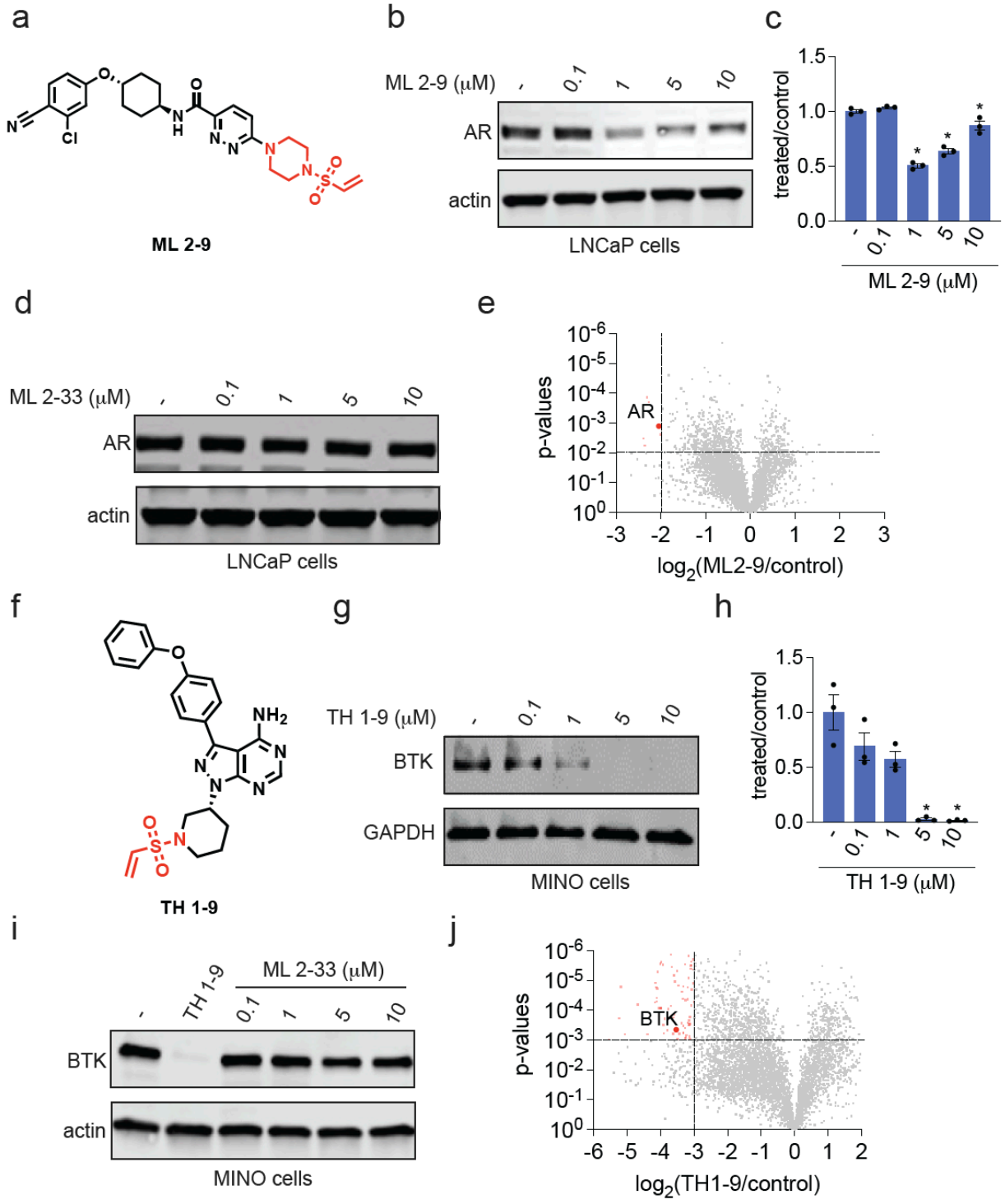

Figure 2.6. Characterization of AR and BTK Monovalent Degraders. (a) Structure of AR monovalent degrader ML 2-9 with AR-targeting ligand derived from the ARV-110 PROTAC bearing the covalent vinylsulfonyl piperazine handle highlighted in red. **(b, c)** AR degradation in LNCaP prostate cancer cells. LNCaP cells were treated with DMSO vehicle or ML 2-9 for 24 h and AR and actin loading control levels were assessed by Western blotting and quantified in **(c)**.

(d) AR levels in LNCaP cells. LNCaP cells were treated with DMSO vehicle or ML 2-33 for 24 h and AR and loading control actin levels were assessed by Western blotting. **(e)** TMT-based quantitative proteomic profiling of ML 2-9 in LNCaP cells. LNCaP cells were treated with DMSO vehicle or ML 2-9 (1 μM) for 24 h. Proteins that were reduced in levels by >4-fold with $p<0.01$ are designated in red with AR labeled. Data are from n=3 biologically independent replicates per group. **(f)** Structure of BTK monovalent degrader TH 1-9 with BTK inhibitor derived from ibrutinib bearing the covalent vinylsulfonyl piperazine handle highlighted in red. **(g, h)** BTK degradation in MINO lymphoma cancer cells. MINO cells were treated with DMSO vehicle or TH 1-9 for 24 h and BTK and GAPDH loading control levels were assessed by Western blotting and quantified in **(h)**. **(i)** BTK levels in MINO cells. MINO cells were treated with DMSO vehicle, TH1-9 (10 μM), or ML 2-33 for 24 h and BTK and loading control actin levels were assessed by Western blotting. **(j)** TMT-based quantitative proteomic profiling of TH 1-9 in MINO cells. MINO cells were treated with DMSO vehicle or TH 1-9 (5 μM) for 24 h. Proteins that were reduced in levels by >8-fold with $p<0.001$ are designated in red with BTK labeled. Data are from n=3 biologically independent replicates per group. Blots in **(b,d,g,f)** are representative of n=3 biologically independent replicates per group. Bar graphs in **(c, h)** show individual replicate values and average ± sem. Significance is expressed as *$p<0.05$ compared to vehicle-treated controls.

2.6 Methods

2.6.1 Cell Culture

HEK293T and HEK293 cells were obtained from the UC Berkeley Cell Culture Facility and were cultured in Dulbecco's Modified Eagle Medium (DMEM) containing 10% (v/v) fetal bovine serum (FBS) and maintained at 37 °C with 5% CO_2. C33A cells were purchased from the American Type Culture Collection (ATCC) and were cultured in DMEM containing 10% (v/v) FBS and maintained at 37 °C with 5% CO_2. K562 cells were obtained from the UC Berkeley Cell Culture Facility and were cultured in Iscove's Modified Dulbecco's Medium (IMDM) containing 10% (v/v) FBS and maintained at 37 °C with 5% CO_2. MV-4-11 cells were obtained from the ATCC and were cultured in IMDM containing 10% (v/v) FBS and maintained at 37 °C with 5% CO_2. Mino cells were obtained from the ATCC and were cultured in RPMI-1640 Medium containing 10% (v/v) FBS and maintained at 37 °C with 5% CO_2. LNCaP cells were obtained from the UC Berkeley Cell Culture Facility and were cultured in DMEM containing 10% (v/v) FBS and maintained at 37 °C with 5% CO_2. HEK293 DCAF16 knockout cells were purchased from Ubigene Biosciences and were cultured in DMEM containing 10% (v/v) FBS and maintained at 37 °C with 5% CO_2. Unless otherwise specified, all cell culture materials were purchased from Gibco. It is not known whether HEK293T cells are from male or female origin.

2.6.2 Western Blotting

Cells were washed twice with cold PBS, scraped, and pelleted by centrifugation (1,200 g, 5 min, 4 °C). Pellets were resuspended in PBS, lysed by sonication or RIPA lysis buffer (Thermo Scientific), clarified by centrifugation (12,000 g, 10 min, 4 °C), and lysate was transferred to new low-adhesion microcentrifuge tubes. Proteome concentrations were determined using the BCA assay and lysate was diluted to appropriate working concentrations. Proteins were resolved by SDS/PAGE and transferred to nitrocellulose membranes using the Trans-Blot Turbo transfer system (Bio-Rad). Membranes were blocked with 5% BSA in Tris-buffered saline containing Tween 20 (TBS-T) solution for 1 hr at RT, washed in TBS-T, and probed with primary antibody diluted in recommended diluent per manufacturer overnight at 4 °C. After 3 washes with TBS-T, the membranes were incubated in the dark with IR680- or IR800-conjugated secondary antibodies at 1:10,000 dilution in 5 % BSA in TBS-T at RT for 1 h. After 3 additional washes with TBS-T, blots were visualized using an Odyssey Li-Cor fluorescent scanner. The membranes were stripped using ReBlot Plus Strong Antibody Stripping Solution (EMD Millipore, 2504) when additional primary antibody incubations were performed. Antibodies used in this study were BRD4 (Abcam ab128874), CDK4 (Abcam ab108357), GAPDH (Cell Signaling Technology 14C10), Beta Actin (Cell Signaling Technology 13E5), c-Abl (Santa Cruz Biotechnology sc-23), SMARCA2 (Abcam ab240648), BRG1 (SMARCA4) (Cell Signaling Technology D1Q7F), BTK (Cell Signaling Technology D3H5), Androgen Receptor (Cell Signaling Technology D6F11).

2.6.3 Bortezomib or MLN4924 Rescue Studies

2E6 of HEK293T cells per 3 mL of media were plated in 6-cm plates and left overnight to adhere. Cells were pretreated for 1 h with either Bortezomib (Cayman, C835F70) or MLN4924 (Tocris Bioscience, 649910) at a final concentration of 1 μM. Cells were then treated with ML1-50 until desired time point. Cells from both the supernatant and on the plate were harvested and assessed via western blot.

2.6.4 Cell Viability Assay

Cells were seeded in 96-well white plates overnight and then treated with DMSO vehicle control or degraders and incubated at 37 °C for 24 h. Cell viability assay was performed using CellTiter-Glo® 2.0 reagent (Promega, G9241) according to manufacturer's protocol. Luminescent signals were measured using the Tecan Spark Plate reader (30086376).

2.6.5 Isotopic desthiobiotin (isoDTB)-ABPP Cysteine Chemoproteomic Profiling of ML1-50

HEK293T cells were treated with either ML1-50 (10 μM) or DMSO for 2 h before cell collection and lysis. The proteome concentrations were determined using BCA assay and adjusted to 2 mg/mL. For each biological replicate, 2 aliquots of 1 mL of 2 mg/mL were used (i.e. 4 mg per condition). Each aliquot was treated with 20 μL of IA-alkyne (26.6 mg/mL in DMSO, 200 μM final concentration) for 1 h at RT. Two master mixes of the click reagents were prepared in the meanwhile, each containing 510 μL TBTA (0.9 mg/mL in 4:1 tBuOH/DMSO), 165 μL CuSO4 (12.5 mg/mL in H_2O), 165 μL TCEP (14.0 mg/mL in H_2O) and 160 μL of either heavy or light isoDTB tags (4 mg in DMSO, Click Chemistry Tools, 1565). The samples were then treated with 120 μL of the heavy (DMSO treated) or light (compound treated) master mix for 1 h at RT. After incubation, one light and one heavy labeled samples were combined and acetone-precipitated overnight at -20 °C. The samples were then centrifuged at 3,500 rpm for 10 min, acetone was removed, and the protein pellets resuspended in cold MeOH by sonication. The samples were centrifuged at 3,500 rpm for 10 min and MeOH was removed (repeated 3× in total). The pellets were dissolved in 600 μL urea (8 M in 0.1 M TEAB) by sonication and the urea concentration was then adjusted to 2 M by adding 1800 μL of TEAB (0.1 M). Two tubes containing solubilized proteins were combined, further diluted with 2400 μL 0.2% NP40 in PBS, and bound to high-capacity streptavidin agarose beads (200 μL/sample, ThermoFisher, 20357) for 1 h at RT with mixing. The beads were then centrifuged for 1 min at 1,000 g, the supernatant was removed, and the beads were washed 3 times with 0.1% NP40 in PBS, 3 times with PBS and 3 times with H_2O. The samples were then resuspended in 8 M urea (600 μL in 0.1 M TEAB) and treated with DTT (30 μL, 31 mg/mL in H_2O) for 45 min at 37 °C. They were then reacted with iodoacetamide (30 μL, 74 mg/mL in H_2O) for 30 min at RT, followed by DTT (30 μL, 31 mg/mL in H_2O) for 30 min at RT. The samples were diluted with 1800 μL TEAB (0.1 M), centrifuged for 1 min at 1,000 g, and the supernatant was removed. The beads were resuspended in 400 μL urea (2M in 0.1 M TEAB), and trypsin (8 μL, 0.5 mg/mL) was added and incubated for 20 h at 37 °C. The samples were then diluted with 800 μL 0.1% NP40 in PBS and the beads were washed 3 times with 0.1%

NP40 in PBS, 3 times with PBS, and 3 times with H_2O. Peptides were then eluted with 0.1% formic acid in 50% acetonitrile (3 × 400 µL). The samples were then dried using a vacuum concentrator at 30 °C, resuspended in 300 µL 0.1% TFA in H_2O, and fractionated using high pH reversed-phase peptide fractionation kits (ThermoFisher, 84868) according to the manufacturer's protocol.

2.6.6 IsoDTB-ABPP Mass Spectrometry Analysis

Mass spectrometry analysis was performed on an Orbitrap Eclipse Tribrid Mass Spectrometer with a High Field Asymmetric Waveform Ion Mobility (FAIMS Pro) Interface (Thermo Scientific) with an UltiMate 3000 Nano Flow Rapid Separation LCnano System (Thermo Scientific). Off-line fractionated samples (5 µl aliquot of 15 µl sample) were injected via an autosampler (Thermo Scientific) onto a 5 µl sample loop which was subsequently eluted onto an Acclaim PepMap 100 C18 HPLC column (75 µm x 50 cm, nanoViper). Peptides were separated at a flow rate of 0.3 µl/min using the following gradient: 2 % buffer B (100 % acetonitrile with 0.1 % formic acid) in buffer A (95:5 water:acetonitrile, 0.1 % formic acid) for 5 min, followed by a gradient from 2 to 40 % buffer B from 5 to 159 min, 40 to 95 % buffer B from 159 to 160 minutes, holding at 95 % B from 160-179 min, 95 % to 2 % buffer B from 179 to 180 min, and then 2 % buffer B from 180 to 200 min. Voltage applied to the nano-LC electrospray ionization source was 2.1 kV. Data was acquired through an MS1 master scan (Orbitrap analysis, resolution 120,000, 400-1800 m/z, RF lens 30 %, heated capillary temperature 250 °C) with dynamic exclusion enabled (repeat count 1, duration 60 s). Data-dependent data acquisition comprised a full MS1 scan followed by sequential MS2 scans based on 2 s cycle times. FAIMS compensation voltages (CV) of -35, -45, and -55 were applied. MS2 analysis consisted of: quadrupole isolation window of 0.7 m/z of precursor ion followed by higher energy collision dissociation (HCD) energy of 38 % with an orbitrap resolution of 50,000.

Data was extracted in the form of MS1 and MS2 files using Raw Converter (Scripps Research Institute) and searched against the Uniprot human database using ProLuCID search methodology in IP2 v.3- v.5 (Integrated Proteomics Applications, Inc.) [59]. Cysteine residues were searched with a static modification for carboxyaminomethylation (+57.02146) and up to two differential modifications for methionine oxidation and either the light or heavy isoDTB tags (+561.33872 or +567.34621, respectively). Peptides were required to be fully tryptic peptides. ProLuCID data were filtered through DTASelect to achieve a peptide false-positive rate below 5%. Only those probe-modified peptides that were evident across two out of three biological replicates were interpreted for their isotopic light to heavy ratios. Light versus heavy isotopic probe-modified peptide ratios are calculated by taking the mean of the ratios of each replicate paired light versus heavy precursor abundance for all peptide-spectral matches associated with a peptide. The paired abundances were also used to calculate a paired sample t-test P value in an effort to estimate constancy in paired abundances and significance in change between treatment and control. P values were corrected using the Benjamini–Hochberg method.

2.6.7 Gel-Based ABPP

Recombinant DCAF16 (MyBioSource.com, MBS1375983) (0.1μg/sample) was pre-treated with either DMSO vehicle or covalent ligand at 37 °C for 30 min in 25 μL of PBS, and subsequently treated with of IA-Rhodamine (concentrations designated in figure legends) (Setareh Biotech) at room temperature for 1 h in the dark. The reaction was stopped by addition of 4×reducing Laemmli SDS sample loading buffer (Alfa Aesar). After boiling at 95 °C for 5 min, the samples were separated on precast 4−20% Criterion TGX gels (Bio-Rad). Probe-labeled proteins were analyzed by in-gel fluorescence using a ChemiDoc MP (Bio-Rad). Imaged gels were stained using Pierce™ Silver Stain Kit (Thermo Scientific™, 24612) following manufacturer's instructions.

2.6.8 ML1-50-Competed Targets from ML2-33 Probe Pulldown Proteomics

HEK293T cells were harvested, lysed, and the proteome concentration was adjusted to 5 mg/mL in 500 μL of PBS using the BCA assay. HEK293T cell lysate were pre-treated with DMSO vehicle or ML1-50 (200 μM) for 1 h at room temperature prior to ML2-33 probe labeling (20 μM) at room temperature for 1 h. To each tube containing cell lysate, the following reagents were added: 10 μL of 10 mM biotin picolyl azide (Sigma Aldrich, 900912) in DMSO, 10 μL of 50 mM TCEP in H_2O, 10 μL of 50 mM $CuSO_4$ in H_2O, and 30 μL of TBTA ligand (1.7 mM in 1:4 DMSO/tBuOH, Cayman Chemical, 18816). The reaction mixture was incubated at room temperature for 60 minutes, and the reaction was quenched by protein precipitation. Precipitated pellets were washed using 500 μL of MeOH and centrifuged again to yield white pellets. Samples were resuspended in 1.2% SDS-PBS (1 mL), completely dissolved, and heated to 90 °C for 5 minutes. The soluble proteome was then diluted with 5 mL of PBS and further incubated with high-capacity streptavidin-agarose beads (100 μL/sample, ThermoFisher Scientific, 20357). Beads and lysates were incubated overnight at 4 °C with rotation. On the following day, beads were suspended and washed three times with 0.1% SDS-PBS, PBS, and H_2O. Washed beads were resuspended in 6 M Urea/PBS (500 μL), and the samples were further treated with DTT and iodoacetamide. After removing the supernatant, beads were resuspended in 100 μL of 50 mM TEAB and enzymatically digested overnight using sequencing-grade trypsin (Promega, V5111). Digested peptides were eluted through centrifugation and labeled using commercially available TMTsixplex tags (ThermoFisher, P/N 90061). After labeling, 35 μg of each labeled sample was combined and dried using a vacufuge. Dried samples were redissolved with 300 μL of 0.1% TFA in H_2O and further fractionated using high-pH reversed-phase peptide fractionation kits (ThermoFisher, P/N 84868) following the manufacturer's protocol. Dried fractions were then resuspended in 25 μL of 0.1 % Formic acid/H_2O (w/v) to be analyzed by LC-MS/MS.

2.6.9 Mapping of ML1-50 Site of Modification on DCAF16 by LC-MS/MS

Pure DCAF16 protein (40 μg, MyBioSource.com, MBS1375983) was diluted in PBS (100 μL) and preincubated with ML1-50 (50 μM final concentration) for 30 min at room temperature. The protein was precipitated by the addition of 25 μL of TCA (100% w/v) and incubation at −80 °C overnight. The sample was then spun at 20,000g for 10 min at 4 °C. The supernatant was carefully

removed, and the sample was washed three times with 200 µL of ice-cold 0.01 M HCl/ 90% acetone solution, with spinning at 20,000 for 5 min at 4 °C between washes. The sample was then resuspended in 30 µL of 8 M urea in PBS and 30 µL of ProteaseMax surfactant (20 µg/mL in 100 mM ammonium bicarbonate, Promega, V2071) with vortexing. Ammonium bicarbonate (40 µL, 100 mM) was then added for a final volume of 100 µL. The sample was reduced with 10 µL of TCEP (10 mM final concentration) for 30 min at 60 °C and alkylated with 10 µL of iodoacetamide (12.5 mM final concentration) for 30 min at 37 °C. The sample was then diluted with 120 µL of PBS before 1.2 µL of ProteaseMax surfactant (0.1 mg mL−1 in 100 mM ammonium bicarbonate, Promega, V2071) and sequencing grade trypsin (10 µL, 0.5 mg mL−1 in 50 mM ammonium bicarbonate, Promega, V5111) were added for overnight incubation at 37 °C. The next day, the sample was acidified with formic acid (5% final concentration) and fractionated using high pH reversed-phase peptide fractionation kits (Thermo Fisher, 84868) following manufacturer's protocol.

2.6.10 Quantitative TMT Proteomics Analysis

Cells were treated with either DMSO vehicle or compound (ML1-50 (1 µM, 24 h), ML1-71 (10µM, 16 h), ML1-96 (10 µM, 16 h), ML2-5 (10 µM, 16 h), TH1-9 (5 µM, 16 h), ML2-9 (1 µM, 24 h)) and lysate was prepared as described above. Briefly, 25-100 µg protein from each sample was reduced, alkylated and tryptically digested overnight. Individual samples were then labeled with isobaric tags using commercially available TMTsixplex (Thermo Fisher Scientific, P/N 90061) kits, in accordance with the manufacturer's protocols. Tagged samples (20 µg per sample) were combined, dried using a vacuum concentrator at 30 °C, resuspended with 300 µL 0.1% TFA in H_2O, and fractionated using high pH reversed-phase peptide fractionation kits (Thermo Fisher Scientific, P/N 84868) according to the manufacturer's protocol. Fractions were dried using a vacuum concentrator at 30 °C, resuspended with 50 µL 0.1% FA in H_2O, and analyzed by LC-MS/MS as described below.

Quantitative TMT-based proteomic analysis was performed as previously described using a Thermo Eclipse with FAIMS LC-MS/MS [30]. Acquired MS data was processed using ProLuCID search methodology in IP2 v.3-v.5 (Integrated Proteomics Applications, Inc.) [59]. Trypsin cleavage specificity (cleavage at K, R except if followed by P) allowed for up to 2 missed cleavages. Carbamidomethylation of cysteine was set as a fixed modification, methionine oxidation, and TMT-modification of N-termini and lysine residues were set as variable modifications. Reporter ion ratio calculations were performed using summed abundances with the most confident centroid selected from the 20 ppm window. Only peptide-to-spectrum matches that are unique assignments to a given identified protein within the total dataset are considered for protein quantitation. High confidence protein identifications were reported with a <1% false discovery rate (FDR) cut-off. Differential abundance significance was estimated using ANOVA with Benjamini-Hochberg correction to determine p-values.

2.6.11 Knock Out Cell Line Generation

To generate a RNF126 knock-out pool in HEK293T, we introduced Cas9 ribonucleoproteins (RNPs) complexed with a custom Alt-R sgRNA synthesized by IDT targeting exon 2 of the RNF126 genomic locus (guide sequence ATGCGAGTCTGGTTTTATCG). spCas9 and sgRNA were introduced into cells by nucleofection. Briefly, 1.6 µL of 62.5 µM Cas9 (IDT, #1081058), 2.88 µL of 50 µM sgRNA (Alt-R from IDT), and 0.52 µL of 1X phosphate-buffered saline were mixed and the RNPs were incubated at room temperature for 30 minutes. Subsequently, the RNPs were added to 200,000 HEK293T cells resuspended in 16.4 µL Nucleofector solution SF plus 3.6 µL of supplement. To this suspension, 1.2 µL of 100 µM Alt-R electroporation enhancer (IDT, #1075916) and 4.32 µL H_2O were added for a final volume of 30 µL. This nucleofection mix was electroporated using a 4D Nucleofector X Unit with program DG-130 in a nucleofector strip. After 10 minutes of recovery, nucleofected cells were grown in a 6-well dish for 7 days. This RNF126 knock-out pool was expanded and aliquoted for storage.

To isolate isogenic RNF126 knock-out clones, the knock-out pool was subjected to single cell sorting into 96-well plates using a WOLF microfluidic cell sorter (Nanocellect). Single cells were allowed to grow into colonies for two weeks, expanded further, and frozen into aliquots for storage. During cell expansion a sample of each clone was processed into lysate and RNF126 knock-out clones were identified by anti-RNF126 immunoblotting (ProteinTech, #66647-1-Ig). Clone 2B8 was designated as the RNF126 knock-out.

The DCAF16 knock-out cell line was purchased from Ubigene with guide sequences AGAGGGGGCCATTCAGGAAT TGG and TTCTGACAAGTGGTCAGGAG AGG (catalog number YKO-H721).

2.6.12 Site-Directed Mutagenesis on FLAG-tagged DCAF16 Plasmid

Site-directed mutagenesis was performed on FLAG-tagged wild type DCAF16 plasmid (Origene, RC208716L3) using Q5® Site-Directed Mutagenesis Kit (NEB, E0552S) according to the manufacturer's protocol. The sequences of the primers used are shown below.

C58S Primer (Forward) : GCAGGTTAAGAGCCTTTTAAAATATTC
C58S Primer (Reverse) : CAGGCAAGACTCTCAAG
C119S Primer (Forward) : TCTGGCCTCTAGCGGAGTCCCAC
C119S Primer (Reverse) : GGGGGCCATTCAGGAATT

2.6.13 Plasmid Isolation

E. coli containing desired plasmids were pelleted, lysed, and neutralized using QIAGEN Plasmid Plus Midi Kit (Qiagen, 12943) according to the manufacturer's protocol. The eluted plasmid concentrations were determined using Nanodrop quantification.

2.6.14 Expression of FLAG-tagged Wild Type DCAF16 and Mutants in DCAF16 Knockout Cells

For lentivirus production, FLAG-tagged wild type DCAF16 or FLAG-tagged DCAF16 mutant plasmids, pMD2.G (Addgene, 12259) and psPAX2 (Addgene, 12260) were transfected

into HEK293T cells using Lipofectamine 2000 (ThermoFisher, 11668027). The virus-containing medium was collected and filtered after 48 hours and was used to infect HEK293 DCAF16 knockout cells with 1:1000 dilution of polybrene (Sigma-Adrich, TR-1003-G). After 48 hours, the infected cells were selected with puromycin (2 μg/mL).

2.6.15 DCAF16 Knockdown Studies

MISSION® shRNA lentiviral construct, pMD2.G (Addgene, 12259) and psPAX2 (Addgene, 12260) were transfected into HEK293T cells using Lipofectamine 2000 (ThermoFisher, 11668027). The virus-containing medium was collected and filtered after 48 hours and was used to infect target cells (K562, Mino or LNCaP cells) with 1:1000 dilution of polybrene (Sigma-Adrich, TR-1003-G). After 48 hours, the infected cells were selected with puromycin. MISSION® pLKO.1-puro Non-Mammalian shRNA Control (Sigma-Adrich, SHC016) was used as a control shRNA.The shRNA sequence used for generation of DCAF16 knockdown lines is shown below.

shDCAF16 (Sigma-Aldrich, TRCN0000143155): CTCTAAATGGAGCACTGCAAT

2.6.16 RT-qPCR Analysis

Total RNA was extracted from cells using Monarch® Total RNA Miniprep Kit (NEB, T2010S) according to the manufacturer's protocol. cDNA was synthesized and gene expression was confirmed by qPCR using Luna® Universal One-Step RT-qPCR Kit (NEB, E3005S) following the manufacturer's protocol with the CFX Connect Real-Time PCR Detection System (BioRad). Relative DCAF16 gene expression was normalized to the GAPDH gene. The sequences of the qPCR primers are shown below.

GAPDH Primer (Forward)	: GTCTCCTCTGACTTCAACAGCG
GAPDH Primer (Reverse)	: ACCACCCTGTTGCTGTAGC
DCAF16 Primer #1 (Forward)	: TGACCACTTGTCAGAATCAGAA
DCAF16 Primer #1 (Reverse)	: AGAGGCGATAAGTTGGGCAC
DCAF16 Primer #2 (Forward)	: TGGATCCAAGCACACCAGTC
DCAF16 Primer #2 (Reverse)	: TGGTTCCAGTTTGGGGACAC
DCAF16 Primer #3 (Forward)	: CAATTCCTGAATGGCCCCCT
DCAF16 Primer #3 (Reverse)	: GTGCTCCATTTAGAGTGGCA
DCAF16 Primer #4 (Forward)	: AGTCTTGCCTGGCAGGTTAAG
DCAF16 Primer #4 (Reverse)	: GGGACTTGTAAGAGGCTTTTGAA

Concluding Remarks

The discovery of the plant hormones auxin and methyl jasmonate as naturally occurring MGDs provided a compelling demonstration of the feasibility of using small molecules to modulate protein degradation through induced proximity. Auxin facilitates degradation of the Aux/IAA transcription repressors by strengthening their interaction with the E3 ligase SCF^{TIR1}, while methyl jasmonate induces the degradation of transcriptional repressor JAZ proteins via SCF^{COI1}, collectively illustrating how nature has evolved small molecules to rewire protein substrate degradation with remarkable selectivity[60,61]. These natural precedents, combined with the clinical success of thalidomide, lenalidomide, pomalidomide and other IMiDs across a range of hematological malignancies, demonstrated the therapeutic power of the MGD mechanism and pushed the field toward a more systematic discovery of MGDs[62]. The serendipitous findings that subtle chemical modifications to existing inhibitors can convert occupancy-based pharmacology into even-driven degradation, exemplified by (*R*)-CR8 and BI-3802, further expanded the conceptual boundaries of MGD discovery. However, these are isolated and mechanistically distinct examples, and the chemical modifications responsible for their degrader activity are not generalizable to inhibitors of other protein targets. The work described in this dissertation addresses this gap by leveraging covalent chemistry and chemoproteomics to identify a generalizable chemical modification that can be appended onto existing protein-targeting ligands to enable the rapid and rational discovery of MGDs, thereby opening new possibilities within the TPD landscape.

We initiated our studies with the BET family protein BRD4, given the availability of the potent, selective and well-validated chemical tool JQ1 as a starting scaffold. Strikingly, recent independent reports of JQ1-based MGDs, including this work, have converged on a shared mechanism: the recruitment of DCAF16 to BRD4[26,33,49,50,63–65]. First identified as a TPD-competent E3 ligase through the use of the "scout" fragment KB02 in PROTAC design, DCAF16 subsequently emerged as the E3 ligase responsible for BRD4 degradation induced by a series of JQ1 derivatives, GNE-0011, TMX1, MMH1, MMH2, IBG1, HRG038, and ML 1-50 from this work. Complementing these findings, Hsia et al. unexpectedly captured an intrinsic affinity between DCAF16 and BRD4 while interrogating the mechanism of their BRD4 degrader IBG1, and Li et al. reported a BRD4 template-assisted covalent modification mechanism for BRD4 degrader discovery. Together, these studies suggest that electrophilic JQ1 derivatives may degrade BRD4 in part by enhancing pre-existing weak interactions between BRD4 and DCAF16. This pattern of convergent discovery resembles the three independent reports of cyclin K MGDs in 2020, which converged on a shared mechanism that stabilizes weak DDB1-CDK12 interaction to achieve cyclin K degradation, further underscoring the therapeutic relevance of exploiting pre-existing native affinities for MGD design[18,25,66,67]. Nevertheless, such weak interactions are typically discovered fortuitously during mechanistic elucidation of MGDs, and the development of experiment workflows capable of systematically identifying native low affinity E3-substrate interactions at scale will be critical to transforming this observation into a rational design strategy.

DCAF16 appears to be a "frequent hitter" E3 ligases in TPD, particularly among compounds bearing cysteine-reactive moieties, with multiple studies reporting covalent modification of DCAF16 at C58, C173, C177-179 by electrophilic PROTACs and MGDs[37,49,64,68–70]. Its susceptibility to covalent modification likely reflects its unusually cysteine-rich character: DCAF16 contains eight cysteines within its 216 amino acids, including a cluster of four cysteines spanning positions 173-179, with C58 positioned in close spatial proximity to this cluster based on the recently solved cryo-EM structure[37,49]. Notably, the two vinyl sulfonamide bearing JQ1-based degraders engage distinct cysteine residues on DCAF16: ML 1-50, with a vinylsulfonyl piperazine in place of the tert-butyl ester group of JQ1 engages C119, while MMH2, which incorporates an N-aryl vinyl sulfonamide linkage on the phenyl exit vector of JQ1, engages C58[26,49]. Structural analysis of the BRD4-MMH2-DCAF16-DDB1 ternary complex cryo-EM structure reveals that C58 is solvent-exposed, whereas C119 is buried near the DDB1-DCAF16 interface. This raises an intriguing possibility that DCAF16 adopts a distinct structural conformation that renders C119 accessible upon engagement by ML 1-50. This conformational flexibility may be a key determinant of DCAF16's permissiveness in TPD and warrants further structural investigation.

Although an intrinsic affinity between BRD4 and DCAF16 has been reported, the vinylsulfonyl piperazine handle described in this work was capable of inducing degradation of CDK4, SMARCA2/4, AR, BTK, and BCR-ABL/c-ABL when appended onto their respective inhibitors. These are targets for which no native interaction with DCAF16 has been demonstrated. This suggests that our degraders do not operate through a template-assisted manner as reported but rather recruit DCAF16 de novo to neosubstrate proteins, a conclusion corroborated by the recent report of a DCAF16- and FBXO22-dependent SMARCA2/4 degrader that similarly does not rely on pre-existing DCAF16-SMARCA2/4 affinity[71]. The broad substrate scope observed in this study showcases the utility of DCAF16 in TPD to degrade a wide range of protein targets supporting is consistent with the structural data suggesting that DCAF16 possesses high conformational flexibility and structural plasticity, enabling it to accommodate a diverse range of neosubstrates beyond its endogenous substrate SPIN4[49,72]. This permissiveness is further supported by independent reports from other groups demonstrating DCAF16-dependent degradation of FKBP12, PARP2, CDK6, HDAC1/2, AR-V7, BRD9, and RPS6KA4, collectively establishing DCAF16 a versatile and broadly exploitable E3 ligases for future TPD applications[37,64,68,69,73–76].

References

(1) Dikic, I. Proteasomal and Autophagic Degradation Systems. *Annu. Rev. Biochem.* **2017**, *86* (1), 193–224. https://doi.org/10.1146/annurev-biochem-061516-044908.

(2) Domostegui, A.; Nieto-Barrado, L.; Perez-Lopez, C.; Mayor-Ruiz, C. Chasing Molecular Glue Degraders: Screening Approaches. *Chem. Soc. Rev.* **2022**, *51* (13), 5498–5517. https://doi.org/10.1039/D2CS00197G.

(3) Cromm, P. M.; Crews, C. M. Targeted Protein Degradation: From Chemical Biology to Drug Discovery. *Cell Chemical Biology* **2017**, *24* (9), 1181–1190. https://doi.org/10.1016/j.chembiol.2017.05.024.

(4) Rehman, W.; Arfons, L. M.; Lazarus, H. M. The Rise, Fall and Subsequent Triumph of Thalidomide: Lessons Learned in Drug Development. *Therapeutic Advances in Hematology* **2011**, *2* (5), 291–308. https://doi.org/10.1177/2040620711413165.

(5) Yamamoto, J.; Ito, T.; Yamaguchi, Y.; Handa, H. Discovery of CRBN as a Target of Thalidomide: A Breakthrough for Progress in the Development of Protein Degraders. *Chem. Soc. Rev.* **2022**, *51* (15), 6234–6250. https://doi.org/10.1039/D2CS00116K.

(6) Zhu, Y. X.; Braggio, E.; Shi, C.-X.; Bruins, L. A.; Schmidt, J. E.; Van Wier, S.; Chang, X.-B.; Bjorklund, C. C.; Fonseca, R.; Bergsagel, P. L.; Orlowski, R. Z.; Stewart, A. K. Cereblon Expression Is Required for the Antimyeloma Activity of Lenalidomide and Pomalidomide. *Blood* **2011**, *118* (18), 4771–4779. https://doi.org/10.1182/blood-2011-05-356063.

(7) Sheskin, J. Thalidomide in the Treatment of Lepra Reactions. *Clin Pharma and Therapeutics* **1965**, *6* (3), 303–306. https://doi.org/10.1002/cpt196563303.

(8) Krönke, J.; Udeshi, N. D.; Narla, A.; Grauman, P.; Hurst, S. N.; McConkey, M.; Svinkina, T.; Heckl, D.; Comer, E.; Li, X.; Ciarlo, C.; Hartman, E.; Munshi, N.; Schenone, M.; Schreiber, S. L.; Carr, S. A.; Ebert, B. L. Lenalidomide Causes Selective Degradation of IKZF1 and IKZF3 in Multiple Myeloma Cells. *Science* **2014**, *343* (6168), 301–305. https://doi.org/10.1126/science.1244851.

(9) Lu, G.; Middleton, R. E.; Sun, H.; Naniong, M.; Ott, C. J.; Mitsiades, C. S.; Wong, K.-K.; Bradner, J. E.; Kaelin, W. G. The Myeloma Drug Lenalidomide Promotes the Cereblon-Dependent Destruction of Ikaros Proteins. *Science* **2014**, *343* (6168), 305–309. https://doi.org/10.1126/science.1244917.

(10) Krönke, J.; Udeshi, N. D.; Narla, A.; Grauman, P.; Hurst, S. N.; McConkey, M.; Svinkina, T.; Heckl, D.; Comer, E.; Li, X.; Ciarlo, C.; Hartman, E.; Munshi, N.; Schenone, M.; Schreiber, S. L.; Carr, S. A.; Ebert, B. L. Lenalidomide Causes Selective Degradation of IKZF1 and IKZF3 in Multiple Myeloma Cells. *Science* **2014**, *343* (6168), 301–305. https://doi.org/10.1126/science.1244851.

(11) Gandhi, A. K.; Kang, J.; Havens, C. G.; Conklin, T.; Ning, Y.; Wu, L.; Ito, T.; Ando, H.; Waldman, M. F.; Thakurta, A.; Klippel, A.; Handa, H.; Daniel, T. O.; Schafer, P. H.; Chopra, R. Immunomodulatory Agents Lenalidomide and Pomalidomide Co-stimulate T Cells by Inducing Degradation of T Cell Repressors I Karos and A Iolos via Modulation of the E 3 Ubiquitin Ligase Complex CRL 4 ^{CRBN} . *Br J Haematol* **2014**, *164* (6), 811–821. https://doi.org/10.1111/bjh.12708.

(12) Krönke, J.; Fink, E. C.; Hollenbach, P. W.; MacBeth, K. J.; Hurst, S. N.; Udeshi, N. D.; Chamberlain, P. P.; Mani, D. R.; Man, H. W.; Gandhi, A. K.; Svinkina, T.; Schneider, R. K.; McConkey, M.; Järås, M.; Griffiths, E.; Wetzler, M.; Bullinger, L.; Cathers, B. E.; Carr, S. A.; Chopra, R.; Ebert, B. L. Lenalidomide Induces Ubiquitination and Degradation of CK1α in Del(5q) MDS. *Nature* **2015**, *523* (7559), 183–188. https://doi.org/10.1038/nature14610.

(13) Donovan, K. A.; An, J.; Nowak, R. P.; Yuan, J. C.; Fink, E. C.; Berry, B. C.; Ebert, B. L.; Fischer, E. S. Thalidomide Promotes Degradation of SALL4, a Transcription Factor Implicated in Duane Radial Ray Syndrome. *eLife* **2018**, *7*, e38430. https://doi.org/10.7554/eLife.38430.
(14) Matyskiela, M. E.; Couto, S.; Zheng, X.; Lu, G.; Hui, J.; Stamp, K.; Drew, C.; Ren, Y.; Wang, M.; Carpenter, A.; Lee, C.-W.; Clayton, T.; Fang, W.; Lu, C.-C.; Riley, M.; Abdubek, P.; Blease, K.; Hartke, J.; Kumar, G.; Vessey, R.; Rolfe, M.; Hamann, L. G.; Chamberlain, P. P. SALL4 Mediates Teratogenicity as a Thalidomide-Dependent Cereblon Substrate. *Nat Chem Biol* **2018**, *14* (10), 981–987. https://doi.org/10.1038/s41589-018-0129-x.
(15) Matyskiela, M. E.; Lu, G.; Ito, T.; Pagarigan, B.; Lu, C.-C.; Miller, K.; Fang, W.; Wang, N.-Y.; Nguyen, D.; Houston, J.; Carmel, G.; Tran, T.; Riley, M.; Nosaka, L.; Lander, G. C.; Gaidarova, S.; Xu, S.; Ruchelman, A. L.; Handa, H.; Carmichael, J.; Daniel, T. O.; Cathers, B. E.; Lopez-Girona, A.; Chamberlain, P. P. A Novel Cereblon Modulator Recruits GSPT1 to the CRL4CRBN Ubiquitin Ligase. *Nature* **2016**, *535* (7611), 252–257. https://doi.org/10.1038/nature18611.
(16) Kerres, N.; Steurer, S.; Schlager, S.; Bader, G.; Berger, H.; Caligiuri, M.; Dank, C.; Engen, J. R.; Ettmayer, P.; Fischerauer, B.; Flotzinger, G.; Gerlach, D.; Gerstberger, T.; Gmaschitz, T.; Greb, P.; Han, B.; Heyes, E.; Iacob, R. E.; Kessler, D.; Kölle, H.; Lamarre, L.; Lancia, D. R.; Lucas, S.; Mayer, M.; Mayr, K.; Mischerikow, N.; Mück, K.; Peinsipp, C.; Petermann, O.; Reiser, U.; Rudolph, D.; Rumpel, K.; Salomon, C.; Scharn, D.; Schnitzer, R.; Schrenk, A.; Schweifer, N.; Thompson, D.; Traxler, E.; Varecka, R.; Voss, T.; Weiss-Puxbaum, A.; Winkler, S.; Zheng, X.; Zoephel, A.; Kraut, N.; McConnell, D.; Pearson, M.; Koegl, M. Chemically Induced Degradation of the Oncogenic Transcription Factor BCL6. *Cell Reports* **2017**, *20* (12), 2860–2875. https://doi.org/10.1016/j.celrep.2017.08.081.
(17) Słabicki, M.; Yoon, H.; Koeppel, J.; Nitsch, L.; Roy Burman, S. S.; Di Genua, C.; Donovan, K. A.; Sperling, A. S.; Hunkeler, M.; Tsai, J. M.; Sharma, R.; Guirguis, A.; Zou, C.; Chudasama, P.; Gasser, J. A.; Miller, P. G.; Scholl, C.; Fröhling, S.; Nowak, R. P.; Fischer, E. S.; Ebert, B. L. Small-Molecule-Induced Polymerization Triggers Degradation of BCL6. *Nature* **2020**, *588* (7836), 164–168. https://doi.org/10.1038/s41586-020-2925-1.
(18) Mayor-Ruiz, C.; Bauer, S.; Brand, M.; Kozicka, Z.; Siklos, M.; Imrichova, H.; Kaltheuner, I. H.; Hahn, E.; Seiler, K.; Koren, A.; Petzold, G.; Fellner, M.; Bock, C.; Müller, A. C.; Zuber, J.; Geyer, M.; Thomä, N. H.; Kubicek, S.; Winter, G. E. Rational Discovery of Molecular Glue Degraders via Scalable Chemical Profiling. *Nat Chem Biol* **2020**, *16* (11), 1199–1207. https://doi.org/10.1038/s41589-020-0594-x.
(19) King, E. A.; Cho, Y.; Hsu, N. S.; Dovala, D.; McKenna, J. M.; Tallarico, J. A.; Schirle, M.; Nomura, D. K. Chemoproteomics-Enabled Discovery of a Covalent Molecular Glue Degrader Targeting NF-κB. *Cell Chemical Biology* **2023**, *30* (4), 394-402.e9. https://doi.org/10.1016/j.chembiol.2023.02.008.
(20) Simonetta, K. R.; Taygerly, J.; Boyle, K.; Basham, S. E.; Padovani, C.; Lou, Y.; Cummins, T. J.; Yung, S. L.; Von Soly, S. K.; Kayser, F.; Kuriyan, J.; Rape, M.; Cardozo, M.; Gallop, M. A.; Bence, N. F.; Barsanti, P. A.; Saha, A. Prospective Discovery of Small Molecule Enhancers of an E3 Ligase-Substrate Interaction. *Nat Commun* **2019**, *10* (1), 1402. https://doi.org/10.1038/s41467-019-09358-9.
(21) Matyskiela, M. E.; Zhu, J.; Baughman, J. M.; Clayton, T.; Slade, M.; Wong, H. K.; Danga, K.; Zheng, X.; Labow, M.; LeBrun, L.; Lu, G.; Chamberlain, P. P.; Thompson, J. W. Cereblon Modulators Target ZBTB16 and Its Oncogenic Fusion Partners for Degradation via

Distinct Structural Degrons. *ACS Chem. Biol.* **2020**, *15* (12), 3149–3158. https://doi.org/10.1021/acschembio.0c00674.

(22) Wang, E. S.; Verano, A. L.; Nowak, R. P.; Yuan, J. C.; Donovan, K. A.; Eleuteri, N. A.; Yue, H.; Ngo, K. H.; Lizotte, P. H.; Gokhale, P. C.; Gray, N. S.; Fischer, E. S. Acute Pharmacological Degradation of Helios Destabilizes Regulatory T Cells. *Nat Chem Biol* **2021**, *17* (6), 711–717. https://doi.org/10.1038/s41589-021-00802-w.

(23) Petzold, G.; Gainza, P.; Annunziato, S.; Lamberto, I.; Trenh, P.; McAllister, L. A.; DeMarco, B.; Schwander, L.; Bunker, R. D.; Zlotosch, M.; SriRamaratnam, R.; Gilberto, S.; Langousis, G.; Donckele, E. J.; Quan, C.; Strande, V.; De Donatis, G. M.; Alabi, S. B.; Alers, J.; Matysik, M.; Staehly, C.; Dubois, A.; Osmont, A.; Garskovas, M.; Lyon, D.; Wiedmer, L.; Oleinikovas, V.; Lieberherr, R.; Rubin, N. T.; Lam, D. T.; Lucas, X.; Liardo, E.; Widlund, N. I.; Ritzén, A.; Caceres, R. M.; Vigil, D.; Tsai, J.; Wallace, O.; Peluso, M.; Sadok, A.; Tiedt, R.; Paterson, A. M.; Zarayskiy, V.; Fasching, B.; Bonenfant, D.; Warmuth, M.; Castle, J. C.; Townson, S. A. Mining the CRBN Target Space Redefines Rules for Molecular Glue–Induced Neosubstrate Recognition. *Science* **2025**, *389* (6755), eadt6736. https://doi.org/10.1126/science.adt6736.

(24) Toriki, E. S.; Papatzimas, J. W.; Nishikawa, K.; Dovala, D.; Frank, A. O.; Hesse, M. J.; Dankova, D.; Song, J.-G.; Bruce-Smythe, M.; Struble, H.; Garcia, F. J.; Brittain, S. M.; Kile, A. C.; McGregor, L. M.; McKenna, J. M.; Tallarico, J. A.; Schirle, M.; Nomura, D. K. Rational Chemical Design of Molecular Glue Degraders. *ACS Cent Sci* **2023**, *9* (5), 915–926. https://doi.org/10.1021/acscentsci.2c01317.

(25) Słabicki, M.; Kozicka, Z.; Petzold, G.; Li, Y.-D.; Manojkumar, M.; Bunker, R. D.; Donovan, K. A.; Sievers, Q. L.; Koeppel, J.; Suchyta, D.; Sperling, A. S.; Fink, E. C.; Gasser, J. A.; Wang, L. R.; Corsello, S. M.; Sellar, R. S.; Jan, M.; Gillingham, D.; Scholl, C.; Fröhling, S.; Golub, T. R.; Fischer, E. S.; Thomä, N. H.; Ebert, B. L. The CDK Inhibitor CR8 Acts as a Molecular Glue Degrader That Depletes Cyclin K. *Nature* **2020**, *585* (7824), 293–297. https://doi.org/10.1038/s41586-020-2374-x.

(26) Lim, M.; Cong, T. D.; Orr, L. M.; Toriki, E. S.; Kile, A. C.; Papatzimas, J. W.; Lee, E.; Lin, Y.; Nomura, D. K. DCAF16-Based Covalent Handle for the Rational Design of Monovalent Degraders. *ACS Cent. Sci.* **2024**, *10* (7), 1318–1331. https://doi.org/10.1021/acscentsci.4c00286.

(27) Scholes, N. S.; Mayor-Ruiz, C.; Winter, G. E. Identification and Selectivity Profiling of Small-Molecule Degraders via Multi-Omics Approaches. *Cell Chem Biol* **2021**, *28* (7), 1048–1060. https://doi.org/10.1016/j.chembiol.2021.03.007.

(28) Schreiber, S. L. The Rise of Molecular Glues. *Cell* **2021**, *184* (1), 3–9. https://doi.org/10.1016/j.cell.2020.12.020.

(29) Mayor-Ruiz, C.; Bauer, S.; Brand, M.; Kozicka, Z.; Siklos, M.; Imrichova, H.; Kaltheuner, I. H.; Hahn, E.; Seiler, K.; Koren, A.; Petzold, G.; Fellner, M.; Bock, C.; Müller, A. C.; Zuber, J.; Geyer, M.; Thomä, N. H.; Kubicek, S.; Winter, G. E. Rational Discovery of Molecular Glue Degraders via Scalable Chemical Profiling. *Nat Chem Biol* **2020**, *16* (11), 1199–1207. https://doi.org/10.1038/s41589-020-0594-x.

(30) King, E. A.; Cho, Y.; Hsu, N. S.; Dovala, D.; McKenna, J. M.; Tallarico, J. A.; Schirle, M.; Nomura, D. K. Chemoproteomics-Enabled Discovery of a Covalent Molecular Glue Degrader Targeting NF-κB. *Cell Chem Biol* **2023**, *30* (4), 394-402.e9. https://doi.org/10.1016/j.chembiol.2023.02.008.

(31) Słabicki, M.; Yoon, H.; Koeppel, J.; Nitsch, L.; Roy Burman, S. S.; Di Genua, C.; Donovan, K. A.; Sperling, A. S.; Hunkeler, M.; Tsai, J. M.; Sharma, R.; Guirguis, A.; Zou, C.; Chudasama, P.; Gasser, J. A.; Miller, P. G.; Scholl, C.; Fröhling, S.; Nowak, R. P.; Fischer, E. S.; Ebert, B. L. Small-Molecule-Induced Polymerization Triggers Degradation of BCL6. *Nature* **2020**, *588* (7836), 164–168. https://doi.org/10.1038/s41586-020-2925-1.

(32) Shergalis, A. G.; Marin, V. L.; Rhee, D. Y.; Senaweera, S.; McCloud, R. L.; Ronau, J. A.; Hutchins, C. W.; McLoughlin, S.; Woller, K. R.; Warder, S. E.; Vasudevan, A.; Reitsma, J. M. CRISPR Screen Reveals BRD2/4 Molecular Glue-like Degrader via Recruitment of DCAF16. *ACS Chem. Biol.* **2023**, *18* (2), 331–339. https://doi.org/10.1021/acschembio.2c00747.

(33) Hsia, O.; Hinterndorfer, M.; Cowan, A. D.; Iso, K.; Ishida, T.; Sundaramoorthy, R.; Nakasone, M. A.; Imrichova, H.; Schätz, C.; Rukavina, A.; Husnjak, K.; Wegner, M.; Correa-Sáez, A.; Craigon, C.; Casement, R.; Maniaci, C.; Testa, A.; Kaulich, M.; Dikic, I.; Winter, G. E.; Ciulli, A. Targeted Protein Degradation via Intramolecular Bivalent Glues. *Nature* **2024**, *627* (8002), 204–211. https://doi.org/10.1038/s41586-024-07089-6.

(34) Backus, K. M.; Correia, B. E.; Lum, K. M.; Forli, S.; Horning, B. D.; González-Páez, G. E.; Chatterjee, S.; Lanning, B. R.; Teijaro, J. R.; Olson, A. J.; Wolan, D. W.; Cravatt, B. F. Proteome-Wide Covalent Ligand Discovery in Native Biological Systems. *Nature* **2016**, *534* (7608), 570–574. https://doi.org/10.1038/nature18002.

(35) Vinogradova, E. V.; Zhang, X.; Remillard, D.; Lazar, D. C.; Suciu, R. M.; Wang, Y.; Bianco, G.; Yamashita, Y.; Crowley, V. M.; Schafroth, M. A.; Yokoyama, M.; Konrad, D. B.; Lum, K. M.; Simon, G. M.; Kemper, E. K.; Lazear, M. R.; Yin, S.; Blewett, M. M.; Dix, M. M.; Nguyen, N.; Shokhirev, M. N.; Chin, E. N.; Lairson, L. L.; Melillo, B.; Schreiber, S. L.; Forli, S.; Teijaro, J. R.; Cravatt, B. F. An Activity-Guided Map of Electrophile-Cysteine Interactions in Primary Human T Cells. *Cell* **2020**, *182* (4), 1009-1026.e29. https://doi.org/10.1016/j.cell.2020.07.001.

(36) Spradlin, J. N.; Hu, X.; Ward, C. C.; Brittain, S. M.; Jones, M. D.; Ou, L.; To, M.; Proudfoot, A.; Ornelas, E.; Woldegiorgis, M.; Olzmann, J. A.; Bussiere, D. E.; Thomas, J. R.; Tallarico, J. A.; McKenna, J. M.; Schirle, M.; Maimone, T. J.; Nomura, D. K. Harnessing the Anti-Cancer Natural Product Nimbolide for Targeted Protein Degradation. *Nat Chem Biol* **2019**, *15* (7), 747–755. https://doi.org/10.1038/s41589-019-0304-8.

(37) Zhang, X.; Crowley, V. M.; Wucherpfennig, T. G.; Dix, M. M.; Cravatt, B. F. Electrophilic PROTACs That Degrade Nuclear Proteins by Engaging DCAF16. *Nat. Chem. Biol.* **2019**, *15* (7), 737–746. https://doi.org/10.1038/s41589-019-0279-5.

(38) Belcher, B. P.; Ward, C. C.; Nomura, D. K. Ligandability of E3 Ligases for Targeted Protein Degradation Applications. *Biochemistry* **2023**, *62* (3), 588–600. https://doi.org/10.1021/acs.biochem.1c00464.

(39) Kuljanin, M.; Mitchell, D. C.; Schweppe, D. K.; Gikandi, A. S.; Nusinow, D. P.; Bulloch, N. J.; Vinogradova, E. V.; Wilson, D. L.; Kool, E. T.; Mancias, J. D.; Cravatt, B. F.; Gygi, S. P. Reimagining High-Throughput Profiling of Reactive Cysteines for Cell-Based Screening of Large Electrophile Libraries. *Nat Biotechnol* **2021**, *39* (5), 630–641. https://doi.org/10.1038/s41587-020-00778-3.

(40) Boatner, L. M.; Palafox, M. F.; Schweppe, D. K.; Backus, K. M. CysDB: A Human Cysteine Database Based on Experimental Quantitative Chemoproteomics. *Cell Chem Biol* **2023**, *30* (6), 683-698.e3. https://doi.org/10.1016/j.chembiol.2023.04.004.

(41) Zhang, X.; Luukkonen, L. M.; Eissler, C. L.; Crowley, V. M.; Yamashita, Y.; Schafroth, M. A.; Kikuchi, S.; Weinstein, D. S.; Symons, K. T.; Nordin, B. E.; Rodriguez, J. L.; Wucherpfennig, T. G.; Bauer, L. G.; Dix, M. M.; Stamos, D.; Kinsella, T. M.; Simon, G. M.; Baltgalvis, K. A.; Cravatt, B. F. DCAF11 Supports Targeted Protein Degradation by Electrophilic Proteolysis-Targeting Chimeras. *J Am Chem Soc* **2021**, *143* (13), 5141–5149. https://doi.org/10.1021/jacs.1c00990.

(42) Sarott, R. C.; You, I.; Li, Y.-D.; Toenjes, S. T.; Donovan, K. A.; Seo, P.; Ordonez, M.; Byun, W. S.; Hassan, M. M.; Wachter, F.; Chouchani, E. T.; Słabicki, M.; Fischer, E. S.; Ebert, B. L.; Hinshaw, S. M.; Gray, N. S. Chemical Specification of E3 Ubiquitin Ligase Engagement by Cysteine-Reactive Chemistry. *J Am Chem Soc* **2023**, *145* (40), 21937–21944. https://doi.org/10.1021/jacs.3c06622.

(43) Luo, M.; Spradlin, J. N.; Boike, L.; Tong, B.; Brittain, S. M.; McKenna, J. M.; Tallarico, J. A.; Schirle, M.; Maimone, T. J.; Nomura, D. K. Chemoproteomics-Enabled Discovery of Covalent RNF114-Based Degraders That Mimic Natural Product Function. *Cell Chem Biol* **2021**, *28* (4), 559-566.e15. https://doi.org/10.1016/j.chembiol.2021.01.005.

(44) Ward, C. C.; Kleinman, J. I.; Brittain, S. M.; Lee, P. S.; Chung, C. Y. S.; Kim, K.; Petri, Y.; Thomas, J. R.; Tallarico, J. A.; McKenna, J. M.; Schirle, M.; Nomura, D. K. Covalent Ligand Screening Uncovers a RNF4 E3 Ligase Recruiter for Targeted Protein Degradation Applications. *ACS Chem Biol* **2019**, *14* (11), 2430–2440. https://doi.org/10.1021/acschembio.8b01083.

(45) Henning, N. J.; Manford, A. G.; Spradlin, J. N.; Brittain, S. M.; Zhang, E.; McKenna, J. M.; Tallarico, J. A.; Schirle, M.; Rape, M.; Nomura, D. K. Discovery of a Covalent FEM1B Recruiter for Targeted Protein Degradation Applications. *J Am Chem Soc* **2022**, *144* (2), 701–708. https://doi.org/10.1021/jacs.1c03980.

(46) Forte, N.; Dovala, D.; Hesse, M. J.; McKenna, J. M.; Tallarico, J. A.; Schirle, M.; Nomura, D. K. Targeted Protein Degradation through E2 Recruitment. *ACS Chem Biol* **2023**, *18* (4), 897–904. https://doi.org/10.1021/acschembio.3c00040.

(47) Meyers, M.; Cismoski, S.; Panidapu, A.; Chie-Leon, B.; Nomura, D. K. Targeted Protein Degradation through Recruitment of the CUL4 Complex Adaptor Protein DDB1. *ACS Chem Biol* **2024**. https://doi.org/10.1021/acschembio.3c00487.

(48) Hong, S. H.; Osa, A.; Huang, O. W.; Wertz, I. E.; Nomura, D. K. Exploiting the Cullin E3 Ligase Adaptor Protein SKP1 for Targeted Protein Degradation. *bioRxiv* **2023**, 2023.10.20.563371. https://doi.org/10.1101/2023.10.20.563371.

(49) Li, Y.-D.; Ma, M. W.; Hassan, M. M.; Hunkeler, M.; Teng, M.; Puvar, K.; Rutter, J. C.; Lumpkin, R. J.; Sandoval, B.; Jin, C. Y.; Schmoker, A. M.; Ficarro, S. B.; Cheong, H.; Metivier, R. J.; Wang, M. Y.; Xu, S.; Byun, W. S.; Groendyke, B. J.; You, I.; Sigua, L. H.; Tavares, I.; Zou, C.; Tsai, J. M.; Park, P. M. C.; Yoon, H.; Majewski, F. C.; Sperling, H. T.; Marto, J. A.; Qi, J.; Nowak, R. P.; Donovan, K. A.; Słabicki, M.; Gray, N. S.; Fischer, E. S.; Ebert, B. L. Template-Assisted Covalent Modification Underlies Activity of Covalent Molecular Glues. *Nat Chem Biol* **2024**, *20* (12), 1640–1649. https://doi.org/10.1038/s41589-024-01668-4.

(50) Hassan, M. M.; Li, Y.-D.; Ma, M. W.; Teng, M.; Byun, W. S.; Puvar, K.; Lumpkin, R.; Sandoval, B.; Rutter, J. C.; Jin, C. Y.; Wang, M. Y.; Xu, S.; Schmoker, A. M.; Cheong, H.; Groendyke, B. J.; Qi, J.; Fischer, E. S.; Ebert, B. L.; Gray, N. S. Exploration of the Tunability of BRD4 Degradation by DCAF16 Trans-Labelling Covalent Glues. *European Journal of Medicinal Chemistry* **2024**, *279*, 116904. https://doi.org/10.1016/j.ejmech.2024.116904.

(51) Winter, G. E.; Buckley, D. L.; Paulk, J.; Roberts, J. M.; Souza, A.; Dhe-Paganon, S.; Bradner, J. E. DRUG DEVELOPMENT. Phthalimide Conjugation as a Strategy for in Vivo Target Protein Degradation. *Science* **2015**, *348* (6241), 1376–1381. https://doi.org/10.1126/science.aab1433.
(52) Farnaby, W.; Koegl, M.; Roy, M. J.; Whitworth, C.; Diers, E.; Trainor, N.; Zollman, D.; Steurer, S.; Karolyi-Oezguer, J.; Riedmueller, C.; Gmaschitz, T.; Wachter, J.; Dank, C.; Galant, M.; Sharps, B.; Rumpel, K.; Traxler, E.; Gerstberger, T.; Schnitzer, R.; Petermann, O.; Greb, P.; Weinstabl, H.; Bader, G.; Zoephel, A.; Weiss-Puxbaum, A.; Ehrenhöfer-Wölfer, K.; Wöhrle, S.; Boehmelt, G.; Rinnenthal, J.; Arnhof, H.; Wiechens, N.; Wu, M.-Y.; Owen-Hughes, T.; Ettmayer, P.; Pearson, M.; McConnell, D. B.; Ciulli, A. BAF Complex Vulnerabilities in Cancer Demonstrated via Structure-Based PROTAC Design. *Nat Chem Biol* **2019**, *15* (7), 672–680. https://doi.org/10.1038/s41589-019-0294-6.
(53) Neklesa, T.; Snyder, L. B.; Willard, R. R.; Vitale, N.; Pizzano, J.; Gordon, D. A.; Bookbinder, M.; Macaluso, J.; Dong, H.; Ferraro, C.; Wang, G.; Wang, J.; Crews, C. M.; Houston, J.; Crew, A. P.; Taylor, I. ARV-110: An Oral Androgen Receptor PROTAC Degrader for Prostate Cancer. *JCO* **2019**, *37* (7_suppl), 259–259. https://doi.org/10.1200/JCO.2019.37.7_suppl.259.
(54) Lanning, B. R.; Whitby, L. R.; Dix, M. M.; Douhan, J.; Gilbert, A. M.; Hett, E. C.; Johnson, T. O.; Joslyn, C.; Kath, J. C.; Niessen, S.; Roberts, L. R.; Schnute, M. E.; Wang, C.; Hulce, J. J.; Wei, B.; Whiteley, L. O.; Hayward, M. M.; Cravatt, B. F. A Road Map to Evaluate the Proteome-Wide Selectivity of Covalent Kinase Inhibitors. *Nat. Chem. Biol.* **2014**, *10* (9), 760–767. https://doi.org/10.1038/nchembio.1582.
(55) Tong, B.; Luo, M.; Xie, Y.; Spradlin, J. N.; Tallarico, J. A.; McKenna, J. M.; Schirle, M.; Maimone, T. J.; Nomura, D. K. Bardoxolone Conjugation Enables Targeted Protein Degradation of BRD4. *Sci Rep* **2020**, *10* (1), 15543. https://doi.org/10.1038/s41598-020-72491-9.
(56) Du, G.; Jiang, J.; Henning, N. J.; Safaee, N.; Koide, E.; Nowak, R. P.; Donovan, K. A.; Yoon, H.; You, I.; Yue, H.; Eleuteri, N. A.; He, Z.; Li, Z.; Huang, H. T.; Che, J.; Nabet, B.; Zhang, T.; Fischer, E. S.; Gray, N. S. Exploring the Target Scope of KEAP1 E3 Ligase-Based PROTACs. *Cell Chem Biol* **2022**, *29* (10), 1470-1481.e31. https://doi.org/10.1016/j.chembiol.2022.08.003.
(57) Schreiber, S. L. Chemistry and Biology of the Immunophilins and Their Immunosuppressive Ligands. *Science* **1991**, *251* (4991), 283–287. https://doi.org/10.1126/science.1702904.
(58) Bayle, J. H.; Grimley, J. S.; Stankunas, K.; Gestwicki, J. E.; Wandless, T. J.; Crabtree, G. R. Rapamycin Analogs with Differential Binding Specificity Permit Orthogonal Control of Protein Activity. *Chem. Biol.* **2006**, *13* (1), 99–107. https://doi.org/10.1016/j.chembiol.2005.10.017.
(59) Xu, T.; Park, S. K.; Venable, J. D.; Wohlschlegel, J. A.; Diedrich, J. K.; Cociorva, D.; Lu, B.; Liao, L.; Hewel, J.; Han, X.; Wong, C. C. L.; Fonslow, B.; Delahunty, C.; Gao, Y.; Shah, H.; Yates, J. R. ProLuCID: An Improved SEQUEST-like Algorithm with Enhanced Sensitivity and Specificity. *J Proteomics* **2015**, *129*, 16–24. https://doi.org/10.1016/j.jprot.2015.07.001.
(60) Tan, X.; Calderon-Villalobos, L. I. A.; Sharon, M.; Zheng, C.; Robinson, C. V.; Estelle, M.; Zheng, N. Mechanism of Auxin Perception by the TIR1 Ubiquitin Ligase. *Nature* **2007**, *446* (7136), 640–645. https://doi.org/10.1038/nature05731.
(61) Sheard, L. B.; Tan, X.; Mao, H.; Withers, J.; Ben-Nissan, G.; Hinds, T. R.; Kobayashi, Y.; Hsu, F.-F.; Sharon, M.; Browse, J.; He, S. Y.; Rizo, J.; Howe, G. A.; Zheng, N. Jasmonate

Perception by Inositol-Phosphate-Potentiated COI1–JAZ Co-Receptor. *Nature* **2010**, *468* (7322), 400–405. https://doi.org/10.1038/nature09430.
(62) King, E. A.; Meyers, M.; Nomura, D. K. Induced Proximity-Based Therapeutic Modalities. *Nat Rev Drug Discov* **2026**, *25* (3), 175–203. https://doi.org/10.1038/s41573-025-01316-z.
(63) Shergalis, A. G.; Marin, V. L.; Rhee, D. Y.; Senaweera, S.; McCloud, R. L.; Ronau, J. A.; Hutchins, C. W.; McLoughlin, S.; Woller, K. R.; Warder, S. E.; Vasudevan, A.; Reitsma, J. M. CRISPR Screen Reveals BRD2/4 Molecular Glue-like Degrader via Recruitment of DCAF16. *ACS Chem. Biol.* **2023**, *18* (2), 331–339. https://doi.org/10.1021/acschembio.2c00747.
(64) Orr, L. M.; Tomlinson, S. J.; Grupe, H. R.; Lim, M.; Ho, E.; Yilmaz, H.; Zhou, G.; Leon, B.; Olzmann, J. A.; Nomura, D. K. DCAF16-Based Covalent Degradative Handles for the Modular Design of Degraders. *ACS Cent. Sci.* **2025**, *11* (7), 1207–1217. https://doi.org/10.1021/acscentsci.5c00959.
(65) Sarott, R. C.; You, I.; Li, Y.-D.; Toenjes, S. T.; Donovan, K. A.; Seo, P.; Ordonez, M.; Byun, W. S.; Hassan, M. M.; Wachter, F.; Chouchani, E. T.; Słabicki, M.; Fischer, E. S.; Ebert, B. L.; Hinshaw, S. M.; Gray, N. S. Chemical Specification of E3 Ubiquitin Ligase Engagement by Cysteine-Reactive Chemistry. *J. Am. Chem. Soc.* **2023**, *145* (40), 21937–21944. https://doi.org/10.1021/jacs.3c06622.
(66) Lv, L.; Chen, P.; Cao, L.; Li, Y.; Zeng, Z.; Cui, Y.; Wu, Q.; Li, J.; Wang, J.-H.; Dong, M.-Q.; Qi, X.; Han, T. Discovery of a Molecular Glue Promoting CDK12-DDB1 Interaction to Trigger Cyclin K Degradation. *eLife* **2020**, *9*, e59994. https://doi.org/10.7554/eLife.59994.
(67) Cao, S.; Kang, S.; Mao, H.; Yao, J.; Gu, L.; Zheng, N. Defining Molecular Glues with a Dual-Nanobody Cannabidiol Sensor. *Nat Commun* **2022**, *13* (1), 815. https://doi.org/10.1038/s41467-022-28507-1.
(68) Hughes, S. J.; Stec, W. J.; Davies, C. T. R.; McGarry, D.; Williams, A.; Carrara, M.; Del Barco Barrantes, I.; Harris, R.; Tasegian, A.; Owens, D. D. G.; Fawcett, A.; Hellicar, J.; Azevedo, A.; Meier, G. P.; Runcie, A. C.; Greger, L.; O'Rourke, M.; Churcher, I.; Pass, M.; Brown, G. A.; Ciulli, A.; Modis, L. K.; Testa, A. Mode of Action of a DCAF16-Recruiting Targeted Glue That Can Selectively Degrade BRD9. *Nat Commun* **2025**, *16* (1), 8516. https://doi.org/10.1038/s41467-025-63594-w.
(69) Campos, M. A.; Riha, I. A.; Zhang, C.; Mozes, C.; Scheidt, K. A.; Zhang, X. Discovery of DCAF16 Binders for Targeted Protein Degradation. *ACS Chem. Biol.* **2025**, *20* (2), 479–488. https://doi.org/10.1021/acschembio.4c00799.
(70) Zhang, X.; Simon, G. M.; Cravatt, B. F. Implications of Frequent Hitter E3 Ligases in Targeted Protein Degradation Screens. *Nat Chem Biol* **2025**, *21* (4), 474–481. https://doi.org/10.1038/s41589-024-01821-z.
(71) Spiteri, V. A.; Segal, D.; Correa-Saez, A.; Iso, K.; Casement, R.; Munoz I Ordono, M.; Nakasone, M. A.; Sathe, G.; Schatz, C.; Peters, H. E.; Doward, M.; Kainacher, L.; Cowan, A. D.; Ciulli, A.; Winter, G. E. Dual E3 Ligase Recruitment by Monovalent Degraders Enables Redundant and Tuneable Degradation of SMARCA2/4. Biochemistry August 4, 2025. https://doi.org/10.1101/2025.08.04.668513.
(72) Zhang, X.; Thielert, M.; Li, H.; Cravatt, B. F. SPIN4 Is a Principal Endogenous Substrate of the E3 Ubiquitin Ligase DCAF16. *Biochemistry* **2021**, *60* (9), 637–642. https://doi.org/10.1021/acs.biochem.1c00067.
(73) Pu, C.; Tong, Y.; Liu, Y.; Lan, S.; Wang, S.; Yan, G.; Zhang, H.; Luo, D.; Ma, X.; Yu, S.; Huang, Q.; Deng, R.; Li, R. Selective Degradation of PARP2 by PROTACs via Recruiting

DCAF16 for Triple-Negative Breast Cancer. *European Journal of Medicinal Chemistry* **2022**, *236*, 114321. https://doi.org/10.1016/j.ejmech.2022.114321.
(74) Pu, C.; Liu, Y.; Deng, R.; Xu, Q.; Wang, S.; Zhang, H.; Luo, D.; Ma, X.; Tong, Y.; Li, R. Development of PROTAC Degrader Probe of CDK4/6 Based on DCAF16. *Bioorganic Chemistry* **2023**, *138*, 106637. https://doi.org/10.1016/j.bioorg.2023.106637.
(75) Sun, T.; Zhai, S.; Lepper, S.; König, B.; Malenica, M.; Honin, I.; Hansen, F. K. DCAF16-Based Covalent Molecular Glues for Targeted Protein Degradation of Histone Deacetylases. *Archiv der Pharmazie* **2025**, *358* (7), e70045. https://doi.org/10.1002/ardp.70045.
(76) Byun, W. S.; Zhuang, Z.; Hnatiuk, A. P.; Jin, C.; Jiang, Z.; Baek, K.; Chao, E.; Donovan, K. A.; Fischer, E. S.; Mercola, M.; Gray, N. S. Discovery of BRD9 Molecular Glue Degraders That Spare Cardiomyocytes. *J. Am. Chem. Soc.* **2025**, *147* (39), 35481–35492. https://doi.org/10.1021/jacs.5c09857.

Appendices

Supplementary Figures

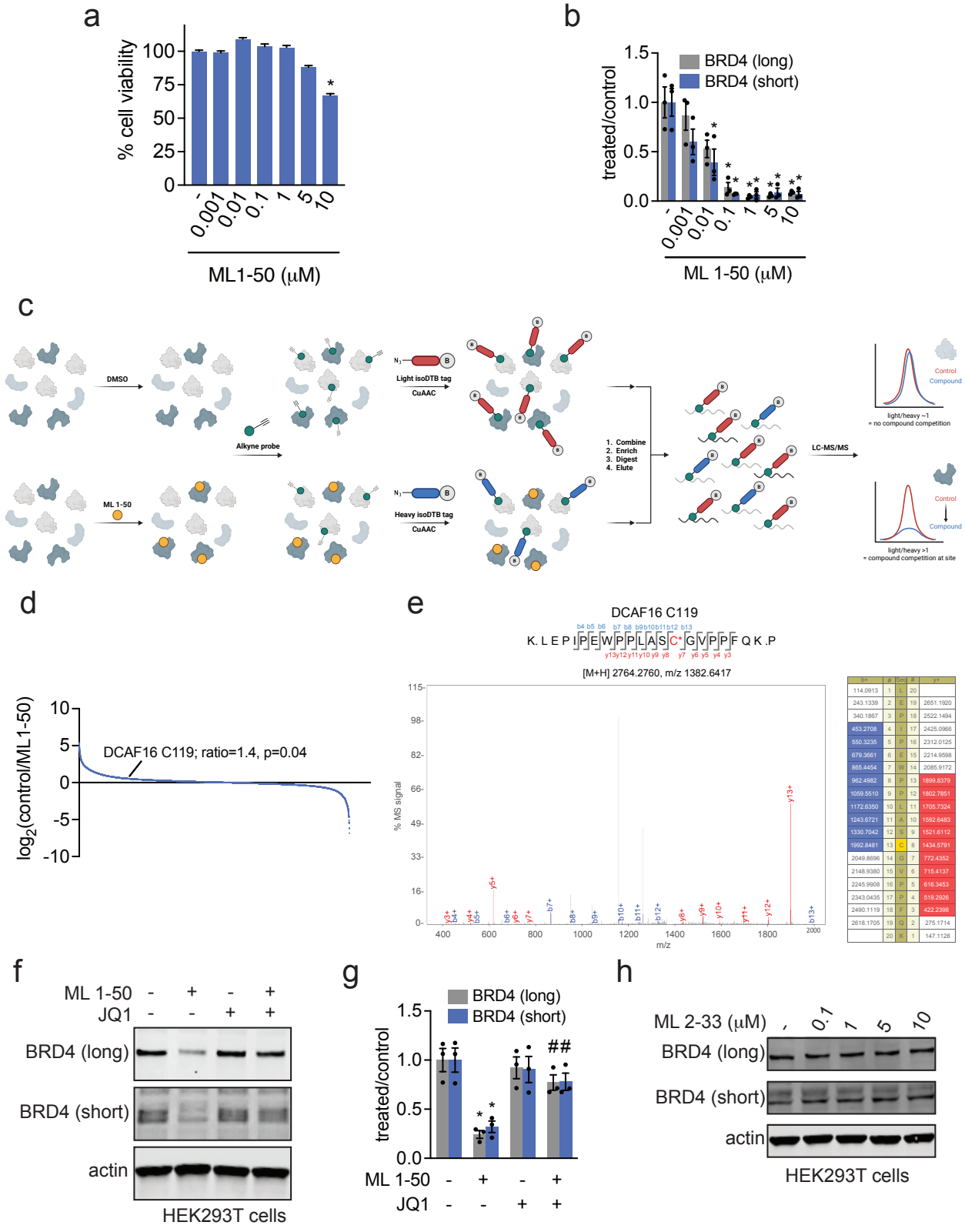

Figure S1. Characterization of ML 1-50. (a) Cell viability of HEK293T cells. HEK293T cells were treated with DMSO vehicle or ML 1-50 for 24 h and cell viability was assessed by CellTiter-Glo. **(b)** Quantification of BRD4 degradation in MDA-MB-231 cells from experiment described in **Figure 2.2h. (c)** Cysteine chemoproteomic profiling isoDTB-ABPP workflow. HEK293T cells were treated with DMSO vehicle or ML 1-50 (10 µM) for 2h. Subsequent lysates were labeled with an alkyne-functionalized iodoacetamide probe (200 µM) for 1 h, followed by CuAAC-mediated attachment of an isotopically light (for control) or heavy (for treated) azide-functionalized desthiobiotin handle, after which probe-modified proteins were streptavidin-enriched, tryptically digested, eluted from beads, and analyzed by LC-MS/MS. **(d)** IsoDTB-ABPP profiling of ML 1-50. The light versus heavy probe-modified peptide ratio for C119 of DCAF16 is noted with associated p-value. Each blue dot corresponds to the average light/heavy ratio of each probe-modified peptide. **(e)** Site of modification analysis of ML 1-50 on pure DCAF16 protein. Pure DCAF16 protein was labeled with ML 1-50 (50 µM) for 1 h. Protein was tryptically digested and analyzed for the ML 1-50 adduct by LC-MS/MS. **(f,g)** ML 1-50-mediated BRD4 degradation attenuated by JQ1 pre-treatment. HEK293T cells were pre-treated with DMSO vehicle or JQ1 (50 µM) for 1 h prior to treatment with DMSO vehicle or ML 1-50 (0.1 µM) for 16 h and BRD4 and loading control actin levels were assessed by Western blotting **(f)** and quantified in **(g). (h)** HEK293T cells were treated with DMSO vehicle or ML 2-33 for 24 h and BRD4 and actin levels were assessed by Western blotting. Data in **(a-b,d-h)** are from n=3 biologically independent replicates per group. Blots shown in **(f,h)** are representative. Bar graphs in **(a)** shows average ± sem and in **(b,g)** show individual replicate values and average ± sem. Significance shown as *p<0.05 compared to vehicle-treated controls and #p<0.05 compared to ML 1-50 treatment in **(g).**

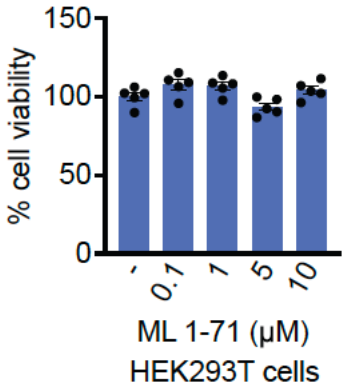

Figure S2. ML 1-71 effects on cell viability. HEK293T cells were treated with HEK293T cells were treated with DMSO vehicle or ML 1-71 for 24 h and cell viability was assessed by CellTiter-Glo. Bar graph shows individual replicate values and average ± sem from n=5 biologically independent replicates per group.

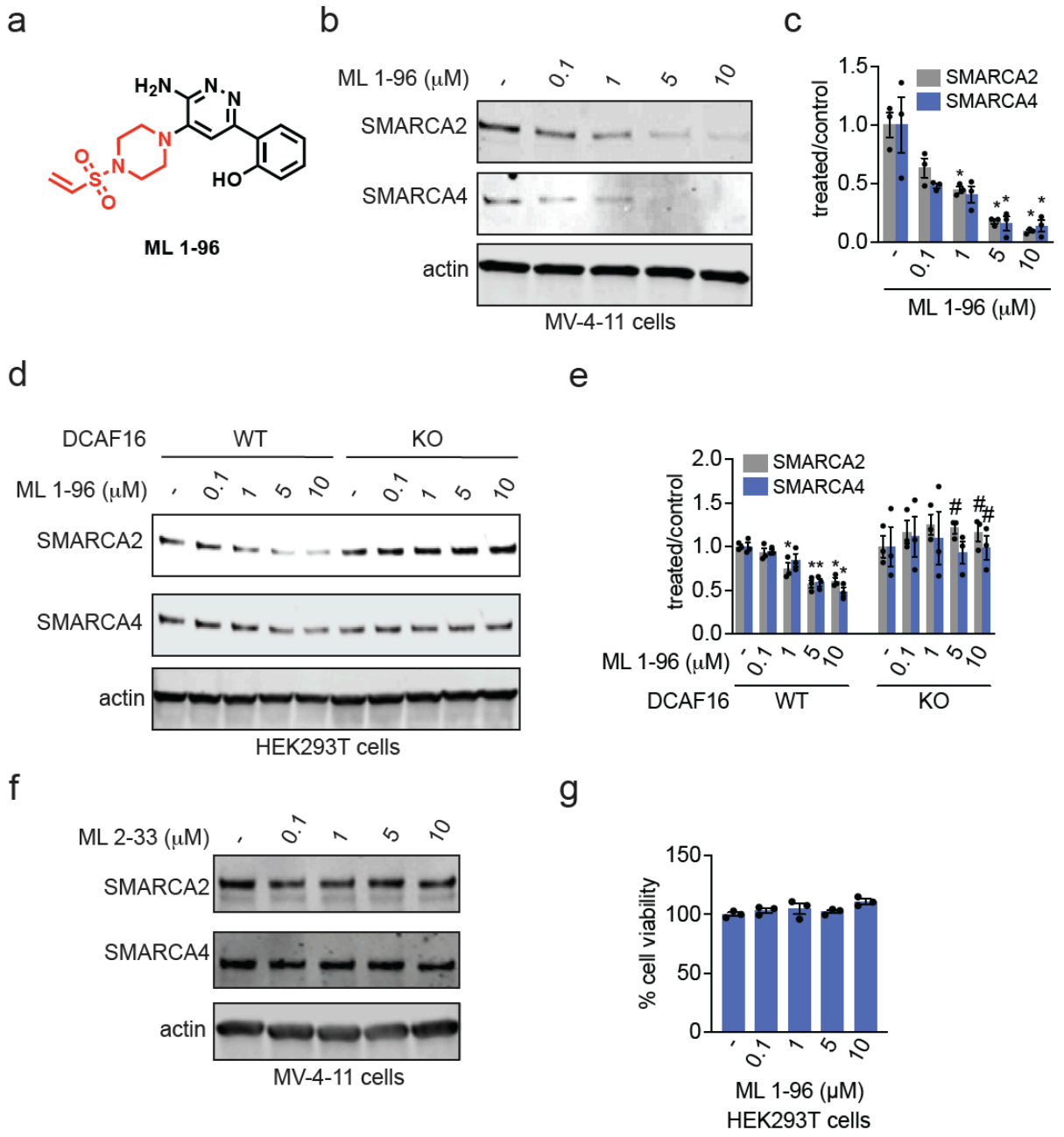

Figure S3. Characterization of SMARCA2 Monovalent Degrader. (a) Structure of ML 1-96 with the vinylsulfonyl piperazine covalent chemical handle in red. **(b,c)** SMARCA2 degradation in MV-4-11 leukemia cancer cells. MV-4-11 cells were treated with DMSO vehicle or ML 1-96 for 24 h and SMARCA2/4 and actin loading control levels were assessed by Western blotting and quantified in **(c)**. **(d, e)** SMARCA2/4 degradation in DCAF16 WT and KO cells. DCAF16 WT and KO HEK293 cells were treated with ML 1-96 for 24 h and SMARCA2, SMARCA4, and actin loading control levels were assessed by Western blotting **(d)** and quantified in **(e). (f)** SMARCA2/4 levels in MV-4-11 cells. MV-4-11 cells were treated with DMSO vehicle or ML 2-33 for 24 h and SMARCA2/4 and loading control actin levels were assessed by Western blotting. **(g)** ML 1-96

effects on cell viability. HEK293T cells were treated with DMSO vehicle or ML 1-96 for 24 h and cell viability was assessed by CellTiter-Glo. Blots in **(b, d, f)** are representative of n=3 biologically independent replicates per group. Bar graphs in **(c, e, g)** show individual replicate values and average ± sem and are from n=3 biologically independent replicates per group. Significance is expressed as *p<0.05 compared to vehicle-treated controls and #p<0.05 compared to ML 1-96 treated DCAF16 WT cells.

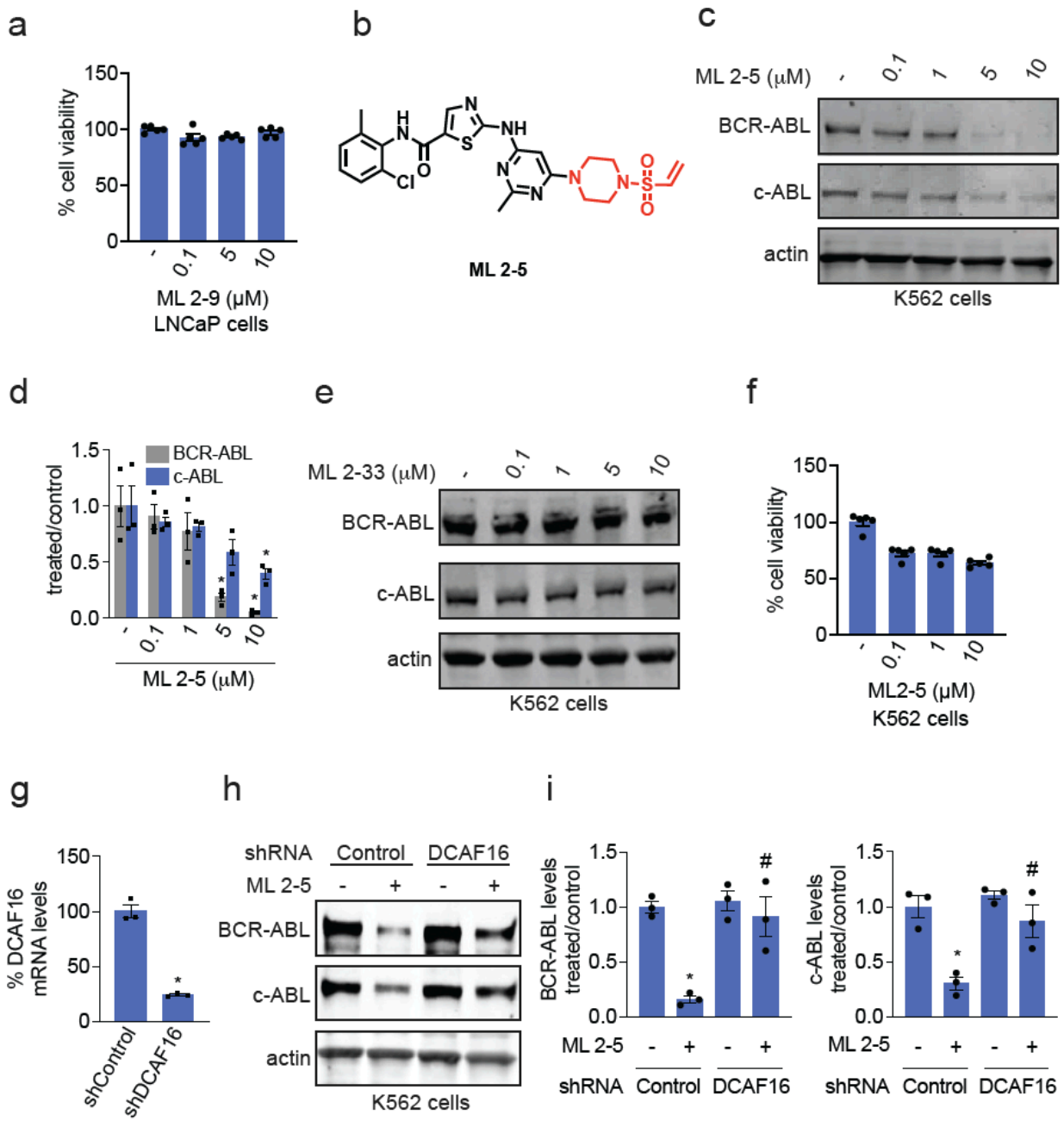

Figure S4. Characterization of AR and BCR-ABL/c-ABL Monovalent Degraders. (a) LNCaP cell viability. LNCaP cells were treated with DMSO vehicle or ML 2-9 for 24 h and cell viability

was assessed by CellTiter-Glo. **(b)** Structure of ML 2-5 with a dasatinib derivative bearing a vinylsulfonyl piperazine covalent chemical handle in red. **(c,d)** BCR-ABL and c-ABL degradation in K562 leukemia cancer cells. K562 cells were treated with DMSO vehicle or ML 2-5 for 24 h and SMARCA2/4 and actin loading control levels were assessed by Western blotting **(c)** and quantified in **(d)**. **(e)** BCR-ABL and c-ABL levels in K562 cells. K562 cells were treated with DMSO vehicle or ML 2-33 for 24 h and BCR-ABL and c-ABL levels were assessed by Western blotting. **(f)** K562 cell viability. K562 cells were treated with DMSO vehicle or ML 2-5 for 24 h and cell viability was assessed by CellTiter-Glo. **(g)** qPCR of DCAF16 knockdown. DCAF16 mRNA expression in shControl and shDCAF16 K562 cells assessed by qPCR. **(h, i)** BCR-ABL and c-ABL levels in shControl and shDCAF16 cells treated with DMSO vehicle or ML 2-5 (5 μM) for 24 h, assessed by Western blotting **(h)** and quantified in **(i)** Data shown in **(a, f)** are n=5 biologically independent replicates per group. Data shown in **(c,d,e,g,h,i)** are n=3 biologically independent replicates per group**,** Blots in **(c,e,h)** are representative. Bar graphs in **(a, d, f, g, i)** show individual replicate values and average ± sem. Significance is expressed as *p<0.05 compared to vehicle-treated controls.

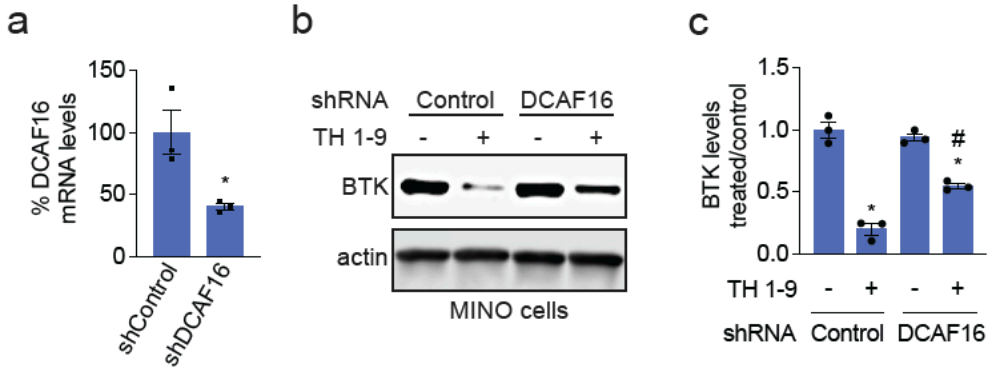

Figure S5. Characterization of the BTK Degrader TH 1-9. (a) qPCR of DCAF16 knockdown. DCAF16 mRNA expression in shControl and shDCAF16 MINO cells assessed by qPCR. **(b,c)** BTK levels in shControl and shDCAF16 cells treated with DMSO vehicle or TH 1-9 (5 μM) for 16 h, assessed by Western blotting **(b)** and quantified in **(c)** Data shown in **(a-c)** are n=3 biologically independent replicates per group. Blot in **(b)** is representative. Bar graphs in **(a,c)** show individual replicate values and average ± sem. Significance is expressed as *p<0.05 compared to shControl cells or vehicle-treated shControl cells and #p<0.05 compared to TH 1-9-treated shControl cells.

Supporting Table Legends

The following supplementary datasets have been deposited online with the submission of this dissertation.

Table S1. Quantitative proteomics of BRD4 degrader ML 1-50. Tandem mass tagging (TMT)-based quantitative proteomic profiling of ML 1-50 in MDA-MB-231 cells. MDA-MB-231 cells were treated with DMSO vehicle or ML 1-50 (1μM) for 24 h. Data are from n=3 biologically independent replicates per group.

Table S2. Chemoproteomic profiling of ML 1-50 competition against ML 2-33 probe. ML 1-50-outcompeted targets enriched by ML 2-33. HEK293T cell lysate were pre-treated with DMSO vehicle or ML 1-50 (200 μM) 1 h prior to treatment with the ML 2-33 probe (20 μM). Probe-modified proteins were subjected to copper-catalyzed azide alkyne cycloaddition (CuAAC) with an azide-functionalized biotin enrichment handle. Probe-modified proteins were avidin-enriched, tryptically digested, and analyzed by TMT-based proteomics. Data are from n=3 biologically independent replicates per group.

Table S3. isoDTB-ABPP analysis of ML 1-50. isoDTB-ABPP profiling of ML 1-50. HEK293T cells were treated with DMSO vehicle or ML 1-50 (10 μM) for 2 h. Subsequent lysates were labeled with an alkyne-functionalized iodoacetamide probe (200 μM) for 1 h, followed by CuAAC-mediated attachment of an isotopically light (for control) or heavy (for treated) azide-functionalized desthiobiotin handle, after which probe-modified proteins were streptavidin-enriched, tryptically digested, eluted from beads, and analyzed by LC-MS/MS. Data are from n=3 biologically independent replicates per group.

Table S4. Quantitative proteomics of DCAF16 WT and KO cells. TMT-based quantitative proteomic analysis of DCAF16 wild-type (WT) versus knockout (KO) cells. Data are from n=3 biologically independent replicates per group.

Table S5. Quantitative proteomics of CDK4 degrader ML 1-71. TMT-based quantitative proteomic profiling of ML 1-71 in C33A cells. C33A cells were treated with DMSO vehicle or ML 1-71 (10 μM) for 24 h. Data are from n=3 biologically independent replicates per group.

Table S6. Quantitative proteomics of AR degrader ML 2-9. TMT-based quantitative proteomic profiling of ML 2-9 in LNCaP cells. LNCaP cells were treated with DMSO vehicle or ML 2-9 (1 μM) for 24 h. Data are from n=3 biologically independent replicates per group.

Table S7. Quantitative proteomics of BTK degrader TH 1-9. TMT-based quantitative proteomic profiling of TH 1-9 in MINO cells. MINO cells were treated with DMSO vehicle or TH 1-9 (5 μM) for 24 h. Data are from n=3 biologically independent replicates per group.

Synthetic Methods and Characterization

All chemical reactions were carried out under a nitrogen atmosphere with dry solvents under anhydrous conditions, unless otherwise noted. Reagents were purchased at the highest commercial quality and used without further purification, unless otherwise stated. Room temperature is defined as between 21-25°C. Reactions were stirred magnetically and monitored by thin layer chromatography (TLC) using TLC plates precoated with silica gel 60 F254 on aluminium (Merck KGaA). Detection was by UV (254 nm and 365 nm) or chemical stain (KMnO4, ninhydrin, iodine). Solvents were removed *in vacuo* using either a Buchi R-300 Rotavapor (equipped with an I-300 Pro Interface, B-300 Base Heating Bath, Welch 2037B-01 DryFast pump, and VWR AD15R-40-V11B Circulating Bath). Solvents for silica gel chromatography were used as supplied by Sigma-Aldrich. Automated flash chromatography was performed on a Biotage Isolera instrument, equipped with a UV detector. Chromatograms were recorded at 254 and 280 nm. If additional purification is needed, compound was further purified using Thermo Scientific's semi-prep reversed phase high-performance liquid chromatography equipped (RP-HPLC: Ultimate 3000 HPLC) equipped with C18 column (Luna® 10 μm c18(2), 100 Å, Serial #:5293-0084). Elution of the sample was monitored using DIONEX UltiMate 3000. Eluting buffer A: 100% distilled water + 0.1% trifluoracetic acid (TFA). Eluting buffer B: 95% acetonitrile + 5% distilled water + 0.1% TFA. High-resolution mass spectra (HRMS) were obtained using Q Exactive™ Plus Hybrid Quadrupole-Orbitrap™ Mass Spectrometer. ^{1}H and ^{13}C Nuclear Magnetic Resonance (NMR) spectra were recorded on BRUKER AV (600 MHz and 700 MHz), AVB (400 MHz), AVQ (400 MHz) and NEO (500 MHz) spectrometers. Measurements were carried out at ambient temperature. Chemical shifts (δ) are reported in ppm with the residual solvent signal as internal standard (chloroform at 7.26 and 77.2 ppm for ^{1}H NMR and ^{13}C NMR, respectively, methanol at 3.31 and 49.0, respectively and DMSO at 2.50 and 39.5, respectively). Multiplicity is reported as follows: singlet (s), doublet (d), doublet of doublet (dd) doublet of triplet (dt), triplet (t), triplet of doublet (td), quartet (q), and multiplet (m). Coupling constants (J) are reported in Hertz (Hz). ^{13}C NMR spectra were recorded with broadband 1 H decoupling.

General Procedures

Amide Couplings

General Procedure A

The corresponding carboxylic acid (1.0 equiv.) was added to a vessel and purged with N_2 for 5 minutes. The acid was dissolved in N,N-dimethylformamide (DMF) (0.1 M) and N,N-diisopropylethylamine (DIPEA) (3 equiv.) was added. A >50% wt. solution of propylphosphonic anhydride (T3P) in EtOAc (1.5 equiv.) was added dropwise, and the reaction mixture was stirred at ambient temperature for 30 minutes. The corresponding amine (1.2 equiv.) was dissolved in DMF (0.1 M) then added dropwise and the reaction mixture was stirred at ambient temperature overnight. The reaction was quenched with 5 times the reaction volume of 5% LiCl(aq) and extracted 3 times with ethyl acetate (EtOAc). The organic extracts were washed once with brine,

dried over Na_2SO_4, vacuum filtered, and concentrated *in vacuo*. The resultant residue was purified by silica gel flash chromatography to afford the title compound.

General Procedure B

A mixture of the corresponding carboxylic acid (1.1 equiv.) and HATU (1.2 equiv.) was purged with N_2 for 5 minutes. The mixture was dissolved in DMF (0.1 M), DIPEA (3 equiv.) was added and the reaction mixture was allowed to stir at ambient temperature for 30 minutes. The corresponding amine (1 equiv.) was dissolved in DMF (0.1 M) then added dropwise and the reaction mixture was stirred at ambient temperature overnight. The reaction was quenched with 5 times the reaction volume of 5% LiCl(aq) and extracted 3 times with EtOAc. The organic extracts were dried over Na_2SO_4, vacuum filtered, and concentrated *in vacuo*. The resultant residue was purified by silica gel flash chromatography to afford the title compound.

Tert-butyloxycarbonyl Deprotection

General Procedure C

The corresponding tert-butyloxycarbonyl protected amine (1 equiv.) was dissolved in DCM (0.1 M). Trifluoroacetic acid (32 equiv.) was added, and the reaction mixture was stirred at ambient temperature for 30 minutes to overnight. The volatiles were removed *in vacuo* and the crude residue was used without further purification, unless otherwise noted.

Synthesis of Vinyl Sulfonamides

General Procedure D

The corresponding amine (1.0 equiv.) was dissolved in dichloromethane (DCM) (0.1 M) and triethylamine (3.0 equiv.) was added at 0 °C. 2-chloroethanesulfonyl chloride (0.8-1.2 equiv.) in DCM (0.1 M) was added dropwise and the resulting reaction mixture was stirred at ambient temperature overnight. The reaction was quenched with 5 times the reaction volume of water and extracted 3 times with DCM. The organic extracts were washed once with brine, dried over Na_2SO_4, vacuum filtered, and concentrated *in vacuo*. The resultant residue was purified by silica gel flash chromatography to afford the title compound.

(S)-4-(2-(4-(4-chlorophenyl)-2,3,9-trimethyl-6H-thieno[3,2-f][1,2,4]triazolo[4,3-a][1,4]diazepin-6-yl)acetamido)benzenesulfonyl fluoride (ML1-10)

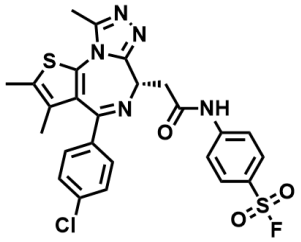

General Procedure A was followed with (S)-2-(4-(4-chlorophenyl)-2,3,9-trimethyl-6H-thieno [3,2-f][1,2,4]triazolo[4,3-a][1,4]diazepin-6-yl)acetic acid (JQ1-Acid) (50.0 mg, 0.12 mmol), T3P (0.1 mL, 0.19 mmol), DIPEA (0.07 mL, 0.37 mmol), and 4-aminobenzenesulfonyl fluoride (24.0

mg, 0.14 mmol). The crude residue was purified by silica gel chromatography (0-7% MeOH in DCM) to afford 16.6 mg (24%) of the title compound as a yellow-white powder.
^{1}H NMR (600 MHz, $CDCl_3$) δ 10.54 (s, 1H), 7.76 (d, *J* = 9.0 Hz, 2H), 7.72 (d, *J* = 9.0 Hz, 2H), 7.40 (d, *J* = 8.5 Hz, 2H), 7.31 (d, *J* = 8.8 Hz, 2H), 4.75 (dd, *J* = 9.7, 4.5 Hz, 1H), 3.99 (dd, *J* = 15.0, 9.7 Hz, 1H), 3.59 (dd, *J* = 15.0, 4.5 Hz, 1H), 2.72 (s, 3H), 2.44 (s, 2H), 1.71 (s, 2H).
^{13}C NMR (151 MHz, $CDCl_3$) δ 169.72, 164.43, 155.93, 150.35, 145.15, 137.14, 136.24, 131.89, 131.42, 131.03, 130.60, 129.90, 129.56, 128.78, 126.48, 126.32, 119.48, 54.24, 40.36, 14.42, 13.14, 11.86.
HRMS (ESI) m/z calcd for $C_{25}H_{21}ClFN_5NaO_3S_2^+$ $[M+Na]^+$: 580.0651; found: 580.0651

(S)-tert-butyl (4-(2-(4-(4-chlorophenyl)-2,3,9-trimethyl-6H-thieno[3,2-f][1,2,4]triazolo[4,3-a][1,4]diazepin-6-yl)acetamido)phenyl) carbonate (ML1-13)

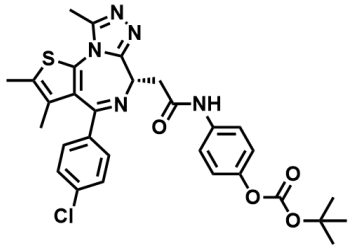

General Procedure A was followed with (S)-2-(4-(4-chlorophenyl)-2,3,9-trimethyl-6H-thieno [3,2-f][1,2,4]triazolo[4,3-a][1,4]diazepin-6-yl)acetic acid (JQ1-Acid) (30.0 mg, 0.07 mmol), T3P (0.07 mL, 0.11 mmol), DIPEA (0.04 mL, 0.22 mmol), and 4-aminophenyl tert-butyl carbonate (17.0 mg, 0.08 mmol). The crude residue was purified by silica gel chromatography (0-7% MeOH in DCM) to afford 30.0 mg (68%) of the title compound as a yellow-white powder.
^{1}H NMR (600 MHz, $CDCl_3$) δ 9.36 (s, 1H), 7.57 (d, *J* = 9.0 Hz, 2H), 7.39 (d, *J* = 8.3 Hz, 2H), 7.30 (d, *J* = 8.8 Hz, 2H), 7.05 (d, *J* = 9.0 Hz, 2H), 4.68 (dd, *J* = 8.1, 5.9 Hz, 1H), 3.81 (dd, *J* = 14.4, 8.2 Hz, 1H), 3.58 (dd, *J* = 14.3, 5.9 Hz, 1H), 2.67 (s, 3H), 2.39 (s, 3H), 1.67 (s, 3H), 1.53 (s, 9H).
^{13}C NMR (151 MHz, $CDCl_3$) δ 168.91, 164.05, 155.79, 151.92, 149.99, 147.08, 136.86, 136.51, 136.00, 132.08, 130.99, 130.96, 130.52, 129.88, 128.72, 121.46, 120.78, 83.35, 54.59, 40.36, 27.71, 14.38, 13.09, 11.82.
HRMS (ESI) m/z calcd for $C_{30}H_{30}ClN_5NaO_4S^+$ $[M+Na]^+$: 614.1599; found:614.1600

(S)-2,4-dichloro-5-(2-(4-(4-chlorophenyl)-2,3,9-trimethyl-6H-thieno[3,2-f][1,2,4]triazolo[4,3-a][1,4]diazepin-6-yl)acetamido)phenyl ethyl carbonate (ML1-14)

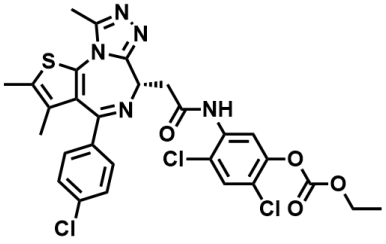

General Procedure A was followed with (S)-2-(4-(4-chlorophenyl)-2,3,9-trimethyl-6H-thieno [3,2-f][1,2,4]triazolo[4,3-a][1,4]diazepin-6-yl)acetic acid (JQ1-Acid) (30.0 mg, 0.07 mmol), T3P

(0.07 mL, 0.11 mmol), DIPEA (0.04 mL, 0.22 mmol), and 5-amino-2,4-dichlorophenyl ethyl carbonate (20.6 mg, 0.08 mmol). The crude residue was purified by silica gel chromatography (0-8% MeOH in DCM) to afford 5.0 mg (10.6%) of the title compound as a yellow-white powder.
^{1}H NMR (600 MHz, $CDCl_3$) δ 8.98 (s, 1H), 8.50 (s, 1H), 7.44 (s, 1H), 7.43 (d, *J* = 8.5 Hz, 2H), 7.34 (d, *J* = 8.8 Hz, 2H), 4.60 (t, *J* = 6.5 Hz, 1H), 4.33 (q, *J* = 7.2 Hz, 2H), 3.77 (dd, *J* = 14.6, 6.9 Hz, 1H), 3.58 (dd, *J* = 14.5, 6.1 Hz, 1H), 2.68 (s, 3H), 2.41 (d, *J* = 0.8 Hz, 3H), 1.71 – 1.68 (m, 3H), 1.38 (t, *J* = 7.1 Hz, 3H).
^{13}C NMR (151 MHz, $CDCl_3$) δ 169.09, 164.38, 152.30, 150.09, 146.02, 137.08, 134.61, 132.26, 130.26, 129.94, 129.68, 128.76, 121.58, 120.49, 116.07, 65.52, 54.22, 40.80, 14.43, 14.16, 13.11, 11.84.
HRMS (ESI) m/z calcd for $C_{28}H_{24}Cl_3N_5NaO_4S^+$ $[M+Na]^+$: 654.0507; found: 654.0512

(S)-2-(4-(4-chlorophenyl)-2,3,9-trimethyl-6H-thieno[3,2-f][1,2,4]triazolo[4,3-a][1,4]diazepin-6-yl)-N-(2,4-dioxo-1,4-dihydro-2H-benzo[d][1,3]oxazin-7-yl)acetamide (ML1-15)

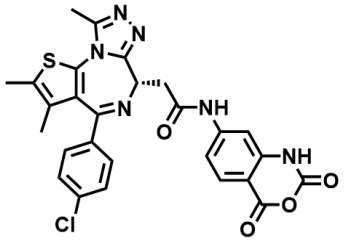

General Procedure A was followed with (S)-2-(4-(4-chlorophenyl)-2,3,9-trimethyl-6H-thieno [3,2-f][1,2,4]triazolo[4,3-a][1,4]diazepin-6-yl)acetic acid (JQ1-Acid) (30.0 mg, 0.07 mmol), T3P (0.07 mL, 0.11 mmol), DIPEA (0.04 mL, 0.22 mmol), and 7-amino-2H-benzo[d][1,3]oxazine-2,4 (1H)-dione (14.7 mg, 0.08 mmol). The crude residue was purified by silica gel chromatography (0-8% MeOH in DCM) to afford 8.6 mg (20.5%) of the title compound as a yellow-white powder.
^{1}H NMR (600 MHz, $CDCl_3$) δ 11.23 (s, 1H), 10.42 (s, 1H), 7.47 (s, 1H), 7.38 (d, *J* = 8.2 Hz, 2H), 7.21 (d, *J* = 8.2 Hz, 2H), 5.03 – 5.00 (m, 1H), 4.24 – 4.21 (m, 1H), 3.76 – 3.73 (m, 1H), 2.72 (s, 3H), 2.38 (s, 3H), 1.72 (s, 3H).
^{13}C NMR (151 MHz, $CDCl_3$) δ 164.37, 156.26, 155.10, 153.41, 150.58, 136.64, 136.56, 131.85, 131.03, 130.95, 130.43, 130.00, 129.78, 129.04, 128.53, 115.66, 54.18, 40.37, 14.38, 13.11, 11.93.
HRMS (ESI) m/z calcd for $C_{27}H_{21}ClN_6NaO_4S^+$ $[M+Na]^+$: 583.0926; found: 583.0934

(S)-2-(4-(4-chlorophenyl)-2,3,9-trimethyl-6H-thieno[3,2-f][1,2,4]triazolo[4,3-a][1,4]diazepin-6-yl)-N-(2-methoxy-3,4-dioxocyclobut-1-en-1-yl)acetamide (ML1-16)

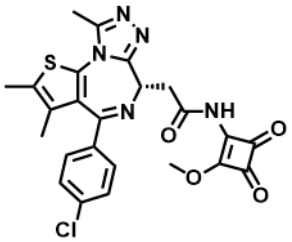

General Procedure A was followed with (S)-2-(4-(4-chlorophenyl)-2,3,9-trimethyl-6H-thieno [3,2-f][1,2,4]triazolo[4,3-a][1,4]diazepin-6-yl)acetic acid (JQ1-Acid) (30.0 mg, 0.07 mmol), T3P (0.07 mL, 0.11 mmol), DIPEA (0.04 mL, 0.22 mmol), and 3-amino-4-methoxycyclobut-3-ene-1,2-dione (10.5 mg, 0.08 mmol). The crude residue was purified by silica gel chromatography (0-7% MeOH in DCM) to afford 8.0 mg (21.0%) of the title compound as a yellow-white powder.
^{1}H NMR (600 MHz, $CDCl_3$) δ 10.97 (s, 1H), 7.42 (d, *J* = 8.3 Hz, 2H), 7.35 (d, *J* = 8.8 Hz, 2H), 4.65 (t, *J* = 6.5 Hz, 1H), 4.50 (s, 3H), 3.81 (dd, *J* = 8.0, 6.5 Hz, 2H), 2.72 (s, 3H), 2.42 (s, 3H), 1.70 (s, 3H).
^{13}C NMR (151 MHz, $CDCl_3$) δ 168.01, 150.62, 150.36, 136.05, 135.32, 132.58, 132.13, 132.12, 131.30, 131.03, 129.94, 128.87, 61.21, 53.67, 39.03, 14.47, 13.13, 11.73.
HRMS (ESI) m/z calcd for $C_{24}H_{20}ClN_5NaO_4S^+$ $[M+Na]^+$: 532.0817; found: 532.0819

(S)-2-(4-(4-chlorophenyl)-2,3,9-trimethyl-6H-thieno[3,2-f][1,2,4]triazolo[4,3-a][1,4]diazepin-6-yl)-N-(6-formylpyridin-3-yl)acetamide (ML1-17)

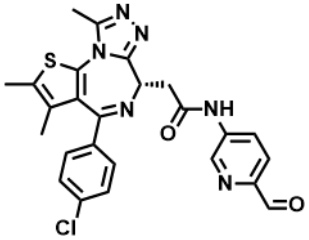

General Procedure A was followed with (S)-2-(4-(4-chlorophenyl)-2,3,9-trimethyl-6H-thieno [3,2-f][1,2,4]triazolo[4,3-a][1,4]diazepin-6-yl)acetic acid (JQ1-Acid) (30.0 mg, 0.07 mmol), T3P (0.07 mL, 0.11 mmol), DIPEA (0.04 mL, 0.22 mmol), and 5-aminopicolinaldehyde (10.5 mg, 0.08 mmol). The crude residue was purified by silica gel chromatography (0-7% MeOH in DCM) to afford 4.0 mg (10.5%) of the title compound as a yellow-white powder.
^{1}H NMR (600 MHz, $CDCl_3$) δ 10.45 (s, 1H), 9.91 (s, 1H), 8.75 (d, *J* = 2.4 Hz, 1H), 8.22 (dd, *J* = 8.5, 2.4 Hz, 1H), 7.78 (d, *J* = 8.5 Hz, 1H), 7.41 (d, *J* = 8.4 Hz, 2H), 7.32 (d, *J* = 8.7 Hz, 2H), 4.76 (dd, *J* = 9.2, 4.6 Hz, 1H), 3.97 (dd, *J* = 14.9, 9.3 Hz, 1H), 3.63 (dd, *J* = 14.9, 4.7 Hz, 1H), 2.72 (s, 3H), 2.44 (s, 3H), 1.71 (s, 3H).
^{13}C NMR (151 MHz, $CDCl_3$) δ 192.15, 169.82, 164.47, 155.82, 150.34, 147.97, 141.08, 139.10, 137.17, 136.22, 131.94, 131.43, 131.02, 130.56, 129.89, 128.81, 126.17, 122.50, 54.27, 40.19, 14.43, 13.16, 11.88.
HRMS (ESI) m/z calcd for $C_{25}H_{21}ClN_6NaO_2S^+$ $[M+Na]^+$: 527.1027; found: 527.1034

(S)-2-(4-(4-chlorophenyl)-2,3,9-trimethyl-6H-thieno[3,2-f][1,2,4]triazolo[4,3-a][1,4]diazepin-6-yl)-N-(6-formylpyridin-2-yl)acetamide (ML1-25)

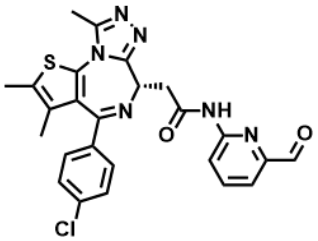

General Procedure A was followed with (S)-2-(4-(4-chlorophenyl)-2,3,9-trimethyl-6H-thieno [3,2-f][1,2,4]triazolo[4,3-a][1,4]diazepin-6-yl)acetic acid (JQ1-Acid) (25.0 mg, 0.06 mmol), T3P (0.06 mL, 0.09 mmol), DIPEA (0.03 mL, 0.19 mmol), and 6-aminopicolinaldehyde (9.1 mg, 0.07 mmol). The crude residue was purified by silica gel chromatography (0-7% MeOH in DCM) to afford 6.0 mg (19.0%) of the title compound as a yellow-white powder.

^{1}H NMR (600 MHz, $CDCl_3$) δ 9.96 (s, 1H), 9.42 (s, 1H), 8.46 (d, *J* = 8.3 Hz, 1H), 7.87 (t, *J* = 7.9 Hz, 1H), 7.69 (d, *J* = 7.4 Hz, 1H), 7.52 (d, *J* = 8.1 Hz, 2H), 7.36 (d, *J* = 8.7 Hz, 2H), 4.66 (t, *J* = 6.8 Hz, 1H), 3.70 (d, *J* = 6.9 Hz, 2H), 2.69 (s, 3H), 2.41 (s, 3H), 1.69 (s, 3H).

^{13}C NMR (151 MHz, $CDCl_3$) δ 192.68, 169.71, 164.55, 155.29, 151.79, 150.99, 150.14, 139.25, 137.16, 136.39, 132.32, 131.06, 130.98, 130.29, 129.98, 128.82, 118.66, 117.83, 54.13, 41.03, 40.35, 14.47, 13.12, 11.88.

HRMS (ESI) m/z calcd for $C_{25}H_{21}ClN_6NaO_2S^+$ $[M+Na]^+$: 527.1027; found: 527.1024

tert-butyl (S)-4-(2-(4-(4-chlorophenyl)-2,3,9-trimethyl-6H-thieno[3,2-f][1,2,4]triazolo[4,3-a] [1,4]diazepin-6-yl)acetyl)piperazine-1-carboxylate (ML1-26)

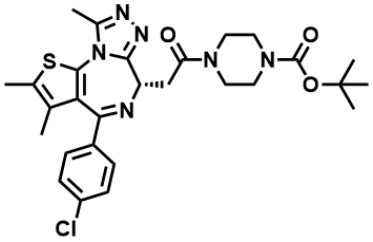

General Procedure A was followed with (S)-2-(4-(4-chlorophenyl)-2,3,9-trimethyl-6H-thieno [3,2-f][1,2,4]triazolo[4,3-a][1,4]diazepin-6-yl)acetic acid (JQ1-Acid) (322.0 mg, 0.80 mmol), T3P (0.53 mL, 0.88 mmol), DIPEA (0.56 mL, 3.21 mmol), and 1-boc-piperazine (179.5 mg, 0.96 mmol). The crude residue was purified by silica gel chromatography (0-5% MeOH in DCM) to afford 338.9 mg (74.1%) of the title compound as a yellow oil.

^{1}H NMR (600 MHz, $CDCl_3$) δ 7.41 (d, *J* = 8.6 Hz, 2H), 7.34 (d, *J* = 8.7 Hz, 2H), 4.84 – 4.79 (m, 1H), 3.84 (ddd, *J* = 13.3, 6.3, 3.5 Hz, 1H), 3.75 (dd, *J* = 15.9, 6.2 Hz, 2H), 3.72 – 3.65 (m, 1H), 3.58 (ddp, *J* = 15.4, 7.6, 4.0 Hz, 4H), 3.52 (s, 1H), 3.41 (ddd, *J* = 13.2, 7.5, 3.6 Hz, 1H), 2.68 (s, 3H), 2.41 (d, *J* = 0.9 Hz, 3H), 1.69 (s, 3H), 1.50 (s, 9H).

^{13}C NMR (151 MHz, $CDCl_3$) δ 169.22, 163.71, 155.82, 154.61, 149.83, 136.82, 136.67, 132.24, 130.91, 130.65, 130.52, 129.80, 128.69, 80.25, 54.47, 45.74, 41.70, 35.35, 28.41, 14.35, 13.06, 11.83.

HRMS (ESI) m/z calcd for $C_{28}H_{33}ClN_6NaO_3S^+$ $[M+Na]^+$: 591.1916; found: 691.1922

(S)-4-(4-(2-(4-(4-chlorophenyl)-2,3,9-trimethyl-6H-thieno[3,2-f][1,2,4]triazolo[4,3-a][1,4]diazepin-6-yl)acetyl)piperazine-1-carbonyl)-2-hydroxybenzaldehyde (ML1-29)

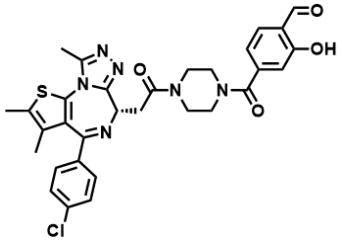

General Procedure C was followed with **ML1-26** (35.0 mg, 0.06 mmol), and TFA (0.15 mL, 1.97 mmol) for 2 hours. The crude material was used without further purification.

General Procedure A was followed with 4-formyl-3-hydroxybenzoic acid (12.8 mg, 0.08 mmol), T3P (0.06 mL, 0.10 mmol), DIPEA (0.06 mL, 0.32 mmol), and the amine from above (30.0 mg, 0.06 mmol). The crude residue was purified by silica gel chromatography (0-7% MeOH in DCM) to afford 10.0 mg (25.3%) of the title compound as a yellow-white powder.

^{1}H NMR (600 MHz, $CDCl_3$) δ 11.12 (s, 1H), 9.95 (s, 1H), 7.67 (d, *J* = 7.8 Hz, 1H), 7.39 (d, *J* = 8.2 Hz, 2H), 7.33 (d, *J* = 8.7 Hz, 2H), 7.06 (d, *J* = 6.4 Hz, 0H), 7.02 (s, 1H), 4.80 (t, *J* = 6.8 Hz, 1H), 4.02 – 3.97 (m, 2H), 3.91 – 3.84 (m, 1H), 3.81 – 3.78 (m, 2H), 3.63 – 3.56 (m, 2H), 3.51 – 3.45 (m, 1H), 3.44 – 3.39 (m, 2H), 2.67 (s, 3H), 2.40 (s, 3H), 1.67 (s, 1H).

^{13}C NMR (151 MHz, $CDCl_3$) δ 196.18, 168.70, 163.96, 161.66, 149.97, 143.44, 136.81, 136.70, 134.37, 132.20, 130.94, 130.45, 129.79, 128.77, 121.11, 118.20, 116.10, 54.36, 46.34, 41.96, 14.42, 13.14, 11.88.

HRMS (ESI) m/z calcd for $C_{31}H_{29}ClN_6NaO_4S^+$ $[M+Na]^+$: 639.1552; found: 639.1562

(*S*)-5-(4-(2-(4-(4-chlorophenyl)-2,3,9-trimethyl-6*H*-thieno[3,2-*f*][1,2,4]triazolo[4,3-*a*][1,4]diazepin-6-yl)acetyl)piperazine-1-carbonyl)-1*H*-pyrrole-3-sulfonyl fluoride (ML1-30)

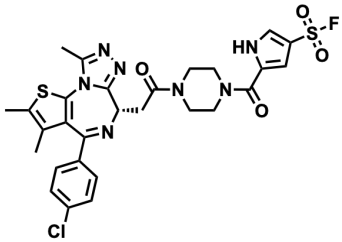

General Procedure C was followed with **ML1-26** (35.0 mg, 0.06 mmol), and TFA (0.15 mL, 1.97 mmol) for 2 hours. The crude material was used without further purification.

General Procedure A was followed with 4-(fluorosulfonyl)-1H-pyrrole-2-carboxylic acid (14.8 mg, 0.08 mmol), T3P (0.06 mL, 0.10 mmol), DIPEA (0.06 mL, 0.32 mmol), and the amine from above (30.0 mg, 0.06 mmol). The crude residue was purified by silica gel chromatography (0-7% MeOH in DCM) to afford 24.8 mg (60.2%) of the title compound as a yellow-white powder.

^{1}H NMR (600 MHz, $CDCl_3$) δ 11.71 (s, 1H), 7.66 (s, 1H), 7.40 (d, *J* = 8.3 Hz, 2H), 7.33 (d, *J* = 8.3 Hz, 2H), 6.93 (d, *J* = 1.5 Hz, 1H), 4.82 (t, *J* = 6.9 Hz, 1H), 4.10 – 4.01 (m, 2H), 3.96 (tt, *J* = 15.2, 6.8 Hz, 3H), 3.89 – 3.75 (m, 3H), 3.67 – 3.60 (m, 1H), 3.52 (dd, *J* = 16.3, 6.4 Hz, 1H), 2.67 (s, 3H), 2.40 (s, 3H), 1.68 (s, 3H).

^{13}C NMR (151 MHz, $CDCl_3$) δ 169.57, 164.00, 160.46, 155.72, 149.99, 136.82, 136.71, 132.16, 130.94, 130.90, 130.54, 129.81, 128.75, 127.05, 126.70, 116.16, 115.96, 111.68, 54.57, 45.44, 41.37, 35.36, 31.92, 22.68, 14.36, 13.09, 11.81.
HRMS (ESI) m/z calcd for $C_{28}H_{27}ClFN_7NaO_4S_2^+$ $[M+Na]^+$: 666.1131; found: 666.1127

(*S*)-4-(4-(2-(4-(4-chlorophenyl)-2,3,9-trimethyl-6*H*-thieno[3,2-*f*][1,2,4]triazolo[4,3-*a*][1,4]diazepin-6-yl)acetyl)piperazine-1-carbonyl)benzenesulfonyl fluoride (ML1-31)

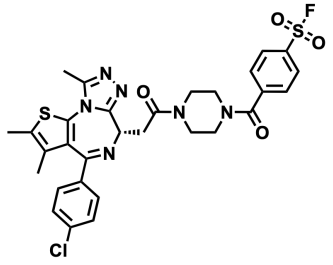

General Procedure C was followed with **ML1-26** (35.0 mg, 0.06 mmol), and TFA (0.15 mL, 1.97 mmol) for 2 hours. The crude material was used without further purification.
General Procedure A was followed with 4-(fluorosulfonyl)benzoic acid (15.7 mg, 0.08 mmol), T3P (0.06 mL, 0.10 mmol), DIPEA (0.06 mL, 0.32 mmol), and the amine from above (30.0 mg, 0.06 mmol). The crude residue was purified by silica gel chromatography (0-7% MeOH in DCM) to afford 22.7 mg (54.2%) of the title compound as a yellow-white powder.
^{1}H NMR (600 MHz, $CDCl_3$) δ 8.10 (d, J = 8.2 Hz, 2H), 7.68 (d, J = 8.0 Hz, 2H), 7.39 (d, J = 8.2 Hz, 2H), 7.33 (d, J = 8.6 Hz, 2H), 4.80 (dd, J = 7.4, 6.4 Hz, 1H), 4.09 – 4.00 (m, 3H), 3.88 – 3.81 (m, 2H), 3.74 – 3.30 (m, 6H), 2.67 (s, 3H), 2.40 (s, 3H), 1.67 (s, 3H).
^{13}C NMR (151 MHz, $CDCl_3$) δ 155.77, 150.10, 142.56, 136.96, 136.83, 134.54, 134.37, 132.31, 131.06, 131.00, 130.61, 129.91, 129.12, 128.88, 128.54, 128.46, 32.04, 30.44, 29.47, 22.81, 14.48, 13.21, 11.92.
HRMS (ESI) m/z calcd for $C_{30}H_{28}ClFN_6NaO_4S_2^+$ $[M+Na]^+$: 677.1178; found: 677.1175

(*S*)-3-(4-(2-(4-(4-chlorophenyl)-2,3,9-trimethyl-6*H*-thieno[3,2-*f*][1,2,4]triazolo[4,3-*a*][1,4]diazepin-6-yl)acetyl)piperazine-1-carbonyl)benzenesulfonyl fluoride (ML1-32)

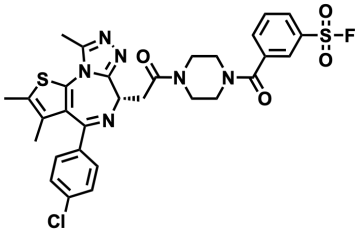

General Procedure C was followed with **ML1-26** (35.0 mg, 0.06 mmol), and TFA (0.15 mL, 1.97 mmol) for 2 hours. The crude material was used without further purification.
General Procedure A was followed with 3-(fluorosulfonyl)benzoic acid (15.7 mg, 0.08 mmol), T3P (0.06 mL, 0.10 mmol), DIPEA (0.06 mL, 0.32 mmol), and the amine from above (30.0 mg, 0.06 mmol). The crude residue was purified by silica gel chromatography (0-7% MeOH in DCM) to afford 10.0 mg (23.9%) of the title compound as a yellow-white powder.

^{1}H NMR (600 MHz, $CDCl_3$) δ 8.10 (dq, *J* = 3.3, 1.7 Hz, 2H), 7.85 (dt, *J* = 7.7, 1.4 Hz, 1H), 7.74 (t, *J* = 8.1 Hz, 1H), 7.40 (d, *J* = 8.3 Hz, 2H), 7.34 (d, *J* = 8.5 Hz, 2H), 4.82 (t, *J* = 6.8 Hz, 1H), 4.11 – 3.95 (m, 2H), 3.84 (dd, *J* = 15.9, 7.1 Hz, 2H), 3.78 – 3.30 (m, 5H), 2.69 (s, 3H), 2.40 (s, 3H), 1.68 (s, 3H).
^{13}C NMR (151 MHz, $CDCl_3$) δ 169.41, 167.64, 164.04, 155.64, 150.02, 137.17, 136.89, 136.64, 134.05, 132.04, 130.99, 130.62, 130.25, 129.79, 129.72, 128.77, 127.31, 35.26, 31.92, 30.32, 22.68, 14.36, 13.09, 11.75.
HRMS (ESI) m/z calcd for $C_{30}H_{28}ClFN_6NaO_4S_2^+$ $[M+Na]^+$: 677.1178; found: 677.1183

(*S*)-butyl (4-(4-(2-(4-(4-chlorophenyl)-2,3,9-trimethyl-6*H*-thieno[3,2-*f*][1,2,4]triazolo[4,3-*a*][1, 4]diazepin-6-yl)acetyl)piperazine-1-carbonyl)phenyl) carbonate (ML1-33)

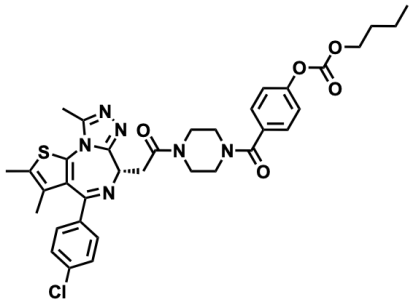

General Procedure C was followed with **ML1-26** (35.0 mg, 0.06 mmol), and TFA (0.15 mL, 1.97 mmol) for 2 hours. The crude material was used without further purification.
General Procedure A was followed with 4-((butoxycarbonyl)oxy)benzoic acid (18.3 mg, 0.08 mmol), T3P (0.06 mL, 0.10 mmol), DIPEA (0.06 mL, 0.32 mmol), and the amine from above (30.0 mg, 0.06 mmol). The crude residue was purified by silica gel chromatography (0-7% MeOH in DCM) to afford 27.0 mg (61.2%) of the title compound as a yellow-white powder.
^{1}H NMR (600 MHz, $CDCl_3$) δ 7.48 (d, *J* = 8.6 Hz, 2H), 7.40 (d, *J* = 8.4 Hz, 2H), 7.33 (d, *J* = 8.6 Hz, 2H), 7.27 (d, *J* = 4.3 Hz, 2H), 4.80 (t, *J* = 6.8 Hz, 1H), 4.27 (t, *J* = 6.7 Hz, 2H), 3.93 (s, 2H), 3.80 (dd, *J* = 15.8, 6.9 Hz, 2H), 3.54 (s, 6H), 2.66 (s, 3H), 2.39 (s, 3H), 1.78 – 1.70 (m, 2H), 1.67 (s, 3H), 1.51 – 1.44 (m, 2H), 0.97 (t, *J* = 7.4 Hz, 3H).
^{13}C NMR (151 MHz, $CDCl_3$) δ 169.74, 169.35, 163.87, 155.72, 153.30, 152.30, 149.89, 136.76, 136.75, 132.83, 132.23, 130.92, 130.74, 130.49, 129.79, 128.74, 128.72, 121.37, 68.97, 54.55, 35.30, 30.57, 29.68, 18.91, 14.35, 13.63, 13.07, 11.81.
HRMS (ESI) m/z calcd for $C_{35}H_{37}ClN_6NaO_5S^+$ $[M+Na]^+$: 711.2127; found: 711.2125

(*S*)-2-(2-(4-(2-(4-(4-chlorophenyl)-2,3,9-trimethyl-6*H*-thieno[3,2-*f*][1,2,4]triazolo[4,3-*a*][1,4]diazepin-6-yl)acetyl)piperazin-1-yl)-2-oxoethoxy)isoindoline-1,3-dione (ML1-43)

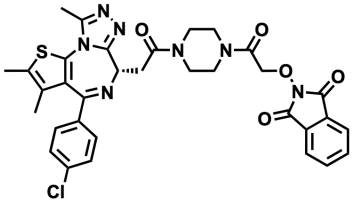

General Procedure C was followed with **ML1-26** (35.0 mg, 0.06 mmol), and TFA (0.15 mL, 1.97 mmol) for 2 hours. The crude material was used without further purification.
General Procedure B was followed with 2-((1,3-dioxoisoindolin-2-yl)oxy)acetic acid (15.6 mg, 0.07 mmol), HATU (29.3 mg, 0.08 mmol), DIPEA (0.05 mL, 0.26 mmol), and the amine from above (30.0 mg, 0.06 mmol). The crude residue was purified by silica gel chromatography (0-7% MeOH in DCM) to afford 5.0 mg (11.6%) of the title compound as a yellow-white powder.
^{1}H NMR (500 MHz, $CDCl_3$) δ 7.88 (dd, *J* = 5.4, 3.0 Hz, 2H), 7.76 (dd, *J* = 5.5, 3.1 Hz, 2H), 7.35 (d, *J* = 8.5 Hz, 2H), 7.26 (d, *J* = 8.7 Hz, 2H), 4.74 (dd, *J* = 7.2, 5.9 Hz, 1H), 4.69 (s, 2H), 3.74 (q, *J* = 5.3 Hz, 2H), 3.71 – 3.62 (m, 2H), 3.63 – 3.51 (m, 2H), 2.77 (ddd, *J* = 6.4, 4.0, 2.2 Hz, 2H), 2.70 – 2.65 (m, 2H), 2.63 (s, 3H), 2.37 (s, 3H), 1.64 (s, 3H).
^{13}C NMR (151 MHz, $CDCl_3$) δ 167.76, 162.97, 149.94, 136.76, 136.72, 134.76, 132.47, 132.06, 131.00, 130.92, 130.88, 130.64, 129.85, 128.85, 128.81, 128.74, 123.81, 77.24, 77.03, 76.82, 68.17, 38.75, 30.37, 28.93, 23.76, 22.98, 14.39, 14.04, 13.10, 11.79, 10.96.
HRMS (ESI) m/z calcd for $C_{33}H_{30}ClN_7NaO_5S^+$ $[M+Na]^+$: 694.1610; found: 694.1589

(*S*)-4-((4-(2-(4-(4-chlorophenyl)-2,3,9-trimethyl-6*H*-thieno[3,2-*f*][1,2,4]triazolo[4,3-*a*][1,4]diazepin-6-yl)acetyl)piperazin-1-yl)methyl)benzenesulfonyl fluoride (ML1-45)

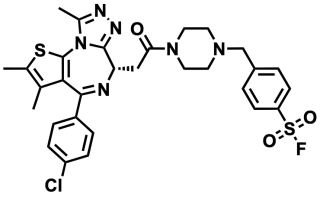

General Procedure C was followed with **ML1-26** (35.0 mg, 0.06 mmol), and TFA (0.15 mL, 1.97 mmol) for 2 hours. The crude material was used without further purification.
To a mixture of the above product (30.0 mg, 0.06 mmol) and 4-(bromomethyl)benzenesulfonyl fluoride (17.8 mg, 0.07 mmol) in DMF (1mL) was added DIPEA (0.06 mL, 0.35 mmol). The reaction was stirred at ambient temperature for 20 min and concentrated *in vacuo* before it was redissolved in EtOAc (20 mL) and saturated aqueous sodium bicarbonate (10 mL). The aqueous phase was extracted 3 times with EtOAc, and the organic extracts were washed with brine (10 mL), dried over Na2SO4, vacuum filtered, and concentrated *in vacuo*. The resultant residue was purified by silica gel chromatography (0-5% MeOH in DCM) to afford 19.9 mg (48.5 %) of the title compound as a yellow-white powder.
^{1}H NMR (600 MHz, $CDCl_3$) δ 7.98 (d, *J* = 8.4 Hz, 2H), 7.64 (d, *J* = 8.2 Hz, 2H), 7.40 (d, *J* = 8.5 Hz, 2H), 7.32 (d, *J* = 8.4 Hz, 2H), 4.83 – 4.77 (m, 1H), 3.90 – 3.84 (m, 1H), 3.80 (ddd, *J* = 13.2, 6.4, 3.3 Hz, 1H), 3.71 (dt, *J* = 15.8, 4.8 Hz, 2H), 3.66 (s, 2H), 3.59 (dtd, *J* = 19.9, 15.2, 9.3 Hz, 2H), 2.66 (s, 3H), 2.63 – 2.54 (m, 2H), 2.50 (ddd, *J* = 10.0, 6.4, 3.4 Hz, 1H), 2.43 (ddd, *J* = 11.1, 7.5, 3.3 Hz, 1H), 2.39 (s, 3H), 1.67 (s, 3H).
^{13}C NMR (151 MHz, $CDCl_3$) δ 168.99, 163.67, 155.89, 149.83, 147.10, 136.85, 136.66, 132.23, 131.90, 131.74, 130.92, 130.66, 130.56, 129.83, 129.80, 128.68, 128.60, 62.03, 54.44, 53.30, 52.86, 45.78, 41.81, 35.23, 14.35, 13.06, 11.83.
HRMS (ESI) m/z calcd for $C_{30}H_{30}ClFN_6NaO_3S_2^+$ $[M+Na]^+$: 663.1386; found: 663.1387

(*S*)-2-(4-(4-chlorophenyl)-2,3,9-trimethyl-6*H*-thieno[3,2-*f*][1,2,4]triazolo[4,3-*a*][1,4]diazepin-6-yl)-1-(4-(vinylsulfonyl)piperazin-1-yl)ethan-1-one (ML1-50)

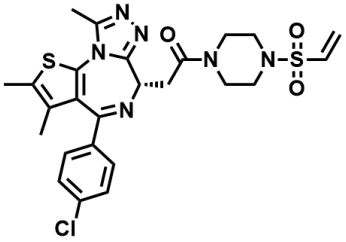

General Procedure C was followed with **ML1-26** (200.0 mg, 0.35 mmol), and TFA (0.86 mL, 11.25 mmol) for 2 hours. The crude material was used without further purification.

General Procedure D was followed with the above product (164.8 mg, 0.06 mmol), triethylamine (0.25 mL, 1.76 mmol), and 2-chloroethanesulfonyl chloride (0.04 mL, 0.39 mmol). The crude residue was purified by silica gel chromatography (0-5% MeOH in DCM) to afford 103.5mg (52.7%) of the title compound as a yellow-white powder.

^{1}H NMR (600 MHz, $CDCl_3$) δ 7.38 (d, *J* = 8.5 Hz, 2H), 7.32 (d, *J* = 8.7 Hz, 2H), 6.44 (dd, *J* = 16.6, 10.0 Hz, 1H), 6.28 (d, *J* = 16.6 Hz, 1H), 6.09 (d, *J* = 10.0 Hz, 1H), 4.77 (t, *J* = 6.8 Hz, 1H), 4.03 – 3.94 (m, 2H), 3.79 – 3.71 (m, 2H), 3.59 – 3.46 (m, 2H), 3.38 (ddd, *J* = 11.8, 5.7, 3.2 Hz, 1H), 3.27 (dddt, *J* = 22.7, 11.6, 8.1, 3.4 Hz, 2H), 3.05 (ddd, *J* = 11.7, 8.2, 3.3 Hz, 1H), 2.65 (s, 3H), 2.39 (s, 3H), 1.67 (s, 3H).

^{13}C NMR (151 MHz, $CDCl_3$) δ 177.74, 172.47, 164.27, 158.48, 145.34, 145.32, 140.79, 140.77, 139.50, 139.33, 139.04, 138.36, 138.06, 137.30, 85.81, 85.60, 85.38, 62.98, 54.25, 54.15, 53.99, 50.01, 43.86, 22.94, 21.66, 20.41.

HRMS (ESI) m/z calcd for $C_{25}H_{27}ClN_6NaO_3S_2^+$ $[M+Na]^+$: 581.1167; found: 581.1171

(*S*)-5-(4-(2-(4-(4-chlorophenyl)-2,3,9-trimethyl-6*H*-thieno[3,2-*f*][1,2,4]triazolo[4,3-*a*][1,4]diazepin-6-yl)acetyl)piperazine-1-carbonyl)picolinaldehyde (ML1-52)

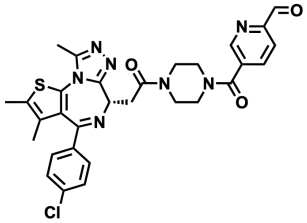

General Procedure C was followed with **ML1-26** (35.0 mg, 0.06 mmol), and TFA (0.15 mL, 1.97 mmol) for 2 hours. The crude material was used without further purification.

General Procedure B was followed with 6-formylnicotinic acid (10.2 mg, 0.07 mmol), HATU (28.1 mg, 0.07 mmol), DIPEA (0.04 mL, 0.25 mmol), and the amine from above (28.8 mg, 0.06 mmol). The crude residue was purified by silica gel chromatography (0-10% MeOH in DCM) to afford 15.0 mg (40.5%) of the title compound as a yellow-white powder.

^{1}H NMR (600 MHz, $CDCl_3$) δ 10.12 (s, 1H), 8.85 (s, 1H), 8.05 (d, *J* = 7.9 Hz, 1H), 7.95 (dd, *J* = 8.0, 2.0 Hz, 1H), 7.40 (d, *J* = 8.3 Hz, 2H), 7.33 (d, 2H), 4.80 (t, *J* = 6.9 Hz, 1H), 4.10 – 4.01 (m,

2H), 3.88 – 3.75 (m, 2H), 3.76 – 3.64 (m, 1H), 3.62 – 3.34 (m, 1H), 2.66 (s, 3H), 2.40 (s, 3H), 1.68 (s, 3H).
^{13}C NMR (151 MHz, $CDCl_3$) δ 192.43, 171.12, 166.92, 153.35, 148.43, 136.82, 136.74, 136.16, 134.90, 132.26, 130.92, 130.44, 129.77, 128.75, 121.49, 60.38, 29.69, 21.03, 14.36, 13.08, 11.83.
HRMS (ESI) m/z calcd for $C_{30}H_{28}ClN_7NaO_3S^+$ $[M+Na]^+$: 624.1555; found: 624.1563

(*S*)-3-(4-(2-(4-(4-chlorophenyl)-2,3,9-trimethyl-6*H*-thieno[3,2-*f*][1,2,4]triazolo[4,3-*a*][1,4]diazepin-6-yl)acetyl)piperazine-1-carbonyl)-4-hydroxybenzenesulfonyl fluoride (ML1-54)

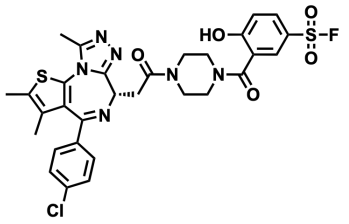

General Procedure C was followed with **ML1-26** (30.0 mg, 0.05 mmol), and TFA (0.13 mL, 1.69 mmol) for 2 hours. The crude material was used without further purification.
General Procedure A was followed with 5-(fluorosulfonyl)-2-hydroxybenzoic acid (13.9 mg, 0.06 mmol), T3P (0.04 mL, 0.06 mmol), DIPEA (0.05 mL, 0.26 mmol), and the amine from above (24.7 mg, 0.05 mmol). The crude residue was purified by silica gel chromatography (0-8% MeOH in DCM) to afford 5.5 mg (15.6%) of the title compound as a yellow-white powder.
^{1}H NMR (600 MHz, $CDCl_3$) δ 7.97 – 7.91 (m, 2H), 7.41 (d, *J* = 8.4 Hz, 2H), 7.34 (d, *J* = 8.7 Hz, 2H), 7.25 (d, *J* = 8.7 Hz, 1H), 4.82 (dd, *J* = 7.7, 6.1 Hz, 1H), 4.09 – 4.04 (m, 2H), 3.97 – 3.89 (m, 2H), 3.87 (dd, *J* = 15.8, 7.9 Hz, 1H), 3.77 (dd, *J* = 13.0, 5.7 Hz, 2H), 3.68 – 3.63 (m, 1H), 3.61 – 3.53 (m, 1H), 3.45 (dd, *J* = 15.8, 6.1 Hz, 1H), 2.68 (s, 3H), 2.42 (s, 3H), 1.69 (s, 3H).
^{13}C NMR (151 MHz, $CDCl_3$) δ 169.32, 168.37, 155.72, 149.97, 136.93, 136.59, 132.57, 132.02, 131.03, 130.98, 130.64, 129.87, 129.79, 129.59, 128.79, 119.25, 118.87, 54.58, 41.51, 35.35, 14.37, 13.10, 11.81.
HRMS (ESI) m/z calcd for $C_{30}H_{28}ClFN_6NaO_5S_2^+$ $[M+Na]^+$: 693.1127; found: 693.1132

(*S*)-2,4-di-*tert*-butyl-5-(2-(4-(4-chlorophenyl)-2,3,9-trimethyl-6*H*-thieno[3,2-*f*][1,2,4]triazolo[4,3-*a*][1,4]diazepin-6-yl)acetamido)phenyl methyl carbonate (ML1-55)

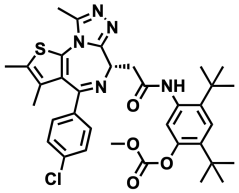

General Procedure A was followed with (S)-2-(4-(4-chlorophenyl)-2,3,9-trimethyl-6H-thieno [3,2-f][1,2,4]triazolo[4,3-a][1,4]diazepin-6-yl)acetic acid (JQ1-Acid) (25.0 mg, 0.06 mmol), T3P (0.05 mL, 0.07 mmol), DIPEA (0.04 mL, 0.25 mmol), and 5-amino-2,4-di-tert-butylphenyl methyl carbonate (19.2 mg, 0.07 mmol). The crude residue was purified by silica gel chromatography (0-8% MeOH in DCM) to afford 5.8 mg (14.0%) of the title compound as a yellow-white powder.

^{1}H NMR (400 MHz, $CDCl_3$) δ 8.03 (s, 1H), 7.49 (s, 1H), 7.42 (s, 1H), 7.39 (d, *J* = 5.1 Hz, 2H), 7.32 (d, *J* = 8.5 Hz, 2H), 4.72 (t, *J* = 6.7 Hz, 1H), 3.87 (s, 3H), 3.71 (dd, *J* = 14.6, 6.2 Hz, 1H), 3.59 (dd, *J* = 14.6, 7.2 Hz, 1H), 2.68 (s, 3H), 2.41 (s, 3H), 1.68 (s, 3H), 1.46 (s, 9H), 1.34 (s, 9H).
^{13}C NMR (151 MHz, $CDCl_3$) δ 168.68, 164.01, 155.70, 154.24, 149.99, 147.53, 139.50, 137.85, 136.82, 136.56, 133.56, 132.14, 131.00, 130.85, 130.53, 129.93, 128.68, 125.25, 121.85, 55.31, 54.23, 40.46, 34.78, 34.72, 30.79, 30.22, 14.40, 13.09, 11.81.
HRMS (ESI) m/z calcd for $C_{35}H_{40}ClN_5NaO_4S^+$ $[M+Na]^+$: 684.2382; found: 684.2385

7-cyclopentyl-*N*,*N*-dimethyl-2-((5-(4-(vinylsulfonyl)piperazin-1-yl)pyridin-2-yl)amino)-7*H*-pyrrolo[2,3-*d*]pyrimidine-6-carboxamide (ML1-71)

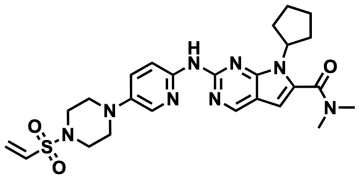

General Procedure D was followed with 7-cyclopentyl-N,N-dimethyl-2-((5-(piperazin-1-yl) pyridin-2-yl)amino)-7H-pyrrolo[2,3-d]pyrimidine-6-carboxamide (ribociclib) (50.0 mg, 0.12 mmol), triethylamine (0.05 mL, 0.35 mmol), and 2-chloroethanesulfonyl chloride (0.01 mL, 0.13 mmol). The crude residue was purified by silica gel chromatography (0-8% MeOH in DCM) to afford 21.7 mg (36.0%) of the title compound as a yellow-white powder.
^{1}H NMR (600 MHz, $CDCl_3$) δ 8.69 (s, 1H), 8.38 (d, J = 8.3 Hz, 1H), 8.00 (d, J = 2.3 Hz, 1H), 7.87 (s, 1H), 7.32 (dd, J = 9.1, 2.9 Hz, 1H), 6.48 (dd, J = 16.6, 10.0 Hz, 1H), 6.44 (s, 1H), 6.30 (d, J = 16.6 Hz, 1H), 6.10 (d, J = 10.0 Hz, 1H), 4.80 (p, J = 8.9 Hz, 1H), 3.38 – 3.34 (m, 4H), 3.25 – 3.20 (m, 5H), 2.58 (qd, J = 10.1, 5.0 Hz, 2H), 2.12 – 2.00 (m, 5H), 1.75 – 1.68 (m, 2H).
^{13}C NMR (151 MHz, $CDCl_3$) δ 164.06, 154.47, 151.96, 151.77, 147.78, 141.85, 132.32, 132.18, 129.16, 128.34, 127.52, 112.80, 112.37, 100.94, 57.90, 50.22, 45.57, 30.20, 24.73.
HRMS (ESI) m/z calcd for $C_{25}H_{33}N_8O_3S^+$ $[M+Na]^+$: 525.2391; found: 525.2382

2-(6-amino-5-(4-(vinylsulfonyl)piperazin-1-yl)pyridazin-3-yl)phenol (ML1-96)

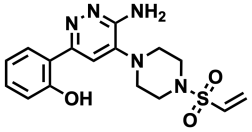

General Procedure D was followed with 2-(6-amino-5-(piperazin-1-yl)pyridazin-3-yl)phenol (50.0 mg, 0.18 mmol), triethylamine (0.08 mL, 0.55 mmol), and 2-chloroethanesulfonyl chloride (0.02 mL, 0.15 mmol). The crude residue was purified by silica gel chromatography (0-8% MeOH in DCM) and another round of purification using HPLC (buffer B : buffer A = 25:75 to 60:40) to afford 12.4 mg (18.6%) of the title compound as a yellow-white powder.
^{1}H NMR (600 MHz, $CDCl_3$) δ 7.61 (dd, *J* = 8.0, 1.6 Hz, 1H), 7.38 (s, 1H), 7.33 (ddd, *J* = 8.5, 7.3, 1.6 Hz, 1H), 7.09 (dd, *J* = 8.2, 1.2 Hz, 1H), 6.99 – 6.92 (m, 1H), 6.52 (dd, *J* = 16.6, 9.9 Hz, 1H), 6.37 (d, *J* = 16.6 Hz, 1H), 6.16 (d, *J* = 9.9 Hz, 1H), 4.81 (s, 2H), 3.43 (t, *J* = 4.9 Hz, 4H), 3.28 (t, *J* = 4.9 Hz, 4H).

^{13}C NMR (151 MHz, $CDCl_3$) δ 159.23, 155.52, 153.88, 140.25, 132.32, 131.13, 129.58, 125.18, 118.82, 118.62, 117.35, 111.46, 48.91, 45.44.
HRMS (ESI) m/z calcd for $C_{16}H_{20}N_5O_3S^+$ $[M+H]^+$: 362.1281; found: 362.1291

(*R*)-3-(4-phenoxyphenyl)-1-(1-(vinylsulfonyl)piperidin-3-yl)-1*H*-pyrazolo[3,4-*d*]pyrimidin-4-amine (TH1-9)

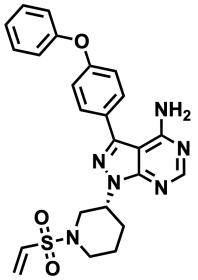

General Procedure C was followed with tert-butyl (R)-3-(4-amino-3-(4-phenoxyphenyl)-1H-pyrazolo[3,4-d]pyrimidin-1-yl)piperidine-1-carboxylate (100.0mg, 0.21mmol), and TFA (0.5 mL, 6.58 mmol) overnight. The crude material was used without further purification.
General Procedure D was followed with the above product (50.0mg, 0.13mmol), triethylamine (0.08 mL, 0.58 mmol), and 2-chloroethanesulfonyl chloride (0.02 mL, 0.19 mmol). The crude residue was purified by silica gel chromatography (0-10% MeOH in DCM) to afford 18.2 mg (29.5%) of the title compound as a yellow-white powder.
^{1}H NMR (600 MHz, $CDCl_3$) δ 8.37 (s, 1H), 7.62 (d, *J* = 8.6 Hz, 2H), 7.38 (dd, *J* = 8.6, 7.4 Hz, 2H), 7.17 (t, 1H), 7.15 (d, 2H), 7.07 (d, *J* = 7.6 Hz, 1H), 6.46 (dd, *J* = 16.6, 10.0 Hz, 1H), 6.24 (d, *J* = 16.6 Hz, 1H), 6.02 (d, *J* = 10.0 Hz, 1H), 5.50 (s, 2H), 5.05 – 4.97 (m, 1H), 4.01 – 3.94 (m, 1H), 3.81 (dt, *J* = 12.2, 2.3 Hz, 1H), 3.28 (t, *J* = 11.2 Hz, 1H), 2.72 (td, *J* = 12.2, 2.9 Hz, 1H), 2.24 – 2.18 (m, 2H), 2.02 – 1.95 (m, 1H), 1.92 – 1.83 (m, 1H).
^{13}C NMR (151 MHz, $CDCl_3$) δ 158.64, 157.76, 156.32, 156.00, 154.38, 144.04, 132.98, 129.99, 129.96, 128.57, 127.65, 124.11, 119.58, 119.13, 98.62, 52.89, 49.19, 45.52, 29.57, 24.37.
HRMS (ESI) m/z calcd for $C_{24}H_{24}N_6NaO_3S^+$ $[M+Na]^+$: 499.1523; found: 499.1523

***N*-(2-chloro-6-methylphenyl)-2-((2-methyl-6-(4-(vinylsulfonyl)piperazin-1-yl)pyrimidin-4-yl)amino)thiazole-5-carboxamide (ML2-5)**

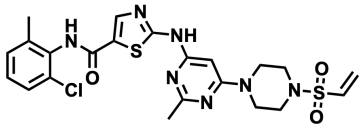

General Procedure D was followed with N-(2-chloro-6-methylphenyl)-2-((2-methyl-6-(piperazin- 1-yl)pyrimidin-4-yl)amino)thiazole-5-carboxamide (100.0 mg, 0.23 mmol), triethylamine (0.09 mL, 0.68 mmol), and 2-chloroethanesulfonyl chloride (0.02 mL, 0.23 mmol). The crude residue was purified by silica gel chromatography (50-100% EtOAc in Hexanes) to afford 35.6 mg (29.6%) of the title compound as a yellow-white powder.
^{1}H NMR (600 MHz, DMSO) δ 11.52 (s, 1H), 9.87 (s, 1H), 8.23 (s, 1H), 7.40 (dd, *J* = 7.8, 1.7 Hz, 1H), 7.28 (dt, *J* = 15.4, 7.5 Hz, 2H), 6.83 (dd, *J* = 16.5, 10.0 Hz, 1H), 6.20 (d, *J* = 10.0 Hz, 1H),

6.16 (d, *J* = 16.5 Hz, 1H), 6.11 (s, 1H), 3.66 (t, *J* = 5.1 Hz, 4H), 3.31 (s, 3H), 3.14 (t, *J* = 5.1 Hz, 4H), 2.43 (s, 3H), 2.25 (s, 3H).
^{13}C NMR (151 MHz, DMSO) δ 170.21, 165.22, 162.37, 162.08, 159.78, 157.01, 140.71, 138.71, 133.41, 132.42, 132.33, 129.64, 128.92, 128.07, 126.90, 125.73, 82.99, 59.63, 44.75, 43.02, 25.44, 20.65, 18.18, 13.98.
HRMS (ESI) m/z calcd for $C_{22}H_{24}ClN_7NaO_3S_2^+$ $[M+Na]^+$: 556.0963; found: 556.0966

***tert*-butyl 4-(6-(((1*r*,4*r*)-4-(3-chloro-4-cyanophenoxy)cyclohexyl)carbamoyl)pyridazin-3-yl) piperazine-1-carboxylate (ML2-8)**

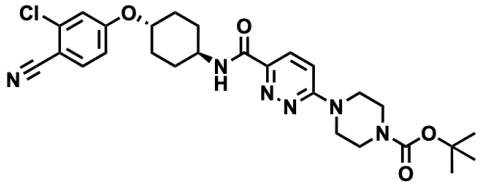

To 6-chloro-N-((1r,4r)-4-(3-chloro-4-cyanophenoxy)cyclohexyl)pyridazine-3-carboxamide (200.0 mg, 0.51 mmol) in DMF (4 mL) was added 1-boc-piperazine (142.8 mg, 0.77 mmol), followed by triethylamine (0.21 mL, 1.53 mmol). The resultant mixture was stirred at 80 °C overnight. It was then cooled to RT and the precipitate was filtered off and dried to afford 156.6mg (56.6%) of the title compound as a white powder.
^{1}H NMR (400 MHz, $CDCl_3$) δ 8.01 (d, *J* = 9.5 Hz, 1H), 7.84 (d, *J* = 8.5 Hz, 1H), 7.54 (d, *J* = 8.6 Hz, 1H), 7.01 – 6.94 (m, 2H), 6.84 (dd, *J* = 8.8, 2.5 Hz, 1H), 4.31 (tt, *J* = 9.9, 3.6 Hz, 1H), 4.04 (dtt, *J* = 10.8, 7.4, 3.9 Hz, 1H), 3.78 – 3.71 (m, 4H), 3.62 – 3.54 (m, 4H), 2.16 (tt, *J* = 10.8, 4.2 Hz, 5H), 1.81 – 1.59 (m, 2H), 1.48 (s, 9H), 1.45 – 1.31 (m, 2H).
^{13}C NMR (151 MHz, $CDCl_3$) δ 162.60, 161.63, 160.20, 154.64, 144.83, 138.35, 135.08, 126.98, 116.94, 116.40, 114.66, 112.28, 104.86, 80.44, 75.68, 47.12, 30.03, 29.67, 28.41.
HRMS (ESI) m/z calcd for $C_{27}H_{33}ClN_6NaO_4^+$ $[M+Na]^+$: 563.2144; found: 563.2146

***N*-((1*r*,4*r*)-4-(3-chloro-4-cyanophenoxy)cyclohexyl)-6-(4-(vinylsulfonyl)piperazin-1-yl)pyridazine-3-carboxamide (ML2-9)**

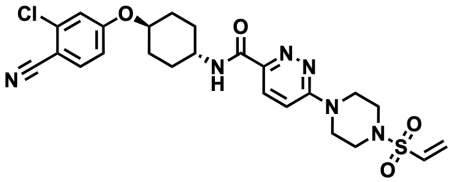

General Procedure C was followed with **ML2-8** (70.0 mg, 0.13 mmol), and TFA (0.32 mL, 4.14 mmol) for 2 hours. The crude material was used without further purification.
General Procedure D was followed with the above product (57.1 mg, 0.13 mmol), triethylamine (0.08 mL, 0.58 mmol), and 2-chloroethanesulfonyl chloride (0.02 mL, 0.16 mmol). The crude residue was purified by silica gel chromatography (0-100% EtOAc in Hexanes) to afford 27.4mg (39.9%) of the title compound as a yellow-white powder.
^{1}H NMR (600 MHz, $CDCl_3$) δ 8.05 (d, *J* = 9.4 Hz, 1H), 7.84 (d, *J* = 8.2 Hz, 1H), 7.55 (d, *J* = 8.7 Hz, 1H), 7.02 (s, 1H), 7.02 – 6.97 (m, 1H), 6.85 (dd, *J* = 8.7, 2.4 Hz, 1H), 6.43 (dd, *J* = 16.6, 9.9

Hz, 1H), 6.30 (d, *J* = 16.6 Hz, 1H), 6.09 (d, *J* = 9.9 Hz, 1H), 4.32 (td, *J* = 10.3, 5.2 Hz, 1H), 4.06 (dtd, *J* = 10.8, 7.4, 4.0 Hz, 1H), 3.89 (t, *J* = 5.1 Hz, 4H), 3.32 (t, *J* = 5.1 Hz, 4H), 2.23 – 2.13 (m, 4H), 1.74 – 1.66 (m, 2H), 1.52 – 1.42 (m, 2H).
^{13}C NMR (151 MHz, $CDCl_3$) δ 162.38, 161.60, 159.99, 145.30, 138.34, 135.09, 132.10, 129.68, 127.20, 116.91, 116.40, 114.66, 112.65, 104.84, 75.62, 47.18, 45.04, 44.65, 30.02, 29.70, 29.66.
HRMS (ESI) m/z calcd for $C_{24}H_{27}ClN_6NaO_4S^+$ $[M+Na]^+$: 553.1395; found: 553.1387

***tert*-butyl 4-(prop-2-yn-1-yl)piperazine-1-carboxylate (ML2-32)**

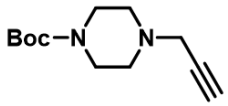

A combination of 1-boc-piperazine (1.50 g, 8.05 mmol) and potassium carbonate (1.67 g, 12.08 mmol) was suspended in acetonitrile (30 mL) and stirred at ambient temperature for 10 minutes. Propargyl bromide (0.84 mL, 8.86 mmol) was added, and the reaction mixture was stirred at 60°C for 2 hours. The reaction mixture was concentrated *in vacuo*, and the crude residue was purified by silica gel chromatography (0-10% MeOH in EtOAc) to afford 1.50 g (82.9%) of the title compound as a yellow oil.
^{1}H NMR (600 MHz, $CDCl_3$) δ 3.38 (t, *J* = 5.1 Hz, 4H), 3.22 (d, *J* = 2.5 Hz, 2H), 2.42 (t, *J* = 5.1 Hz, 4H), 2.19 (t, *J* = 2.4 Hz, 1H), 1.37 (s, 9H).
^{13}C NMR (151 MHz, $CDCl_3$) δ 154.55, 79.54, 78.35, 73.41, 51.54, 46.90, 28.35.

1-(prop-2-yn-1-yl)-4-(vinylsulfonyl)piperazine (ML2-33)

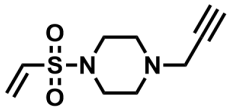

General Procedure C was followed with **ML2-32** (500.0 mg, 2.23 mmol), and TFA (5.5 mL, 73.3 mmol) for 2 hours. The crude material was used without further purification.
General Procedure D was followed with the above product (28 mg, 0.23 mmol), triethylamine (0.14 mL, 1.01 mmol), and 2-chloroethanesulfonyl chloride (0.03 mL, 0.27 mmol). The reaction mixture was concentrated *in vacuo*, and the crude residue was purified by silica gel chromatography (0-10% MeOH in EtOAc) to afford 13.0 mg (26.9%) of the title compound as a yellow oil.
^{1}H NMR (600 MHz, $CDCl_3$) δ 6.42 (dd, *J* = 16.6, 10.0 Hz, 1H), 6.24 (d, *J* = 16.6 Hz, 1H), 6.04 (d, *J* = 10.0 Hz, 1H), 3.33 (d, *J* = 2.4 Hz, 2H), 3.22 (t, *J* = 5.0 Hz, 4H), 2.68 – 2.63 (m, 4H), 2.28 (t, *J* = 2.5 Hz, 1H).
^{13}C NMR (151 MHz, $CDCl_3$) δ 132.32, 128.81, 77.98, 73.72, 51.10, 46.68, 45.45.